CHAPTER 12

ANALYSIS OF ALDEHYDES IN CLOUD AND FOG WATER SAMPLES BY HPLC WITH A POSTCOLUMN REACTION DETECTOR

by

Manabu Igawa†, J. William Munger, and Michael R. Hoffmann*

California Institute of Technology
W. M. Keck Laboratories 138–78
Pasadena, CA 91125

Submitted to: *Environmental Science & Technology*
26 May 1988

Revised: 4 November 1988

* To whom correspondence should be addressed.

†Faculty of Engineering, Kanagawa University, Rokkakubashi,
Kanagawa–ku, Yokohama, 221 Japan.

Abstract

High performance liquid chromatography (HPLC) coupled with a segmented–flow analyzer was used for the analysis of aldehydes. The aldehydes, which were separated on a reversed–phase C_{18} column, were derivatized with 3–methyl–2–benzothiazolinone hydrazone (MBTH) and detected at 640 nm. MBTH reacts readily with all aliphatic aldehydes to form MBTH derivatives with high molar absorptivities. Aldehydes below 1 μM can be easily detected by this method. Because aldehydes and other solutes are separated by HPLC before derivatization, free aldehydes are detected without interference. Aldehydes in cloud– and fogwater samples were analyzed. Formaldehyde, acetaldehyde, glyoxal, and methylglyoxal concentrations were determined. Results obtained with the MBTH method were consistent with those obtained with the 2,4–dinitrophenylhydrazine (DNPH) method. The MBTH method allows for the rapid determination of the concentration of free aldehydes; the DNPH method will yield the similar results, although the procedure is more cumbersome and time consuming.

Introduction

Aldehydes are highly reactive in the atmosphere and in some cases intrinsically hazardous. Furthermore they function as reservoirs for S(IV) in cloud and fog water (1). Formaldehyde or total aliphatic aldehydes can be easily determined by the Nash method (2) or the MBTH method (3) but these colorimetric procedures must be coupled to a chromatographic technique in order to analyze many aldehydes at a same time. In addition aldehydes can be determined quantitatively by derivatization with 2,4–dinitrophenylhydrazine (DNPH) followed by HPLC analysis (4,5) or by formation of bisulfite adducts followed by ion chromatography (6). These methods involve precolumn reactions. However, the derivatization reactions may be affected by the other components in the sample. In addition, the resultant signals, absorptivities, conductivities are sensitive to matrix effects.

We have developed an analytical procedure for aldehydes that couples high performance liquid chromatography (HPLC) with a segmented–flow analyzer. This technique involves a postcolumn reaction (7). The aldehydes, which were separated on a reversed–phase C_{18} column, were derivatized with MBTH (3–methyl–2–benzothiazolinone hydrazone) and detected at 640 nm. The derivatization proceeds as follows: aldehydes react with MBTH to form the corresponding azide (eq. 1); MBTH is oxidized by Fe^{3+} to yield a reactive cation (eq. 2); and a blue cation forms from the combination of the azide and the reactive cation (eq. 3) (8). MBTH reacts with almost all aliphatic aldehydes; the derivatives of these aldehydes have much higher molar absorptivity than those of other methods using UV or VIS detectors (9). Since aldehydes and other solutes are separated by HPLC before derivatization, free aldehydes are detected without interference.

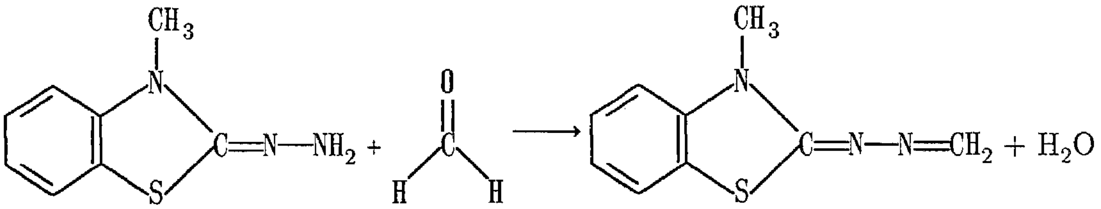

(1)

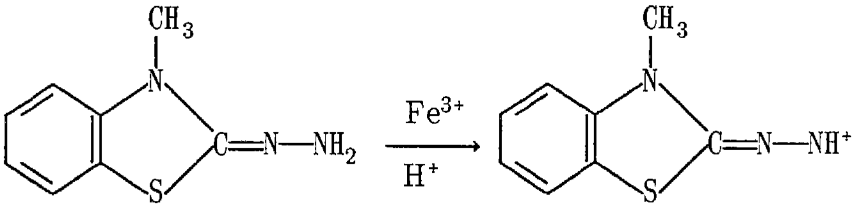

(2)

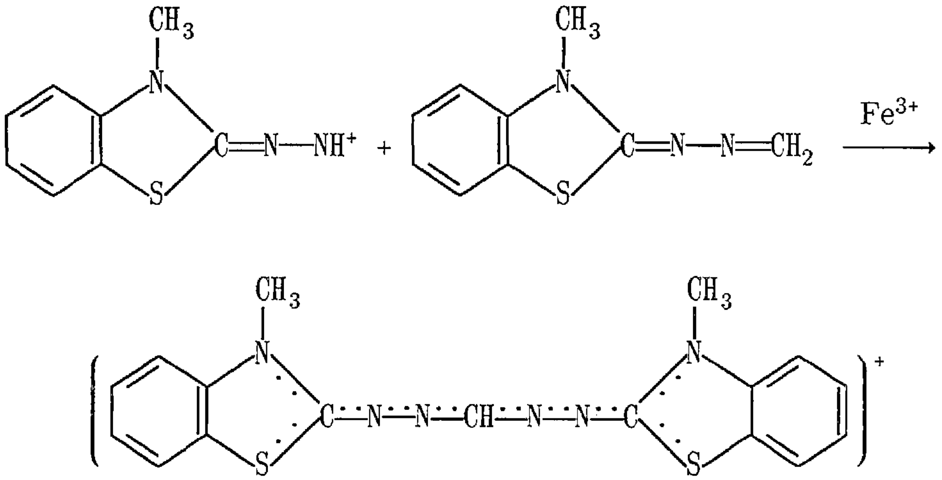

(3)

In this paper, we will report on the optimal conditions for formation of the chromophore of eq. 3, the separation conditions, the sensitivity and the reproducibility of this method, the analysis of free aldehydes and their adducts of bisulfite, and some results for aldehydes in cloud– and fogwater samples.

Experimental Section

Solutions.

The eluent was an acetonitrile–water mixture prepared from HPLC–grade acetonitrile and purified Milli–Q/Milli–RO water. All analytical solutions were prepared from AR grade reagents and Milli–Q water. The reagents used in the reaction detector were MBTH, Fe^{3+}, and a surfactant, Triton X–100. MBTH solutions were prepared by dissolving 3–methyl–2–benzothiazolinone hydrazone hydrochloride monohydrate (from Sigma Chemical Company, Saint Louis, MO) in water to 0.5% (wt/vol). Fe^{3+} solutions were prepared daily by dissolving $FeCl_3 \cdot 6H_2O$ in 0.01 M HCl to 10% (wt/vol). Triton X–100 solutions were prepared by dilution with water to 0.1% (v/v).

Analysis System.

The analysis system couples a HPLC (Hewlett Packard 1084B high performance liquid chromatograph) to a rapid flow analyzer (RFA–300^{TM}, Alpkem Corp.) as shown in Figure 1. The HPLC was equipped with a reversed–phase C_{18} analytical column, {Sperisorb ODS–2 ($5 \mu m$, 4.6×250 mm)} and with Adsorbosphere C_{18} guard column connected just before the analytical column. Samples were injected with a variable volume injector. The separation of aldehydes was performed with isocratic elution using a 40% / 60% or 1% / 99% by volume acetonitrile–water solvent mixture. The eluent flow rate and the column temperature were maintained throughout at 0.5 mL/min and 30 ^{0}C, respectively.

The reactor for the postcolumn reaction was a segmented–stream tubular reactor. The derivatization reaction occurred in an Alpkem glass coil, whose inner diameter, coil diameter, and the number of turns were 1 mm, 1 cm, and 25, respectively, and heat bath equipped with a long coil with 3 mL inner volume. A standard Alpkem air–injector and T–pieces were used and the pump of the analyzer was equipped with standard Tygon tubing to deliver the reagents. The absorbance of the air–segmented colored solution was detected at 640 nm intermittently using the bubble gate of the analyzer. The path length was 1 cm. The signal was recorded on a chart recorder and the concentrations were measured from the peak heights.

The dinitrophenylhydrazone derivatives of carbonyls were extracted 3 times in 60/40 hexane/dichloromethane after adding cyclohexanone 2,4–dinitropheylhydrazone (Aldrich) as an internal standard. The organic fraction was washed with H_2O to remove excess acid and unreacted DNPH. The solvent phase was evaporated to dryness under a stream of N_2. The extracted and dried hydrazones were stored in the refrigerator until analysis. Immediately before analysis the residue was dissolved in THF. The derivatized carbonyls were separated by HPLC on a C_{18} column (Alltech Spherisorb ODS–2); a 45/27.5/27.5 (v/v/v) mixture of $H_2O/CH_3CN/THF$ was used as the mobile phase. Aldehydes and ketones were determined by absorbance at 365nm; each analysis was repeated at 430 nm to determine the dicarbonyls, which absorb at a higher wavelength. Stored and fresh standards gave comparable peak areas at the time of analysis, indicating that the derivatives were stable. The spectra taken at the peaks of selected samples were compared to sample spectra to aid in identification of the compounds present. Standards were prepared from carbonyl hydrazones that were previously synthesized and purified.

Formaldehyde in some samples was also determined by the Nash method using a variation for automated analysis (2). Samples were treated with a buffered S(IV) preservative upon receipt in the laboratory (i.e. within 12 hours of collection) and analyzed within a few days. Alkaline H_2O_2 is added before analysis to prevent interference by S(IV). The results of this analysis give the total CH_2O concentration.

Sample Collection.

Cloudwater was collected at three sampling stations in the Los Angeles Basin. They were located at San Pedro Hill on the Palos Verdes Peninsula overlooking Los Angeles Harbor, at Henninger Flats in the San Gabriel Mountains, and on the roof of a one story building on the eastern edge of the University of California, Riverside campus. The elevations of the sampling points are 427 m, 762 m, and 350 m, respectively. All the samples were collected using the Caltech Active Strand Collector as described elsewhere

(10). The samples were stored in a refrigerator at 4 °C from the sampling station to our laboratory and they were stored in a freezer until analysis. Samples collected for DNPH derivatization were treated in the field according to the method of Grosjean and Wright (5b).

Results and Discussion

Optimal Conditions for the MBTH Method.

The detection sensitivity of the aldehydes depends on the relative concentrations of the colorimetric reagents, on the volume of the reagent solutions, on pH, and on the temperature of the derivatization reaction. The volumes of reagent solutions need to be small to minimize the effects of dilution. The flow rate of each solution was fixed at 37 μL min^{-1}; concentrated solutions were used for coloring. Normally the reaction of aldehydes with MBTH requires 1 hour at room temperature (8). To overcome this problem, the reaction chamber was maintained at 45 °C. A reactor made of glass tubing with 25 turns gave a enough time for the coloring reaction after mixing with Fe^{3+}.

The detection sensitivity increased with an increase in MBTH and Fe^{3+} concentrations. In order to determine the optimal concentrations of MBTH and Fe^{3+}, the effects of a variation in the concentrations on the peak heights of acetaldehyde, glyoxal, and acrolein were investigated; the results are shown in Figure 2. With an increase in the MBTH concentration at a fixed ratio of Fe^{3+} to MBTH, the sensitivity of the least sensitive aldehydes such as glyoxal and acrolein increased; however the selectivities decreased. This was convenient for the coloration of all the aldehydes although the noise of the base line also increased proportionally because Triton X–100, which was used as a stabilizer for the flow system, and acetonitrile in the eluent reacted with MBTH resulting in an increase in the blank absorbance. Hydrochloric acid HCl was added to Fe^{3+} solutions to prevent the precipitation of $Fe(OH)_3$. HCl was added to a maximum level 0.01 M; sensitivity decreased by 1/2 with a one pH unit decrease. For these reasons, each reagent concentration in the system was optimized as described in the experimental section.

Acetone is normally added in the MBTH analysis to prevent turbidity in the sample solution but in our system acetone was not added because of the potential adverse effect on the plastic tubing. Sulfamic acid may be substituted for acetone (11), but it was avoided because the sensitivity was lowered by its addition. The flow system of the reactor was rinsed with concentrated acid daily after the end of the experiment to remove the precipitates that had formed on the inner wall of the glass tubings.

The eluents other than acetonitrile were tested. However alternative solvents such as THF, DMF, DMSO, ethylene glycol, and acetone could not be used because of their high blank absorbances. Alcohols were tested as eluents but their separation properties were found to be poorer than that of acetonitrile.

Analysis of Aldehydes by the MBTH Method.

Figure 3 shows a chromatogram of C_1– C_6 carbonyls using a 40% acetonitrile–water eluent in which each compound is clearly separated. Thus, analysis of aldehydes by this method is possible. The correlation between the log of the retention time and the carbon number for the analysis of aldehydes by this method compares well with the analogous correlation obtained for paraffins separated by GC (12).

Table 1 shows the retention times and the sensitivities of representative aldehydes obtained by using a single component solution for a sample solution and 40% acetonitrile–water for the eluent. The sensitivity was defined as (absorbance of the peak height)/(injection volume (L) × sample concentration (M)) and the detection limit was calculated when the ratio of signal–to–noise was 2. The retention time excludes the period in the postcolumn reactor. Most of the aldehydes can be easily detected below 1 μM but the sensitivity decreases with an increase in carbon number. This may occur for the following reasons: first, hydrophobic aldehydes with higher carbon numbers tend to adsorb strongly on the column and yield peaks that are diffuse; second, the molar absorptivity decreases with an increase in the carbon number. When the sensitivity was evaluated by the peak area, the sensitivities of acetaldehyde and the C_3–C_6 aliphatic carbonyls were 68% and 38 to 30% of that of formaldehyde, respectively. With the increase in the number of carbonyl and hydroxide groups, the hydrophilicity of the aldehydes increases and the retention times decrease. When the number of carbon and hydrophilic groups of an aldehyde were the same as those of another aldehyde, the aldehydes had similar retention times. For example, acrolein ($H_2C{=}CHCHO$) and propionaldehyde (CH_3CH_2CHO) have similar retention times (6.8 vs 7.1 min).

Some aldehydes have very similar retention times but they can be separated from each other by decreasing the acetonitrile concentration in the eluent as shown in Figure 4. When acetonitrile concentration was 40%, the hydrophilic aldehydes, glyoxal, formaldehyde, and pyruvaldehyde, eluted in one peak but they were clearly separated from each other when the acetonitrile concentration was lowered to 1%. Hydroxyacetaldehyde, which has the retention time close to that of formaldehyde (Table 1) was eluted 0.2 min. faster than formaldehyde and could be separated from other aldehydes when acetonitrile concentration was lowered to 1%.

Figure 5 shows a chromatogram of the hydrophilic aldehydes using an eluent of 1% acetonitrile–water. Under this elution condition the analysis of dicarbonyls, glyoxal and methylglyoxal is feasible, although they were not completely resolved due to band broadening in the reactor (7). An important advantage of the MBTH method compared to the DNPH method is that dicarbonyls can be readily analyzed. In the DNPH method two peaks for a dicarbonyl (i.e. mono– and di–DNPH derivatives) are obtained (13). Furthermore the solubilities of the di–DNPH derivatives are low in water, thus they precipitate easily in the analytical column (14). If a gradient elution were applied to the MBTH/HPLC method, it is possible to analyze all aldehydes at once. However because acetonitrile reacts with MBTH, the absorbance of the blank increases with an increase in the acetonitrile concentration; thereby reducing the efficiency of a single chromatographic separation.

Fractionation of Free Aldehydes from Total Aldehydes.

In this method, only free aldehydes are determined. Consequently, it is possible to distinguish between free aldehydes and aldehyde adducts. In fog– and cloudwater, bisulfite ion reacts with aldehydes to form sulfonate adducts (1). Figure 6A and 6B show a chromatogram of a 0.1 mM formaldehyde solution and that of 0.1 mM formaldehyde solution at after the addition of a 10–fold excess of bisulfite, respectively. The formaldehyde peak of Figure 6A is that of free formaldehyde. This peak is almost absent from Figure 6B. Formaldehyde is converted to hydroxymethanesulfonate (HMSA) completely in less than one hour after the addition of bisulfite under these conditions (6, 15). The effects of HCl and NaOH addition to a solution of 0.1 mM formaldehyde and 1 mM bisulfite are shown in Figures 6C, 6D, and 6E. No change in free formaldehyde was observed 30 min. after the addition of HCl to 0.01 mM; but 50% of the hydroxymethanesulfonate (HMSA) was dissociated to free formaldehyde 30 min. after the addition of NaOH to 0.01 M. Only 7% of HMSA was changed 30 min. after the addition of NaOH to 1.0 mM. Addition of NaOH results in the partial dissociation of HMSA to free formaldehyde and sulfite. The net dissociation rate depends on not only NaOH concentration but also on the HMSA and bisulfite concentrations (15,16). The concentration ratio of free formaldehyde to bisulfite adduct after the addition of NaOH increased with the decrease of HMSA and/or bisulfite concentration. When NaOH added to the solution to 0.1 M, the free aldehyde concentration increased to over 85% just after its addition but it gradually decreased again possibly because of CH_2O destruction via the Cannizzaro reaction ($2\ RCHO \xrightarrow{OH^-} RCH_2OH + RCO_2^-$) involving HCHO. The oxidation of bisulfite to sulfate by the addition of hydrogen peroxide to be 1 mM in alkali solution (16) changed 97% of HMSA to free formaldehyde as shown in Figure 6E. However, the addition of hydrogen peroxide sometimes caused positive error in the analysis of natural water samples because of the oxidation of some of the organic components to aldehydes via Fenton's reagent (17) formed from the added H_2O_2 and the Fe^{3+}/Fe^{2+} present in the sample. The addition of EDTA or CDTA could minimize this interference.

In this paper only free aldehydes were determined because the base of C_{18} packing material will be dissolved by the repeated injection of strong alkali solution, although the addition of NaOH was effective for the estimation of the total aldehydes in some cases.

Calibration Curves.

The calibration curves for formaldehyde, acetaldehyde, glyoxal, and methylglyoxal using a 1% acetonitrile–water eluent were found to be highly linear for the relationship between the peak height and concentration. The correlation coefficients (r^2) for these aldehydes were close to one; 1.000 for formaldehyde, 0.997 for acetaldehyde, 0.994 for glyoxal, 0.999 for methylglyoxal.

Analysis of Aldehydes in Cloudwater samples.

Figure 7 shows a typical chromatogram of aldehydes in a cloudwater sample. All of these sample solutions were acidic in the pH range of 2.6 to 3.6. When the acetonitrile concentration in the eluent was 40%, there were only two peaks corresponding to the retention times of formaldehyde and acetaldehyde. No peaks were observed at the retention times of carbonyls containing more than three carbon atoms in most of the samples. However, when the acetonitrile concentration was maintained at 1%, five peaks were observed. They were due to glyoxal, formaldehyde, methylglyoxal, acetaldehyde, and some matrix ions colored by MBTH. The shoulder on the front of the formaldehyde peak suggests the existence of the small amount of hydroxyacetaldehyde. The aldehydes can be determined by comparing the absorbances with a standard solution. The peaks of glyoxal and methylglyoxal were on the shoulder of the formaldehyde peak and their absorbances were obtained as the difference between the absorbance of their peak and the extrapolated absorbance of the peak shoulder of formaldehyde. The analytical errors were estimated by repeated experiments to be at most ± 2%, ± 5%, ± 10%, and ± 25% for formaldehyde, methylglyoxal, acetaldehyde, and glyoxal, respectively. The relative error for glyoxal was high because it was not separated well from other components and its sensitivity was low.

The analyzed values are summarized in Table 2. Formaldehyde was the predominant species found in all the samples. The aldehyde concentrations in the ambient air have been reported; acetaldehyde concentrations are on same order as or a little lower than that of formaldehyde (19,20). However, in Table 2 acetaldehyde concentrations were much lower than the formaldehyde concentration in cloudwater as reported previously by Steinberg et al. (13). The cloudwater samples were collected successively over discrete time intervals. The concentration of each aldehyde decreased at first during the cloud event and then increased with the passage of time in most of the cases. This concentration vs time profile can be explained by the initial dilution that occurs during the condensational growth of the water droplet and the subsequent concentration effect that occurs as the droplet assemblage evaporates (21,22). Note that the concentrations of carbonyls are greater at the inland site than along the coast.

Free CH_2O determined by the MBTH post–column reactor method was 66–89% of the total aldehyde determined by the Nash method. The absolute difference was typically 10–25 μM. None of the San Pedro Hill samples were analyzed by both methods. However, the range of CH_2O determined in 80 samples from other cloud events is comparable to the values determined by the MBTH method.

Fogwater samples collected at Riverside were analyzed by the DNPH method; these results are summarized in Table 3. A large number of carbonyls were found to be present in the fog samples. Formaldehyde was the dominant aldehyde; the longer chain aldehydes decreased in importance as the carbon chain length increased. Glyoxal and methylglyoxal had appreciable concentrations in all samples. The results obtained by the DNPH method are consistent with those obtained by the MBTH method, therefore we feel that the MBTH method provides a suitable alternative especially when it is desirable to know the concentration of free aldehyde as compared to the total aldehyde (free + bisulfite adduct). The MBTH method is more convenient and subject to fewer interferences; thus for samples in the higher concentration domain it may prove to be more satisfactory.

Conclusions

The analytical method of HPLC with a post–column analyzer is useful for the analysis of aldehydes in natural water samples for several reasons. First, the interference from the other components is very small and the reliability of the data is high because each aldehyde, that is separated in the column, is colored and detected. Second, dicarbonyls can be chromatographed by the MBTH method without the generation of two peaks for one dicarbonyl and losses due to the precipitation during analysis as in the case of the DNPH procedure. These advantages are very important in the analysis of aldehydes.

References

1) Munger, J. W.; Tiller, C.; Hoffmann, M. R. *Science* **1986**, *17*, 247–249.

2) a. Dong, S.; Dasgupta, P. K. *Environ. Sci. Technol.* **1987**, *21*, 581–588.

b. Nash, T. *Biochem. J.* **1953**, *55*, 416–421.

3) Nebel, G. J. *Anal.Chem.* 1981, *53*, 1708–1709.

4) Papa, L. J.; Turner, L. P. *J. Chromatogr. Sci.* **1972**, *10*, 747–750.

5) a. Grosjean, D.; Fung, K. *Anal. Chem.* **1981**, *53*, 168–171.

b. Grosjean, D.; Wright, B. *Atmos. Environ.* **1983**, *17*, 2093–2096.

6) Duval, D. L.; Rogers, M.; Fritz, J. S. *Anal. Chem.* **1985**, *57*, 1583–1586.

7) Frei, R. W.; Jansen, H.; Brinkman, U. A. T. *Anal. Chem.* **1985**, *57*, 1529A–1539A.

8) Sawicki, E.; Hauser, T. R.; Stanley, T. W.; Elbeert, W. *Anal. Chem.* **1961**, *33*, 93–96.

9) Sawicki, E.; Stanley, T. W.; Pfaff, J. *Anal. Chim. Acta* **1963**, *28*, 156–163.

10) a. Jacob, D. J.; Waldman, J. M.; Haghi, M.; Hoffmann, M. R.; Flagan, R. C. *Rev. Sci. Instrum.* **1985**, *56*, 1291–1293.

b. Daube, B. C., Jr.; Flagan, R. C.; M. R. Hoffmann United States Patent 1987, 4,697,462 (10–6–87).

11) Hauser, T. R.; Cummins, R. L. *Anal. Chem.* **1964**, *56*, 679–681.

12) Skoog, D. A. *Principles of Instrumental Analysis*, 3rd ed.; Saunders College Publishing, New York: 1985; p.770.

13) Steinberg, S.; Kaplan, I. R. *Intern. J. Environ. Anal. Chem.* **1984**, *18*, 253–266.

14) Hull, L. A. *Analysis of aldehydes and ketones in the gas phase*, EPA report (EPA/600/3–85/021), 1985.

15) Boyce, S.; Hoffmann, M. R. *J. Phys. Chem.* **1984**, *88*, 4740–4746.

16) Olson, T. M.; Hoffmann, M. R. *Atmos. Environ.* **1986**, *20*, 2277–2278.

17) Dong, S.; Dasgupta, P. K. *Environ. Sci. Technol.* 1987, *21*, 581–588.

18) Bhargava, M.; Sethuram, B.; Rao, T. N. *Indian J. Chem.* **1976**, *14A*, 770–772.

19) Grosjean, D. *Environ. Sci. Technol.* **1982**, *16*, 254–262.

20) Kuwata, K.; Uebori, M.; Yamasaki, H.; Kuge, Y.; Kiso, Y. *Anal. Chem.* **1983**, *55*, 2013–2016.

21) Waldman, J. M.; Munger, J. W.; Jacob, D. J.; Flagan, R. C.; Morgan, J. J.; Hoffmann, M. R. *Science* **1982**, *218*, 677–679.

22) Munger, J. W.; Jacob, D. J.; Waldman, J. M.; Hoffmann, M. R. *J. Geophys. Res.* 1983, *88*, 5109–5121.

Table 1. Retention time and sensitivity of aldehydes.

Aldehydes	Retention time (min)*	Sensitivity** (x 10^8)	Detection limit (μM)*** 20 μL	100 μL
			injection volumes	
HCOCHO	4.1	1.31	0.95	0.190
CH_3COCHO	4.5	2.03	0.49	0.099
HCHO	4.3	4.79	0.21	0.042
CH_3CHO	5.6	2.79	0.36	0.072
C_2H_5CHO	7.1	1.14	0.88	0.180
C_3H_7CHO	10.0	0.73	1.40	0.280
C_4H_9CHO	15.3	0.31	3.20	0.640
$C_5H_{11}CHO$	25.3	0.12	8.70	1.700
$HOCH_2CHO$	4.30	3.61	0.28	0.055
$H_2C{=}CHCHO$	6.80	0.14	7.00	1.4
$H_2C{=}CH(CH_3)CHO$	9.80	0.023	44.0	9.0

HPLC column; Spherisorb ODS–2 (5μm), 4.6 x 250 mm.

HPLC eluent: 40% acetonitrile + 60% water.

* Retention times exclude the time in the postcolumn reaction detector (4.9 min).

** Sensitivity is defined as (absorbance of peak height)/(injection volume (L) x sample concentration (mol/L)).

*** Detection limit was calculated when the signal–to–noise ratio was 2.

Table 2. Concentration of aldehydes (μM) in cloudwater at San Pedro Hill and at Henninger Flats as determined by the MBTH method.

Date	Time	HCHO	CH_3CHO	$\mathrm{H\overset{\overset{O}{\Vert}}{C}{-}\overset{\overset{O}{\Vert}}{C}H}$	$\mathrm{CH_3\overset{\overset{O}{\Vert}}{C}CHO}$	$\mathrm{HCHO}_T^{\dagger}$
		San Pedro Hill (a coastal site)				
6–13–87	20:43–21:22	22.7	4.2	8.1	7.5	——
6–14–87	00:56–01:41	16.4	3.6	7.8	4.9	——
	04:09–04:31	21.9	4.3	9.0	7.1	——
	05:40–06:16	21.6	5.1	6.9	6.7	——
6–26–87	01:48–02:08	30.7	3.0	10.2	7.8	——
	03:06–03:15	27.7	1.9	2.0	4.6	——
	04:04–04:24	13.6	2.3	3.3	3.7	——
	05:27–05:45	36.3	2.5	1.2	5.0	——
	06:26–09:19	37.3	1.7	8.6	8.3	——
		Henninger Flat (an inland mountainous site)				
6–20–87	05:00–06:19	61.5	4.5	4.7	13.4	75
	08:47–09:30	57.5	3.1	10.1	21.3	66
6–21–87	02:49–05:06	50.6	1.9	31.0	15.2	76
	06:20–06:34	45.9	1.4	20.2	8.2	54
	07:08–07:41	55.1	1.2	19.4	13.0	62
	08:39–09:19	59.9	3.8	23.3	26.9	75

Cloud events: 20:43–08:39 on 6/13 to 6/14 and 01:48–09:19 on 6/26 at San Pedro Hill and 05:00–11:09 on 6/20 and 01:28–10:03 on 6/21 at Henninger Flat. † Total CH_2O determined by the Nash method.

Table 3. Carbonyl Concentrations (μM) determined by HPLC analysis of DNPH Derivatives of Riverside Fogwater.

Date	Time		CH_2O	$\mathrm{H\overset{\overset{O}{\|}}{C}-\overset{\overset{O}{\|}}{C}H}$	$\mathrm{CH_3\overset{\overset{O}{\|}}{C}-\overset{\overset{O}{\|}}{C}H}$	$(CH_3CO)_2$
01–23–86	05:55	06:30	109	65.3	45.9	4.7
	06:30	07:00	122	32.3	25.8	3.7
	07:00	07:30	162	34.6	26.7	3.5
	07:30	08:00	228	59.9	44.1	5.8
	08:00	08:30	119	55.3	42.7	5.1
	08:30	09:00	142	56.8	47.7	5.8
	09:00	09:35	104	121	83.9	1.4
	09:35	10:12	84	139	108	0.0
	Blank		0.4	0.0	0.0	0.0
02–28–86	07:44	08:20	36.3	38.6	35.5	3.9
	08:20	08:45	40.8	45.0	41.1	4.9
	08:45	09:30	57.3	77.1	60.5	6.6
	09:30	10:00	107	198	128	14.0
	Blank		21.0	0.8	0.0	0.0
03–01–86	00:00	01:00	4.1	147.8	79.1	8.8
	01:00	02:06	8.7	142.3	74.9	8.9
	00:06	03:00	8.2	144.1	77.4	8.8
	03:00	04:05	36.0	276.2	124	17.7
	Blank		13	0.6	0	0

Sample Concentrations are corrected for blank concentrations. The concentrations given for the blanks are the actual concentrations in the blank.

Figure Captions

Figure 1. Schematic diagram of the apparatus used in this study. 1) from HPLC (500 μL min^{-1}). 2) Triton X–100 (37 μL min^{-1}). 3) Air (118 μL min^{-1}). 4) MBTH (37 μL min^{-1}). 5) Fe^{3+} (37 μL min^{-1}). P, pump. HB, heat bath. RC, reaction coil. D, detector (640 nm).

Figure 2. Effects of Fe^{3+} and MBTH concentrations on peak heights. Eluent, 40% acetonitrile + 60% water. Injection volume, 20 μL. ———, acetaldehyde (10 μM); ———, glyoxal (10 μM); –·–·–, acrolein (10 μM). Open symbols (e.g. ○) are 0.5% MBTH soln.; half–shaded symbols (e.g. ⬓) are 1% MBTH soln.; and shaded symbols (e.g. ▲) are 2% MBTH soln. The value of [MBTH(%)] was calculated from the weight(g) of 3–methyl–2–benzo-thiazolinone hydrazone hydrochloride monohydrate in 100 mL aqueous solution.The value of [Fe^{3+}(%)] was calculated from the weight(g) of $FeCl_3 \cdot 6H_2O$ in 100 mL aqueous solution.

Figure 3. HPLC separation of C_1–C_6 carbonyls. Column, Spherisorb ODS–2 (5μm), 4.6 x 250 mm. Injection volume, 20 μL. Eluent, 40% Acetonitrile + 60% water. 1) 25 μM HCHO; 2) 50 μM CH_3CHO; 3) 75 μM C_2H_5CHO; 4) 100 μM C_3H_7CHO; 5) 150 μM C_4H_9CHO; 6) 200 μM $C_5H_{11}CHO$.

Figure 4. Effect of acetonitrile concentration on retention time. Column, Spherisorb ODS–2 (5μm), 4.6 x 250 mm. Injection volume, 20 μL. ○, glyoxal; ●, formaldehyde; ◑., methylglyoxal; ◐ , acetaldehyde; ◒ , propionaldehyde.

Figure 5. HPLC separation of selected hydrophilic aldehydes. Column, Spherisorb ODS–2 (5μm), 4.6 x 250 mm. Injection volume, 20 μL. Eluent, 1% Acetonitrile + 99% water. 1) 200 μM HCOCHO; 2) 50 μM HCHO; 3) 150 μM CH_3COCHO; 4) 100 μM CH_3CHO

Figure 6. Effect of bisulfite on free aldehyde concentration. Column, Spherisorb ODS–2 (5μm), 4.6 x 250 mm. Injection volume, 20 μL. Eluent, 40% acetonitrile + 60% water. Sample composition: A) 0.1mM HCHO. B) 0.1 mM formaldehyde and 1 mM $NaHSO_3$. C) 0.1 mM formaldehyde, 1 mM $NaHSO_3$, and 0.01 M HCl. D)

0.1 mM formaldehyde, 1 mM $NaHSO_3$, and 0.01 M NaOH. E) 0.1 mM formaldehyde, 1 mM $NaHSO_3$, and 1 mM H_2O_2.

Figure 7. Typical chromatogram of aldehydes in a cloudwater sample. Column, Spherisorb ODS–2 (5 μm), 4.6 x 250 mm. A) Eluent, 40% acetonitrile + 60% water. Injection volume, 50 μL. B) Eluent, 1% acetonitrile + 99% water. Injection volume, 100 μL. 0) some matrix ions; 1) HCOCHO; 2) HCHO; 3) CH_3COCHO; 4) CH_3CHO

BRIEF

HPLC coupled with a segmented–flow analyzer was used for the analysis of aldehydes. Aldehydes in cloudwater samples were analyzed and C_1– C_3 aldehydes concentrations were determined.

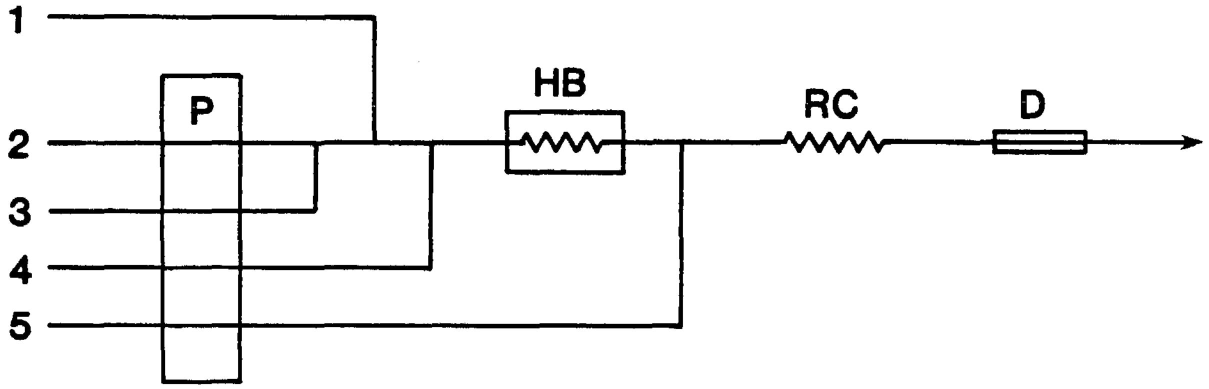

Figure 1

Flow diagram for the postcolumn MBTH detection system: 1) effluent flow from the HPLC (500 μL min^{-1}). 2) Triton X–100 (37 μL min^{-1}). 3) Air (118 μL min^{-1}). 4) MBTH (37 μL min^{-1}). 5) Fe^{3+} (37 μL min^{-1}). P, pump. HB, heat bath. RC, reaction coil. D, detector (640 nm).

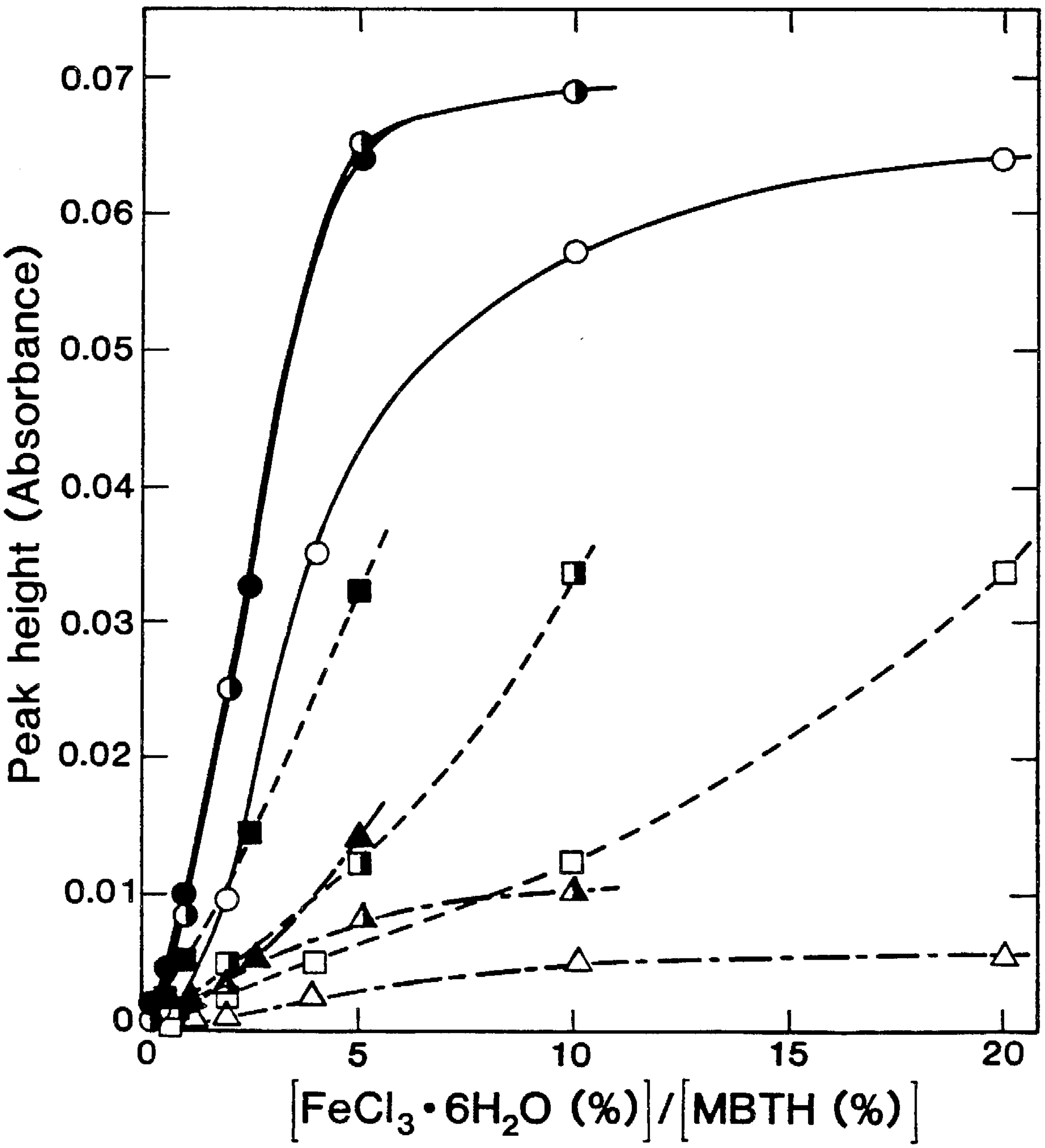

Figure 2

Effects of Fe^{3+} and MBTH concentrations on peak heights. Eluent, 40% acetonitrile + 60% water. Injection volume, 20 μL. ———, acetaldehyde (10 μM); ———, glyoxal (10 μM); —·—·—, acrolein (10 μM). Open symbols (e.g. ○) are 0.5% MBTH soln.; half–shaded symbols (e.g. ◧) are 1% MBTH soln.; and shaded symbols (e.g. ▲) are 2% MBTH soln. The value of [MBTH(%)] was calculated from the weight(g) of 3–methyl–2–benzo-thiazolinone hydrazone hydrochloride monohydrate in 100 mL aqueous solution.The value of [Fe^{3+}(%)] was calculated from the weight(g) of FeCl$_3$·6H$_2$O in 100 mL aqueous solution.

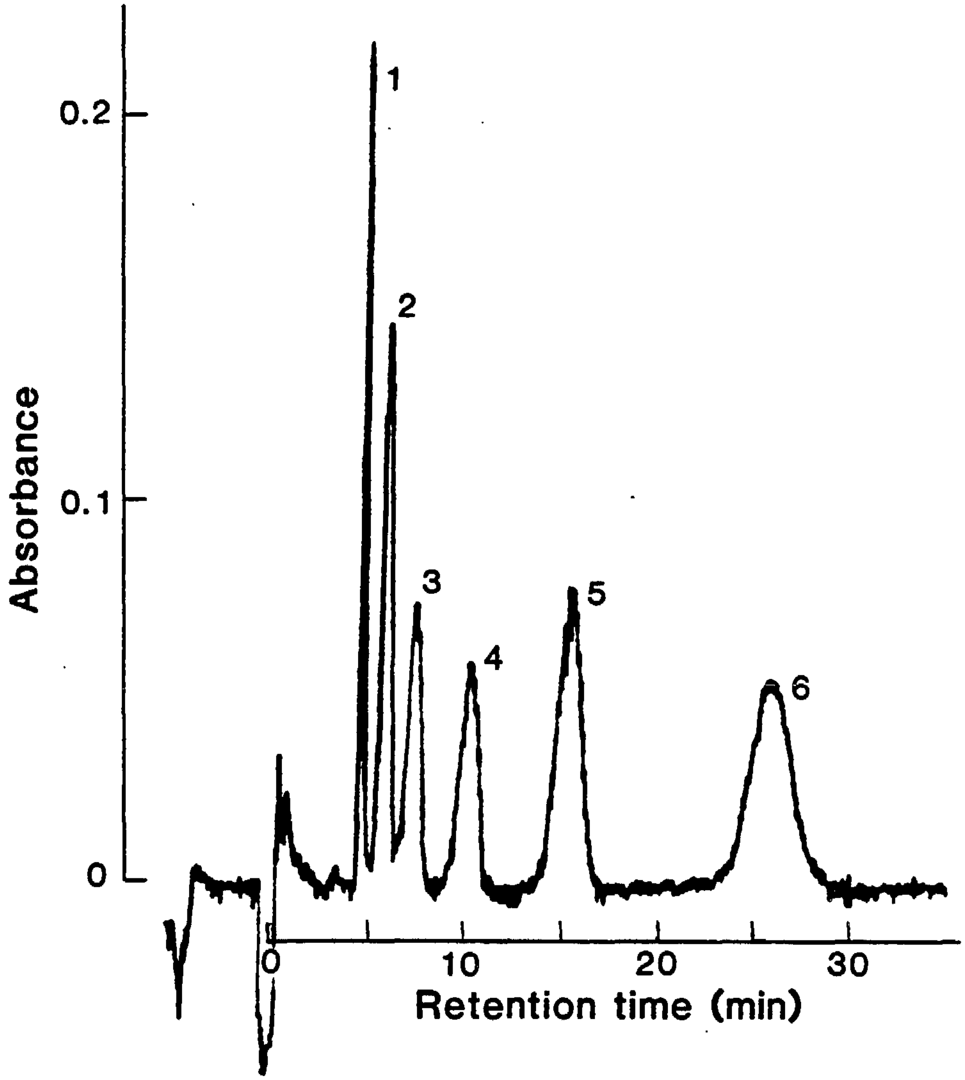

Figure 3

HPLC separation of C_1–C_6 carbonyls. Column, Spherisorb ODS–2 (5μm), 4.6 x 250 mm. Injection volume, 20 μL. Eluent, 40% Acetonitrile + 60% water. 1) 25 μM HCHO; 2) 50 μM CH_3CHO; 3) 75 μM C_2H_5CHO; 4) 100 μM C_3H_7CHO; 5) 150 μM C_4H_9CHO; 6) 200 μM $C_5H_{11}CHO$.

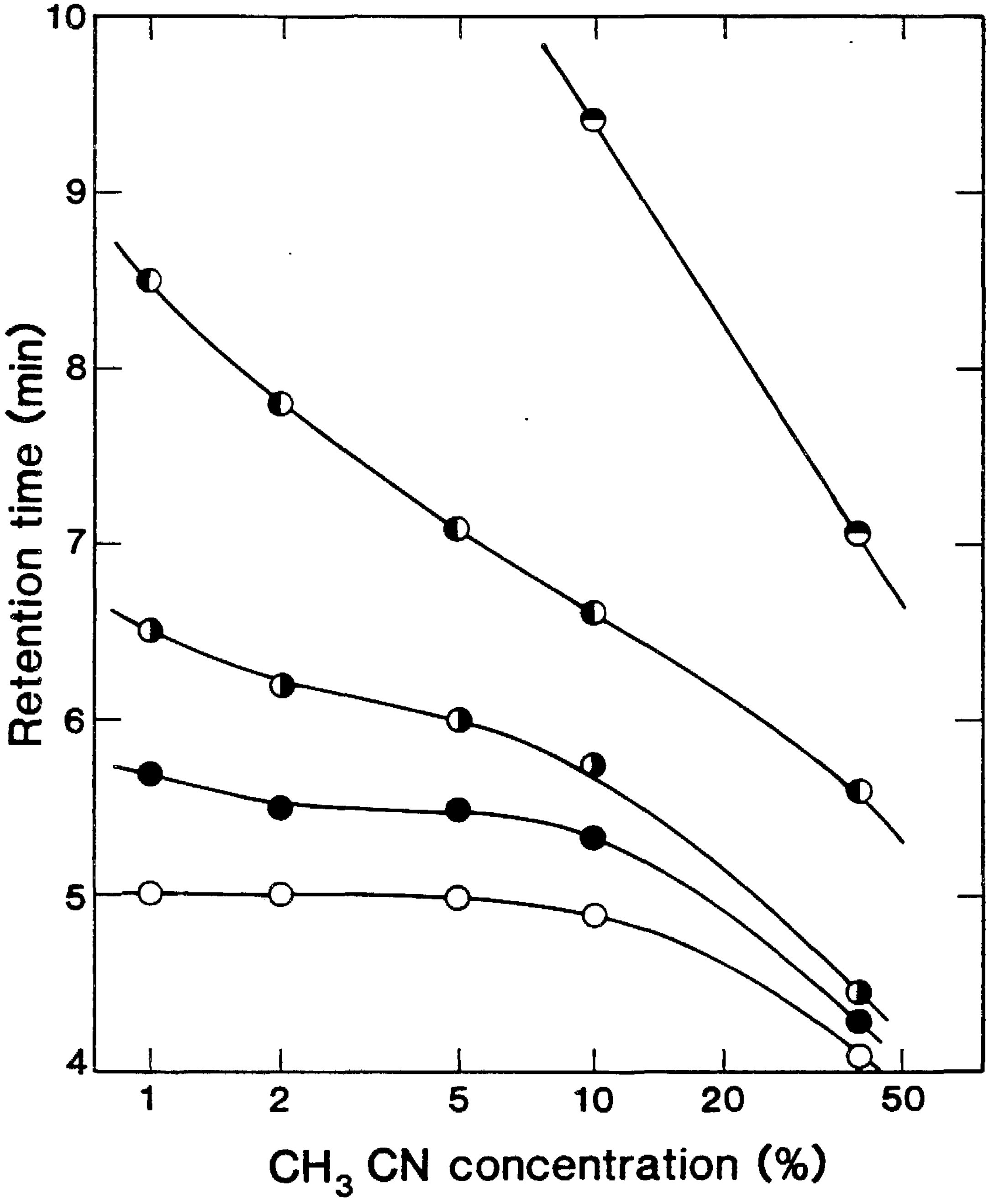

Figure 4

Effect of acetonitrile concentration on retention time. Column, Spherisorb ODS–2 (5μm), 4.6 x 250 mm. Injection volume, 20 μL. ○, glyoxal; ●, formaldehyde; ◑, methylglyoxal; ◐, acetaldehyde; ⊖, propionaldehyde.

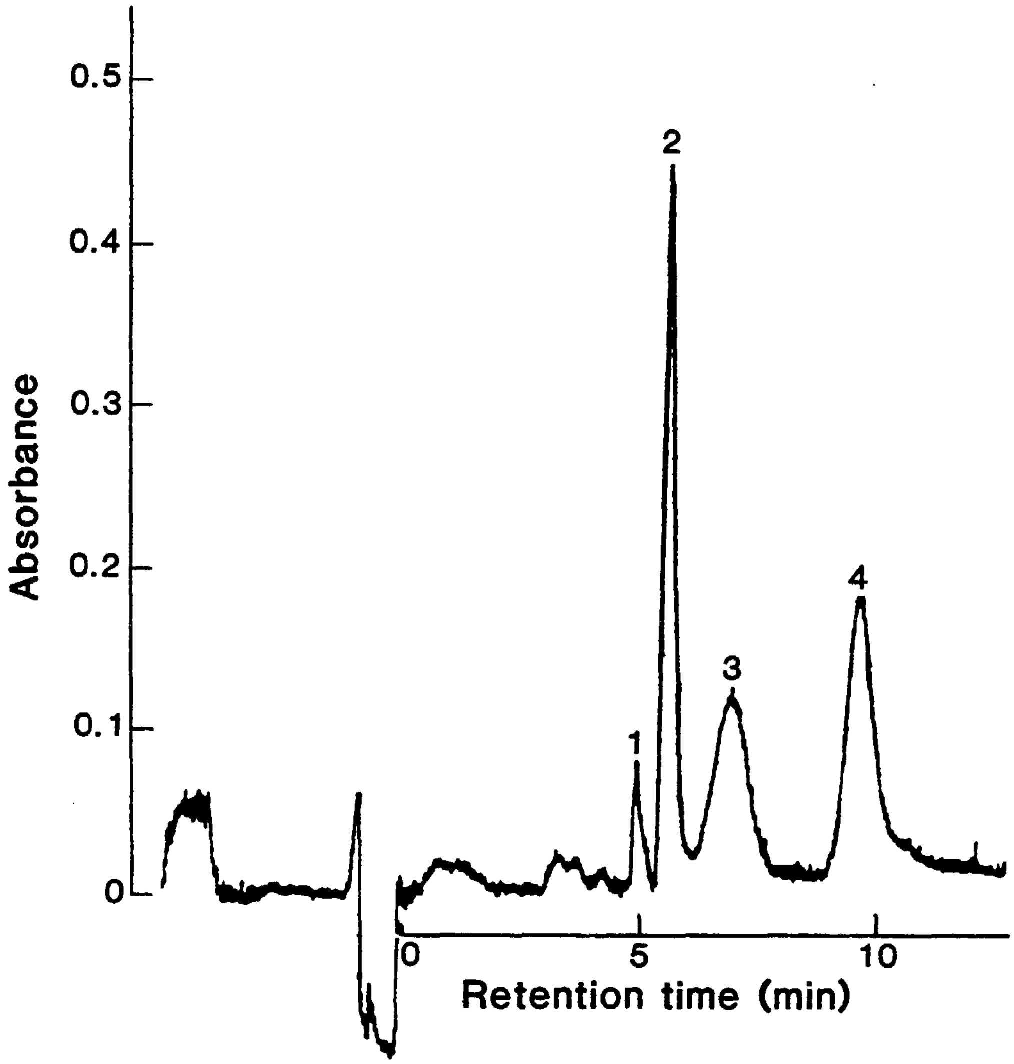

Figure 5

HPLC separation of selected hydrophilic aldehydes. Column, Spherisorb ODS–2 (5μm), 4.6 x 250 mm. Injection volume, 20 μL. Eluent, 1% Acetonitrile + 99% water. 1) 200 μM HCOCHO; 2) 50 μM HCHO; 3) 150 μM CH_3COCHO; 4) 100 μM CH_3CHO

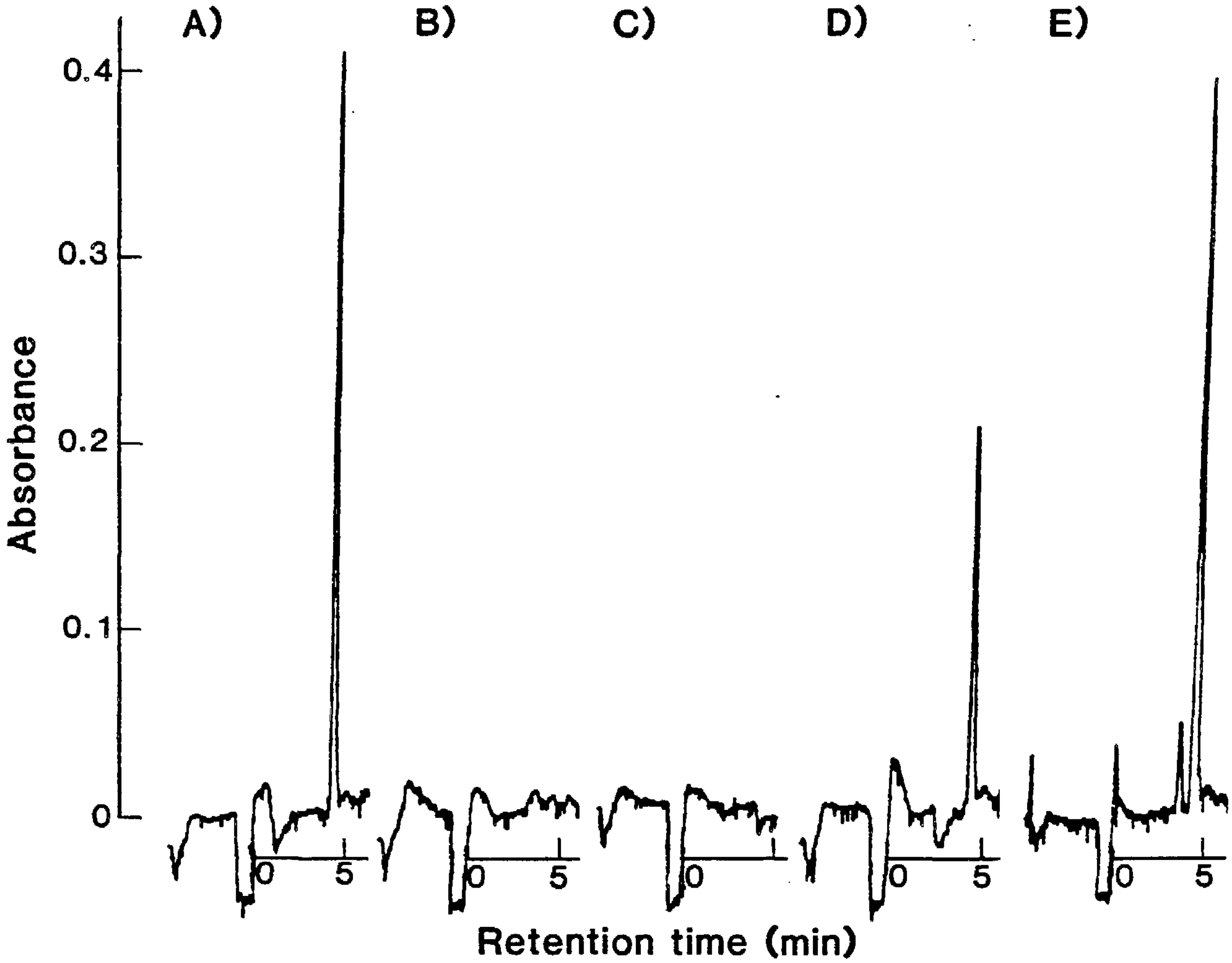

Figure 6

Effect of bisulfite on free aldehyde concentration. Column, Spherisorb ODS–2 (5μm), 4.6 x 250 mm. Injection volume, 20 μL. Eluent, 40% acetonitrile + 60% water. Sample composition: A) 0.1mM HCHO. B) 0.1 mM formaldehyde and 1 mM $NaHSO_3$. C) 0.1 mM formaldehyde, 1 mM $NaHSO_3$, and 0.01 M HCl. D) 0.1 mM formaldehyde, 1 mM $NaHSO_3$, and 0.01 M NaOH. E) 0.1 mM formaldehyde, 1 mM $NaHSO_3$, and 1 mM H_2O_2.

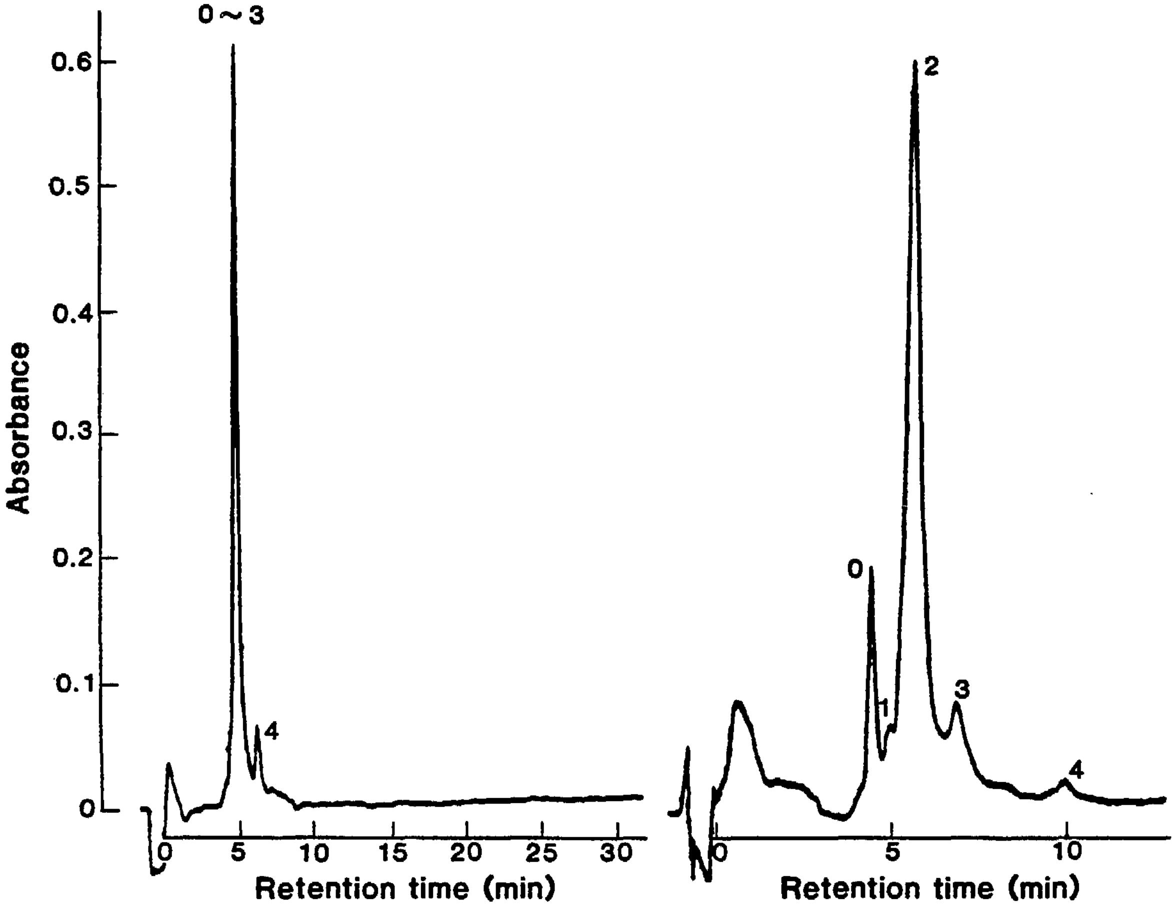

Figure 7

Typical chromatogram of aldehydes in a cloudwater sample. Column, Spherisorb ODS–2 (5 μm), 4.6 x 250 mm. A) Eluent, 40% acetonitrile + 60% water. Injection volume, 50 μL. B) Eluent, 1% acetonitrile + 99% water. Injection volume, 100 μL. 0) some matrix ions; 1) HCOCHO; 2) HCHO; 3) CH_3COCHO; 4) CH_3CHO

CHAPTER 13

Carboxylic Acids and Carbonyl Compounds in Southern California Clouds and Fogs

by

J. William Munger, Jeff Collett, Jr.,
Bruce C. Daube, Jr., and Michael R. Hoffmann*

Environmental Engineering Science
W. M. Keck Laboratories, 138–78
California Institute of Technology
Pasadena, CA 91125, U.S.A.

Submitted to *Tellus* (CACGP Symposium Volume – Paper OR O9)
March 8, 1988

* to whom correspondence should be addressed

ABSTRACT

Formaldehyde, formate, and acetate have been determined in fog and cloudwater from several areas of southern California. Up to 190 μM formate and acetate was seen in high pH fog samples from the San Joaquin Valley. Formaldehyde concentrations as high as 500 μM were observed. Organic acid concentrations were much lower at an acidic site along the margin of the valley. Fog from Riverside, CA had maximum concentrations of 1500 and 500 μM formate and acetate. The highest concentrations were observed in the samples with highest pH. Formaldehyde at Riverside was as high as 380 μM. Average formate and acetate concentrations in intercepted stratus clouds from the Santa Barbara Channel coast and San Pedro Hill were 20 – 60 μM and 10 – 30 μM, respectively. Formaldehyde concentrations in stratus clouds were about 10 – 20 μM.

Because the lifetime of a cloud or fog droplet is usually much longer than the characteristic time for interfacial mass transport, hydration or dissociation, droplets can be assumed to be in equilibrium with their surroundings. High aqueous–phase concentrations of organic acids are observed either near sources where ambient levels are high or at sites where cloudwater pH is high.

1. INTRODUCTION

Soluble organic carbon is an important component of the atmosphere. Liljestrand and Morgan (1981) observed that organic carbon was the dominant component by mass of rainwater collected in Los Angeles, while Likens et al. (1983) established that carbonyl compounds and carboxylic acids contribute a major portion of the dissolved organic carbon in rainwater. Organic acids can be the dominant source of free acidity in rainwater, particularly in remote regions where strong mineral acids are scarce (Galloway et al., 1982; Keene et al., 1983). At high pH the salts of organic acids (e.g. $NH_4^+COO^-$) become a component of atmospheric alkalinity (Jacob et al., 1986). Carbonyls play a well known role in gas–phase photochemistry (Finlayson–Pitts and Pitts, 1986; Seinfeld, 1986). In the aqueous phase formation of gem diols reduces their susceptibility to photolysis. However, model calculations indicate that the following reaction may be important (Chameides 1984).

$$CH_2(OH)_2 + OH\cdot \xrightarrow{O_2} HCOOH + HO_2\cdot + H_2O$$

The fate of HCOOH formed via this reaction is pH dependent (Jacob 1986). At $pH > pK_a$, $HCOO^-$ is rapidly oxidized by $OH\cdot$, while in acidic droplets HCOOH may be released to the surrounding atmosphere. In addition the formation of carbonyl–S(IV) adducts (hydroxyalkylsulfonates) may enhance S(IV) scavenging in droplets (Munger et al., 1984; 1986).

The equilibria that control partitioning of carbonyls and carboxylic acids between droplets and the surrounding air are shown in Table 1. Even though equilibrium constants have been measured for many environmentally important species, some constants have not been determined. In these cases, Taft correlations can be used to estimate values for carbonyl hydration constants and sulfonate stability constants (Betterton et al., 1988). Because the characteristic times for interfacial mass transfer and the equilibrium reactions in Table 1 are short compared to cloud droplet lifetimes, droplets can be assumed to be in equilibrium with their surroundings (Schwartz and Freiberg, 1981). Raindrops, however, which are larger and fall through layers with different compositions may not achieve equilibrium with their surroundings.

Some general predictions may be made about the distribution of carbonyls and carboxylic acids in the presence of liquid water. Carbonyl solubility is primarily a function of the hydration constant. Formaldehyde is easily hydrated, but the higher alkyl carbonyls are not. Aldehydes with low hydration constants will be less important in the aqueous phase. Because electron withdrawing substituents adjacent to the carbonyl carbon enhance its hydration, dicarbonyls and halo–substituted acetaldehyde should have large hydration constants. The carbonyl group on ketoacids, such as pyruvic, should be strongly hydrated when the acid is protonated, but not when it dissociates. Sulfonate stability is also enhanced by adjacent electron withdrawing substituents, so it should follow the same trend as the hydration constants. The distribution of organic acids between vapor and aqueous phase will be strongly pH dependent. At droplet pH values below the pK_a for the acid, most of it will be present in the gas phase. When the pH of the droplet is above the pK_a, the droplet will be an efficient sink for weak acids. At 25°C in a cloud with liquid water content $= 0.5$ g m^{-3}, formate and acetate are predicted to be found predominantly in the aqueous phase above $\simeq$ pH 5 and 6, respectively. Furthermore, the solubility of carbonyls and carboxylic acids is increased at low temperatures.

Combustion processes are the major source of primary aldehydes (Rogozen et al., 1984). Vegetation and combustion are thought to be direct sources of organic acids (Graedel et al., 1986). Bacterial metabolism produces a variety of short–chain carboxylic acids; thus decomposing organic matter (e.g. soils, manure) could be sources of organic acids. However, atmospheric reactions are the most important sources of carbonyls and carboxylic acids. A wide variety of aldehydes, ketones and substituted carbonyls are formed from the oxidation of hydrocarbons. Ozonolysis of isoprene, a natural hydrocarbon emitted by vegetation, is potentially a major source of HCOOH (Jacob and Wofsy, 1986). Carbonyls are sensitive to photolysis and attack by oxidants. Atmospheric residence times for aldehydes are less than a day (NRC, 1981). Organic acids are generally more stable. The major sink for organic acids is surface deposition.

Keene and Galloway (1986) have summarized much of the recent data on HCOOH and CH_3OOH in rainwater. However, fog and cloudwater measurements made in conjunction with gas–phase measurements are less extensive. Carlier et al. (1986) have summarized the literature on gas–phase formaldehyde. Fewer data are available on aqueous–phase formaldehyde. In this paper we present data on formaldehyde, formate and acetate concentrations in cloud and fogwater from several sites in Southern California. Our objective is to establish the range of concentrations in these environments and identify differences and similarities among the various sites.

2. METHODS

Samples have been collected from four regions of southern California (see Figure 1) with a variety of meteorological and pollution characteristics. The San Joaquin Valley (inset A of Figure 1) is subject to persistent stagnation episodes, lasting several days at a time. These are accompanied by fog or low stratus, during the early winter months. Emissions from urban centers, oil field steam generators, and animal feedlots accumulate in the stagnant air mass. Samples were collected at four locations during the period December 1983 – January 1984. Bakersfield is a major population center adjacent to the oilfields on the east side of the valley. Visalia is a small city in a predominantly agricultural area. Buttonwillow is a small town surrounded by cropland. McKittrick is located on the west slope of the valley and is surrounded by oilfields; because of its higher elevation it is impacted by stratus clouds that do not affect the valley floor. Fogwater pH values in the San Joaquin Valley range from near 3 to above 6, depending on the local balance between acids and NH_3 (Jacob et al., 1986). Photochemical activity is reduced because of the cloud cover and low sun angle.

At Riverside, California (inset B of Figure 1) radiation fogs form during the winter months. Samples were collected there during the winter of 1986. Frequent temperature inversions over the Los Angeles basin trap emissions near the ground. Prevailing winds that blow from the coast are funneled through the Riverside area during the day; nocturnal land breezes recycle the air mass back toward the coast. Very high pollutant levels are observed under these conditions. In addition to urban emissions from urban Los Angeles and Orange County, the Riverside area is affected by numerous dairy operations around Chino. These activities are a strong source of NH_3 and possibly some organic compounds.

Stratus clouds are frequent occurrence along the California coast. Temperature inversions associated with subsidence in the Pacific High seals the top of the mixed layer. As noted above, sea/land breeze cycles recirculate emissions and secondary pollutants (Cass and Shair, 1984). In addition, extensive areas are covered with chaparral and forest outside the immediate urban areas; these are potential sources for natural hydrocarbons. Three sites along the Santa Barbara Channel coast were sampled in July and August of 1986 (see Figure 1). Samples were collected from two elevations on Laguna Peak, which is at the southeastern end of the Channel. The upper site is identified as Laguna Peak; the lower site is identified as Laguna Road. The Ventura site was located on a hill overlooking the city, while the third site, Casitas Pass, was located at the head of a valley. Emission sources in this area include numerous offshore oil platforms and the population centers along the coastal plain. Transport of emissions from Los Angeles to the Santa Barbara Channel has been observed (Shair et al., 1982). Stratus clouds were sampled from San Pedro Hill overlooking Los Angeles Harbor (see inset B of Figure 1) during June and July

1987. This site is affected at times by nearby refineries, as well as by the overall mix of emissions from throughout the Los Angeles basin.

The San Joaquin Valley samples were collected with a Rotating Arm Collector (Jacob et al., 1984). The remainder of the samples were collected with a Caltech Active Strand Collector (Daube et al., 1987). Although the CASC does not isolate the collected droplets from the air stream as quickly as the RAC, it collects the entire droplet size spectrum effectively, generates larger sample volumes, and its operation is automated (Daube et al., 1987). Side–by–side comparison of the two collectors does not indicate any bias in CH_2O concentrations.

A size–fractionating inlet has been constructed for the CASC. A series of teflon rods at the mouth of the inlet collect the larger droplets. The 50% size cut for the rods is $\simeq 16$ μm diameter. The remaining droplets penetrate to the strands and are collected there. A series of cloudwater samples were collected at San Pedro Hill using this inlet on the morning of July 15, 1987.

Attempts were made to sample organic acids in the gas phase using NaOH impregnated filters. However, because of a possible interference by aldehydes (Keene et al., 1986), these data are not reported.

Formaldehyde in fog and cloud samples was determined by the Nash method (Nash 1953; Reitz, 1980). The reagent mixture was added to the sample in the field to stabilize the CH_2O as 3,5-diacetyl,1,4-dihydrolutidine (DDL). Iodine was used in most cases to eliminate S(IV), which complexes with CH_2O (Smith and Erhardt, 1975). The San Pedro Hill samples were analyzed according to Dong and Dasgupta's (1987) modification for use with an autoanalyzer. Sulfite was added to the samples shortly after collection to form the stable sulfonate salt (Boyce and Hoffmann, 1984). Prior to analysis, the samples were treated with strong base and H_2O_2 to release CH_2O.

Chloroform was added to an aliquot of sample shortly after collection to retard decomposition of the organic acids (Keene and Galloway, 1984). Samples were analyzed by Ion Exclusion Chromatography on a Dionex 2020i Ion Chromatograph. The San Joaquin Valley samples were analyzed with a Dionex ICE anion separator column and Ag^+ resin packed-bed suppressor. Subsequent samples were analyzed using the Dionex HPICE AS1 column preceded by an MPIC (uncharged resin) guard column. The guard column was installed to protect the separator column from nonpolar material in the samples. The eluents used in all cases were HCl at 1 − 5 mM concentration. A Dionex ICE AMMS suppressor was tested, but high baselines and a limited lifetime made it impractical for these analyses. Parallel analysis by normal ion chromatography using 2 mM $Na_2B_4O_7$ as eluent gave equivalent results for HCOOH concentrations, but acetate coeluted under these conditions with propionate and lactate and perhaps other acids. In addition to formate and acetate, which are reported here, several other acids were frequently observed in the chromatograms. These peaks have been tentatively identified as lactate and pyruvate.

3. Results and Discussion

Formic and acetic acid concentrations in fogwater collected at the four sites in the San Joaquin Valley are illustrated in Fig. 2. Organic acid concentrations were consistently low at McKittrick. Concentrations at Bakersfield were quite variable; the most highly concentrated samples had large excesses of CH_3COOH relative to CHOOH. At Buttonwillow both the formic acid concentrations and formic/acetic ratio were fairly high. Visalia, on the other hand had an excess of acetic acid.

McKittrick had the lowest formaldehyde concentrations, followed by Visalia (see Fig.3). Most of the samples from these two sites had $< 50\mu M$ [CH_2O]. The Buttonwillow samples fell in the range 70 – 120 μM. The highest concentrations of formaldehyde (up to 500 μM) occurred at Bakersfield.

When the effect of pH on organic acid scavenging is accounted for by calculating the equilibrium partial pressure of formic and acetic acid in the San Joaquin Valley fogs a different pattern emerges. The high pH fog at Visalia essentially scrubs all the organic acid from the atmosphere. Very low gas–phase concentrations can support the observed aqueous–phase concentrations. The McKittrick fog with formate concentrations of 10 – 30 μM was predicted to be in equilibrium with 0.15 – 0.7 ppb formic acid in the gas phase. The same gas–phase concentration would give aqueous–phase concentrations $\geq$ 120 μM in fog at Buttonwillow and Bakersfield. The observed concentration patterns are related to the proximity to sources. McKittrick and Bakersfield are adjacent to oil fields, or major urban areas. The major hydrocarbon sources, which are precursors to organic acids and formaldehyde, are well to the south of Visalia. Formaldehyde and total organic acid levels were low there. Bakersfield, being closest to the emission sources has the highest CH_2O concentrations. The inorganic anions, NO_3^- and SO_4^{2-}, which are derived from combustion sources, were also highest at Bakersfield. The formation of the S(IV)–CH_2O adduct, hydroxymethanesulfonate, also contributes to high CH_2O concentrations at Bakersfield (Munger et al., 1984; 1986). Buttonwillow, which is in the middle of the valley may be influenced by oilfield emissions from either side of the valley.

Formic and acetic acid concentrations in the Riverside fogwater samples were extremely high (see Fig.4A). Formic acid exceeded 1000 μM during the 3/1/86 event; acetic acid was around 500 μM. Formaldehyde levels (Fig.5) ranged from 150 to near 400 μM; the variation within an event was as great as between events. High concentrations of organic carbon species in the Riverside fogwater are not surprising considering its location downwind of the Los Angeles urban area, with its heavy concentration of vehicle emissions and active photochemical smog chemistry. The concentration increases at the end of the fog events coincide with morning traffic and wind reversal, which would advect fresh emissions to the site. The large differences in aqueous–phase organic acid concentrations between the three events are due to the fogwater acidity. The range of equilibrium partial pressures of the acids for each event overlap (Fig. 4B). The calculated equilibrium partial pressures were considerably higher in Riverside fogs than in the San Joaquin Valley. Formate always exceeded acetate in the aqueous phase, although the magnitude of the excess increased with concentration. The calculated gas–phase concentrations were not as consistent. The January samples, which were the most acidic, had excess formic acid. The February 28 – March 1 samples had comparable levels of acetic and formic acid.

Figures 6 and 7 indicate that the distributions of formate, acetate, and formaldehyde concentrations at the four Santa Barbara Channel sites have considerable overlap. Because these samples were routinely acidic the calculated equilibrium partial pressures of organic acid follow the same trend as the aqueous–phase concentrations, however, the excess of formic over acetic acid was greater in the gas phase. Casitas Pass, which had the lowest concentrations of inorganic components, also had the lowest organic concentrations. Because of its location at the head of a valley it may be isolated from the major emission sources and is affected more by cleaner, upper level air, entrained in drainage flows from the surrounding mountains. Two features distinguish these samples from the San Joaquin Valley and Riverside samples. Formate consistently exceeds acetate and the formaldehyde concentrations are relatively low.

Figure 8 shows an apparently linear relationship between formate and acetate at the San Pedro Hill site. The line fit through the data has a slope of about 0.5. Calculated gas-phase concentrations follow the same trend, but have more scatter and a smaller slope. The organic acid concentrations at this site were generally less than those observed elsewhere. Formaldehyde levels at San Pedro Hill (Figure 9) were comparable to the stratus cloud samples from the Santa Barbara Channel area.

The size–fractionated samples from San Pedro Hill were collected after several hours of fog. Fog initially formed at 1900 the previous evening and continued throughout the night. The size–fractionated sampling began at 0400 and continued until the fog was too thin to sample. Drizzle, falling intermittently from 0630 to 1000, contributed to the coarse fraction of the cloudwater.

Comparison of the inorganic components suggests that size–dependent differences in the composition of the precursor aerosol are retained in the droplet. The large drops had higher concentrations of soil dust and sea salt components, which would reside in the larger aerosol. The small drops had higher levels of SO_4^{2-}, NH_4^+, and H^+, which would derive from the smaller secondary aerosol. Components that exist partly in the gas phase (NO_3^- and Cl^-) did not appear to be size segregated. Figure 10 shows that there is little difference in the organic acid concentrations of the two cloudwater fractions, which would be expected if the cloud were in equilibrium with the surrounding air. The calculated partial pressures give similar results. Over the cloudwater pH range of 3 to 3.6 most of the organic acid will be in the gas phase. Even during periods of drizzle when some of the large droplets could have originated from near the top of the cloud, equilibrium appears to be maintained. The CH_2O concentrations (Fig. 11) in the initial fractionated samples are equivalent, which is consistent with equililbrium considerations. Beginning at 0530 there was a spike in $[CH_2O]$, $[HCOOH]$, and $[CH_3COOH]$ as well as the major inorganic ions. The organic acids appear to maintain their equilibrium; however, the small–droplet fraction has a much higher $[CH_2O]$ during this spike. The difference decays away over the next 3 hours. The sharpness of this pulse suggests passage of a plume or a major wind shift. The CH_2O data imply that the precursor nuclei for the smaller droplets contain CH_2O that is not in equilibrium with the gas phase. The presence of the S(IV) adduct, hydroxymethanesulfonate (HMSA) (Munger et al., 1984), could account for this. At the observed pH of ≃ 3.5 the kinetics of HMSA dissociation would be quite slow (Boyce and Hoffmann, 1984), thus HMSA in the precursor aerosol would be retained in the droplet where it would be measured as CH_2O. Preliminary measurements of S(IV) and HMSA itself in these samples are consistent with this explanation.

Tables 2–4 summarize the data for these sampling sites. High concentrations of organic acid are observed in fog and clouds where pH is high or near sources where high concentrations exist in the gas phase as well. Riverside, where both conditions are met for some events, has the highest organic acid concentrations. The apparent lower concentrations of organic acid in stratus clouds at San Pedro Hill relative to the Santa Barbara Channel sites is surprising if urban pollution is a major source of carboxylic acids. The elevation of the sampling sites and meteorological conditions are similar for both sets of samples. A more detailed analysis of air mass histories will be required to interpret these data. Proximity to sources alone does not account for the CH_2O concentrations in fog and cloud. Bakersfield, which is adjacent to major combustion sources has high concentrations of CH_2O in fogwater, but clouds at San Pedro Hill, which is affected by Los Angeles air pollution, does not. The shallower mixed layer, weaker insolation, and higher SO_2 concentrations (which would support sulfonate formation) at Bakersfield are factors that would account for higher $[CH_2O]$. Furthermore, the Bakersfield samples were collected at ground level, whereas, the San Pedro sampling site is on a 450 m hill. The hilltop location and night time sampling at San Pedro Hill may account for the apparent low P_{CH_2O} compared to previous measurements of gas–phase CH_2O in Los Angeles (Grosjean, 1982). In general [HCOOH] exceeded $[CH_3COOH]$ in these fog and cloudwater samples, which agrees with the trends noted by Keene and Galloway (1986). The San Joaquin Valley and high pH Riverside fog samples, which are the most strongly affected by feedlot emissions, are notable exceptions.

If this latter observation is not due simply to coincidence, it suggests that CH_3COOH is emitted from animal wastes or that destruction of $HCOO^-$ is accelerated in high pH droplets as suggested by Jacob (1986). It should also be pointed out that ground level fogs may be strongly influenced by local emissions, which may have different $HCOOH/CH_3COOH$ ratios. The components in clouds, on the other hand, are derived from a variety of sources that have had longer times to undergo reaction.

REFERENCES

Betterton, E., Erel, Y., and Hoffmann, M. R. 1988. Aldehyde–bisulfite adducts: Prediction of some of their thermodynamic and kinetic properties. *Environ. Sci. Technol.* **22**, 000–000.

Boyce, S. D. and Hoffmann, M. R. 1984. Kinetics and mechanism of the formation of hydroxymethanesulfonic acid at low pH. *J. Phys. Chem.* **88**, 4740–4746.

Carlier, P., Hannachi, H., and Mouvier, G. 1986. The Chemistry of carbonyl compounds in the atmosphere — A Review. *Atmos. Environ.* **20**, 2079–2099.

Cass, G. R., and Shair, F. H. 1984. Sulfate accumulation in a sea breeze/land breeze circulation system. *J. Geophys. Res.* **89**, 1429–1438.

Chameides, W. L. 1984. The photochemistry of a remote marine stratiform cloud. *J. Geophys. Res.* **89**, 4739–4755.

Daube, B. C., Jr., Flagan, R. C., and Hoffmann, M. R. 1987. *Active Cloudwater Collector* United States Patent # 4,697,462, Oct. 6, 1987.

Dong, S. and Dasgupta, P. K. 1987. Fast flourimetric flow injection analysis of formaldehye in atmospheric water. *Environ. Sci. Technol.* **21**, 581–588.

Finlayson–Pitts, B. J. and Pitts, J. N (jr.) 1986. Atmospheric Chemistry: Fundamentals and Experimental Techniques. John Wiley, New York, 1098.

Galloway, J. N., Likens, G. E., Keene, W. C. and Miller, J. M. 1982. The composition of precipitation in remote areas of the world. *J. Geophys. Res.* **87**, 8771–8786.

Graedel, T. E., Hawkins, D. T., and Claxton, L. D. 1986. *Atmospheric chemical compounds: Sources, occurrence, and bioassay.* Academic Press, New York.

Grosjean, D. 1982. Formaldehyde and other carbonyls in Los Angeles ambient air. *Environ. Sci. Technol.* **16**, 254–262.

Jacob, D. J., Munger, J. W., Waldman, J. M., and Hoffmann, M. R. 1986. The H_2SO_4–HNO_3–NH_3 system at high humidities and in fogs: I. Spatial and temporal patterns in the San Joaquin Valley of California. *J. Geophys. Res.* **91**, 1073–1088.

Jacob, D. J., Wang, R.–F. T. and Flagan, R. C. 1984. Fogwater Collector Design and characterization. *Environ. Sci., Technol.* **18**, 827–833.

Jacob., D. J. 1986. The chemistry of OH in remote clouds and its role in the production of formic acid and peroxymonosulfate. *J. Geophys. Res.* **91**, 9807–9826.

Jacob, D. J. and Wofsy, S. C. (1986) Photochemical production of carboxylic acids in a remote continental atmosphere, Presentation at NATO Advanced Research Workshop: Acid Deposition Processes at Highe Elevation Sites, Edinburgh, U. K. 8–12 September 1986.

Keene, W. C. and Galloway, J. N. 1984. Organic acidity in precipitation of North America. *Atmos. Environ.* **18,** 2491–2497.

Keene, W. C. and Galloway, J. N. 1986. Considerations regarding sources for formic and acetic acids in the troposphere. *J. Geophys. Res.* **91,** 14466–14474.

Keene, W. C., Galloway, J. N., and Holden, J. D. 1983. Measurement of weak organic acidity in precipitation from remote areas of the world. *J. Geophys. Res.* 88, 5122–5130.

Keene, W. C. et al. 1986. An intercomparison of measurement systems for vapor and particulate phase concentrations of formic and acetic acids. *J. Geophys Res.*(submitted).

Likens, G. E., Edgerton, E. S., and Galloway, J. N. 1983. The composition and deposition of organic carbon in precipitation. *Tellus* **35,** 16–24.

Liljestrand, H. M. and Morgan, J. J. 1981. Spatial variations of acid precipitation in Southern California. *Environ. Sci. Technol.* **15,** 333–338.

Munger, J. W., Jacob, D. J., and Hoffmann, M. R. 1984. The occurrence of bisulfite–aldehyde adducts in fog– and cloudwater. *J. Atmos. Chem.* **1,** 335–350.

Munger, J. W., Tiller, C. T., and Hoffmann, M. R. 1986. Determination of hydroxymethanesulfonate in fog water. *Science* **231,** 247–249.

Nash, T. 1953. The colorimetric estimation of formaldehyde by means of the Hantszch reaction. *Biochem. J.* **55**, 416–421.

National Research Council (1981) *Formaldehyde and other aldehydes,* National Academy Press Washington, D. C., 340 pp.

Reitz E. B. 1980. The stabilization of small concentrations of formaldehyde in aqueous solutions. *Analyt. Lett.* **13**, 1073–1084.

Rogozen, M. B., Maldonado, G. , Grosjean, D., Shochet, A., and Rapoport, R. 1984. Formaldehyde: A survey of airborne concentrations and sources. Final Report to California Air Resources Board. Sacramento, CA.

Schwartz, S. E. and Freiberg, J. E. 1981. Mass–transport limitation to the rate of reaction of gases in liquid droplets: Application to oxidation of SO_2 in aqueous solutions. *Atmos. Environ.* **15**, 1129–1144.

Seinfeld, J. H. 1986. *Atmospheric Chemistry and Physics of Air Pollution,* John Wiley. New York, 738 pp..

Shair, F. H., Sasaki, E. J., Carlan, D. E., Cass, G. R., Goodin, W. R., Edinger, J. G., and Schacher, G. E. 1982. Transport and dispersion of airborne pollutants associated with the land breeze–sea breeze system. *Atmos. Environ.* **16**, 2043–2053.

Smith, R. V., and Erhardt, P. W. 1975. Nash determination for formaldehyde in the presence of bisulfite. *Anal. Chem.* **47**, 2462–2454.

ACKNOWLEDGEMENTS

This research was supported by a contract with the California Air Resources Board contract #A4–075–32. We thank the California Air Resources Board, Avenue Cable TV of Ventura, the U. S. Navy, the Federal Aviation Administration and Dr. Robert. Musselman of Univ. Calif. Riverside for the permission to use their facilities as sampling sites. This work would not have been possible without the field and laboratory assistance of Carol. Choy, Gary. Gibb, Walter. Chong, and Aram Kaloustian.

Table 1. Generalized Equilibrium Reactions

Henry's Law Aldehyde	$RCHO_{(g)} \overset{H_R}{\rightleftharpoons} RCHO_{(aq)}$
Henry's Law Organic Acid	$HA_{(g)} \overset{H_A}{\rightleftharpoons} HA_{(aq)}$
Dissociation	$HA_{(aq)} \overset{K_a}{\rightleftharpoons} H^+ + A^-$
Hydration	$RCHO_{(aq)} \overset{K_H}{\rightleftharpoons} RCH(OH)_2$
Sulfonate Formation	$RCHO_{(aq)} \overset{K_S}{\rightleftharpoons} RCH(OH)SO_3^-$

Table 2. Formate Concentrations

Measured Aqueous Phase (µM)

Site	N	Min	Max	Avg
Casitas Pass	25	16	58	27
Ventura	16	31	96	60
Laguna Peak	16	24	103	42
Laguna Road	18	21	74	39
San Pedro Hill	21	12	43	20
Riverside	11	106	1517	627
Bakersfield	6	40	169	77
McKittrick	26	0	56	21
Visalia	11	40	187	71
Buttonwillow	2	133	157	145

Calculated Gas Phase (ppb)

Site	N	Min	Max	Avg
Casitas Pass	25	0.64	5.8	1.5
Ventura	17	0.0	12	6.7
Laguna Peak	16	2.7	12	4.8
Laguna Road	18	2.0	9.7	4.5
San Pedro Hill	21	0.79	4.5	1.8
Riverside	11	1.55	33.	9.3
Bakersfield	6	0.001	0.75	0.16
McKittrick	26	0	1.4	0.41
Visalia	11	0.001	0.11	0.013
Buttonwillow	2	0.2	0.56	0.38

Table 3 Acetate Concentrations

Measured Aqueous Phase (µM)

Site	N	Min	Max	Avg
Casitas Pass	25	4	14	10
Ventura	17	3	173	32
Laguna Peak	16	11	44	18
Laguna Road	17	7	34	15
San Pedro Hill	21	5	30	10
Riverside	11	56	581	245
Bakersfield	6	0	244	83
McKittrick	25	0	28	3
Visalia	11	35	187	86
Buttonwillow	2	47	74	60

Calculated Gas Phase (ppb)

Site	N	Min	Max	Avg
Casitas Pass	25	0.20	0.74	0.44
Ventura	17	0.18	9.2	1.7
Laguna Peak	16	0.59	2.3	0.96
Laguna Road	17	0.38	1.8	0.76
San Pedro Hill	21	0.27	1.6	0.52
Riverside	11	1.6	8.5	4.0
Bakersfield	6	0	0.33	0.11
McKittrick	26	0	0.44	0.05
Visalia	11	0.003	0.37	0.05
Buttonwillow	2	0.21	0.64	0.42

Table 4 Formaldehyde Concentrations

Measured Aqueous Phase (μM)

Site	N	Min	Max	Avg
Casitas Pass	30	3	13	7.8
Ventura	32	7	18	13
Laguna Peak	15	7	32	17
Laguna Road	20	11	15	13
San Pedro Hill	20	5	38	13
Riverside	16	65	384	236
Bakersfield	16	27	498	168
McKittrick	49	6	93	26
Visalia	15	18	65	31
Buttonwillow	6	61	115	88

Calculated Gas Phase (ppb)

Site	N	Min	Max	Avg
Casitas Pass	30	0.31	1.2	0.78
Ventura	32	0.75	1.8	1.28
Laguna Peak	15	0.72	3.2	1.7
Laguna Road	20	1.1	1.5	1.3
San Pedro Hill	20	0.53	3.8	1.3
Riverside	16	12.8	30.	18.
Bakersfield	16	1.6	30.	10.1
McKittrick	49	0.36	5.6	1.6
Visalia	15	1.1	3.9	1.9
Buttonwillow	6	3.7	6.9	5.3

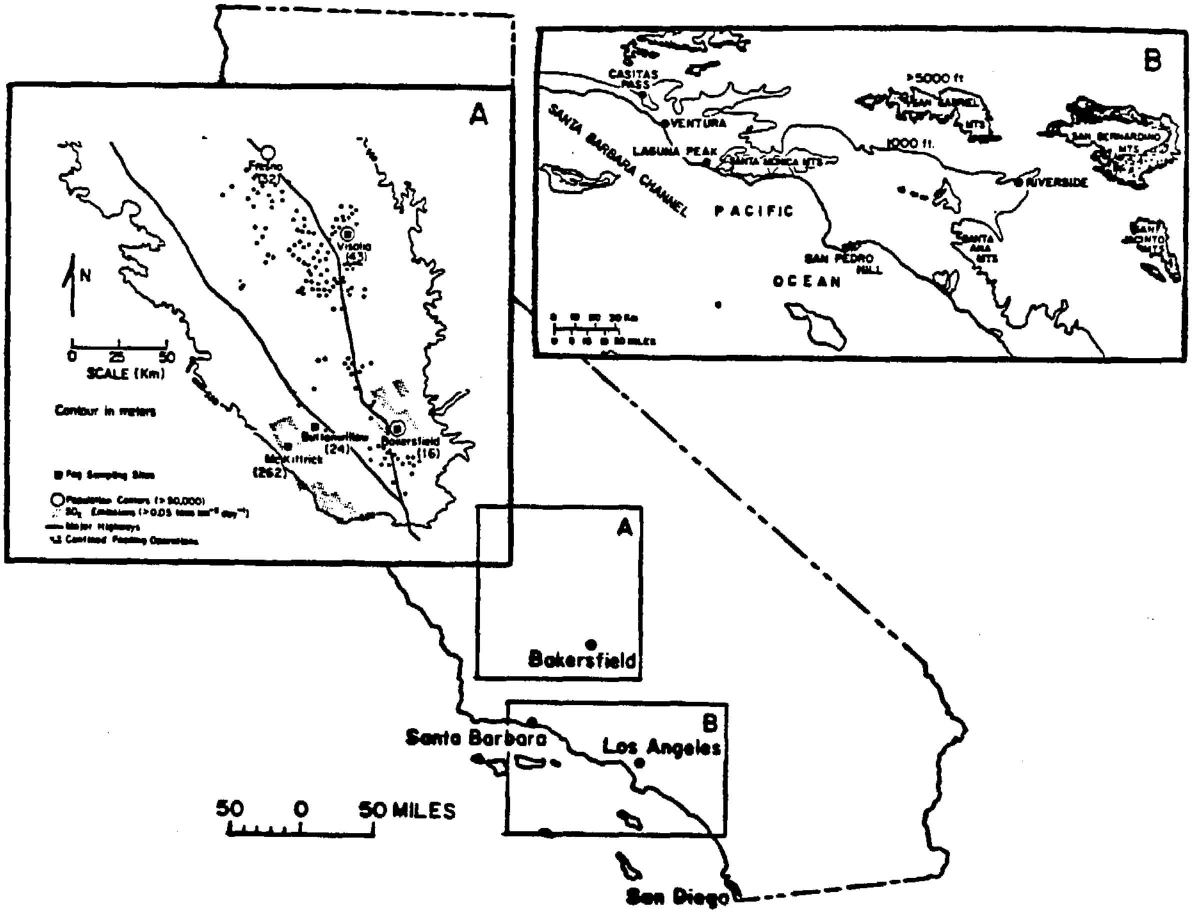

Figure 1. Map of southern California showing the location of fog and cloud sampling sites. Inset A shows the San Joaquin Valley sampling locations in relation to major oil fields, feedlots and population centers. Inset B shows the Los Angeles Basin and Santa Barbara Channel area.

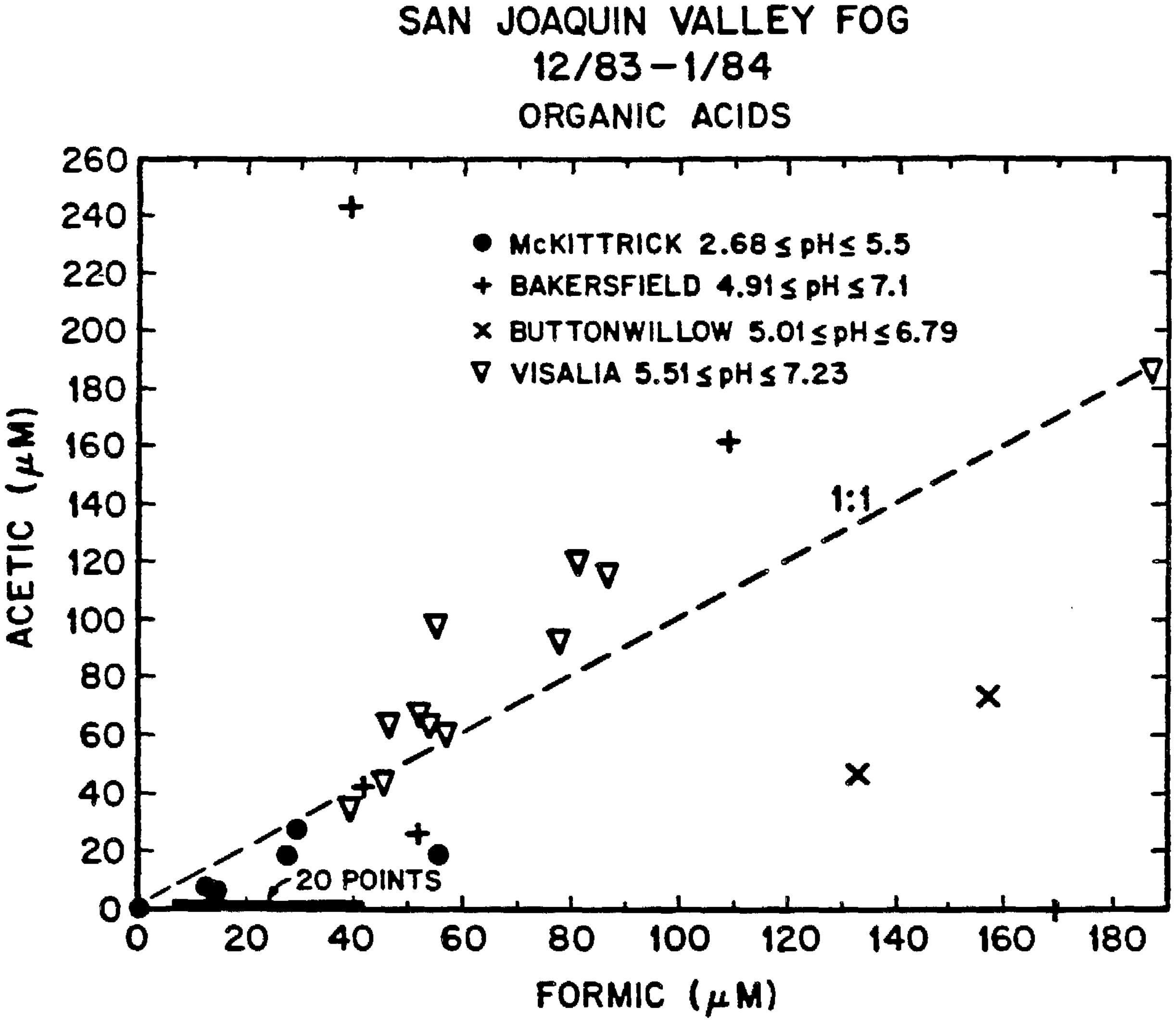

Figure 2. Formic and acetic acid concentrations in San Joaquin Valley fog samples. The range of pH in the samples is noted in the symbol legend. Data from Jacob et al. (1986)

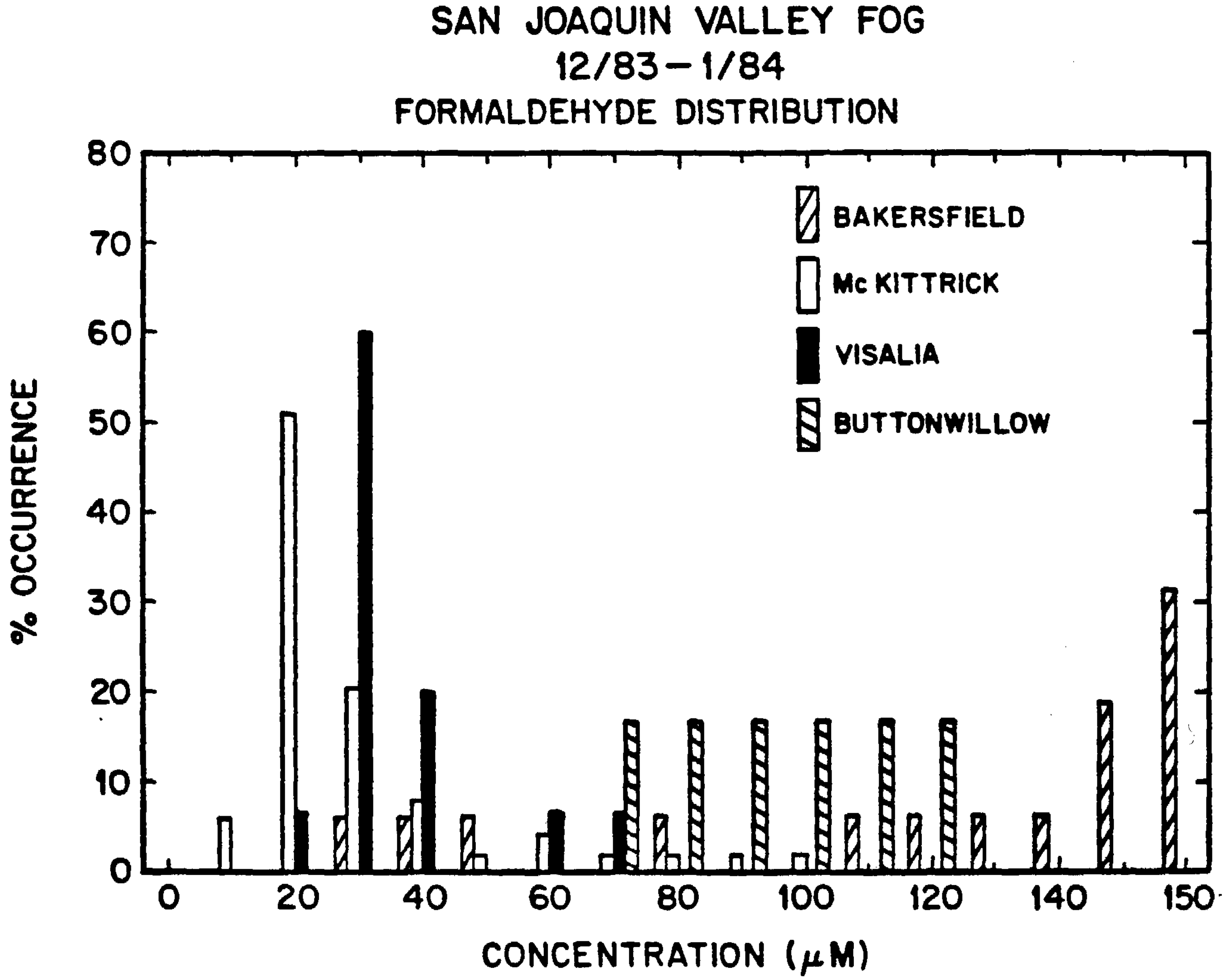

Figure 3. Distribution of CH_2O concentrations in San Joaquin Valley fog samples. Data from Jacob et al. (1986)

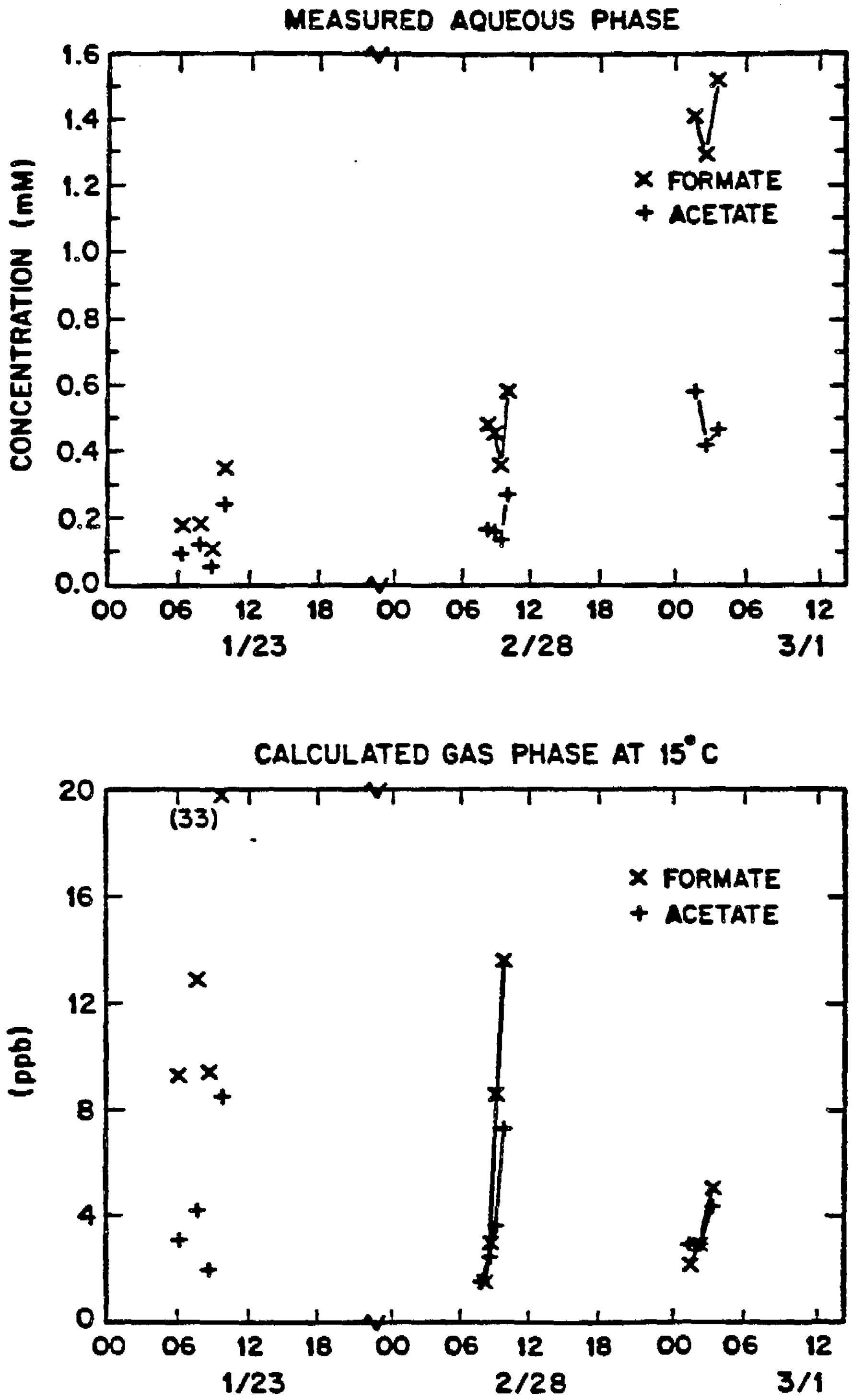

Figure 4. Formic and acetic acid concentrations vs time in Riverside, CA fog samples collected during the winter of 1986. Points not connected by lines were not consecutive samples. Panel A shows the measured concentrations. Panel B shows the calculated equilibrium partial pressure at 15° C

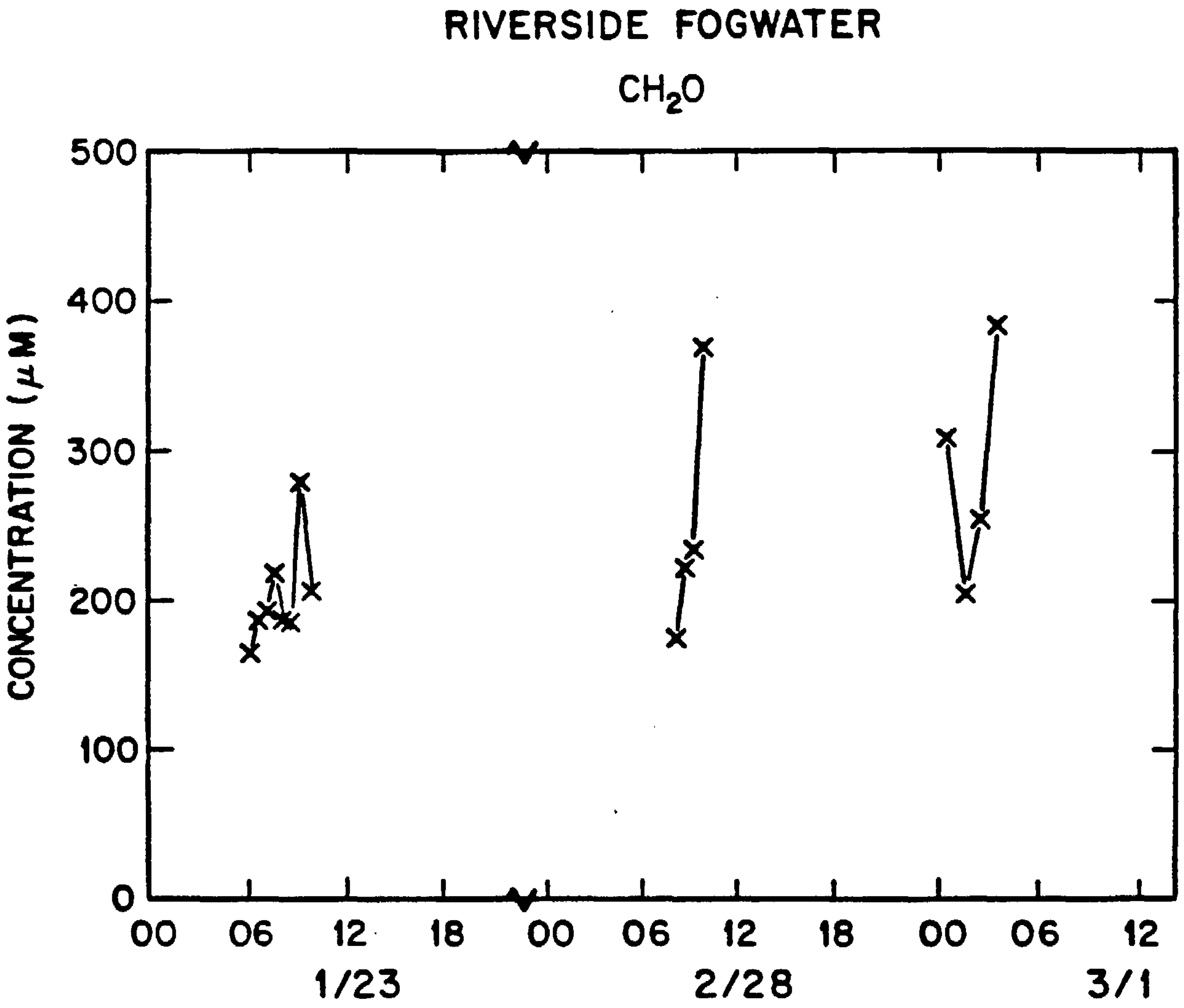

Figure 5. Formaldehyde concentrations vs time in Riverside, CA fogwater samples collected during the winter of 1986. Points not connected by lines were not consecutive samples.

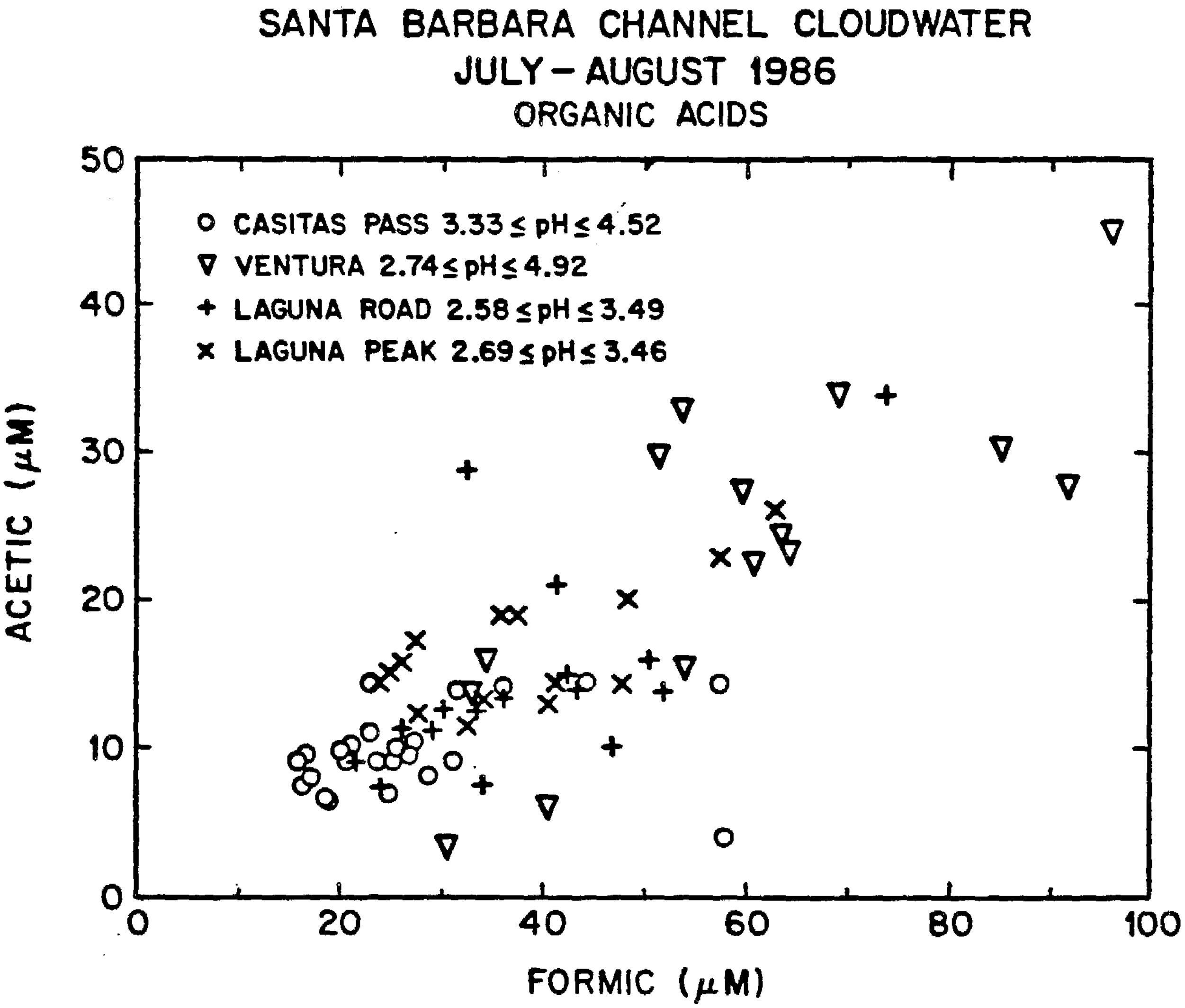

Figure 6. Formic and acetic acid concentrations in intercepted stratus cloud samples from four sites along the Santa Barbara Channel coast. The range of pH in each set of samples is indicated in the symbol legend.

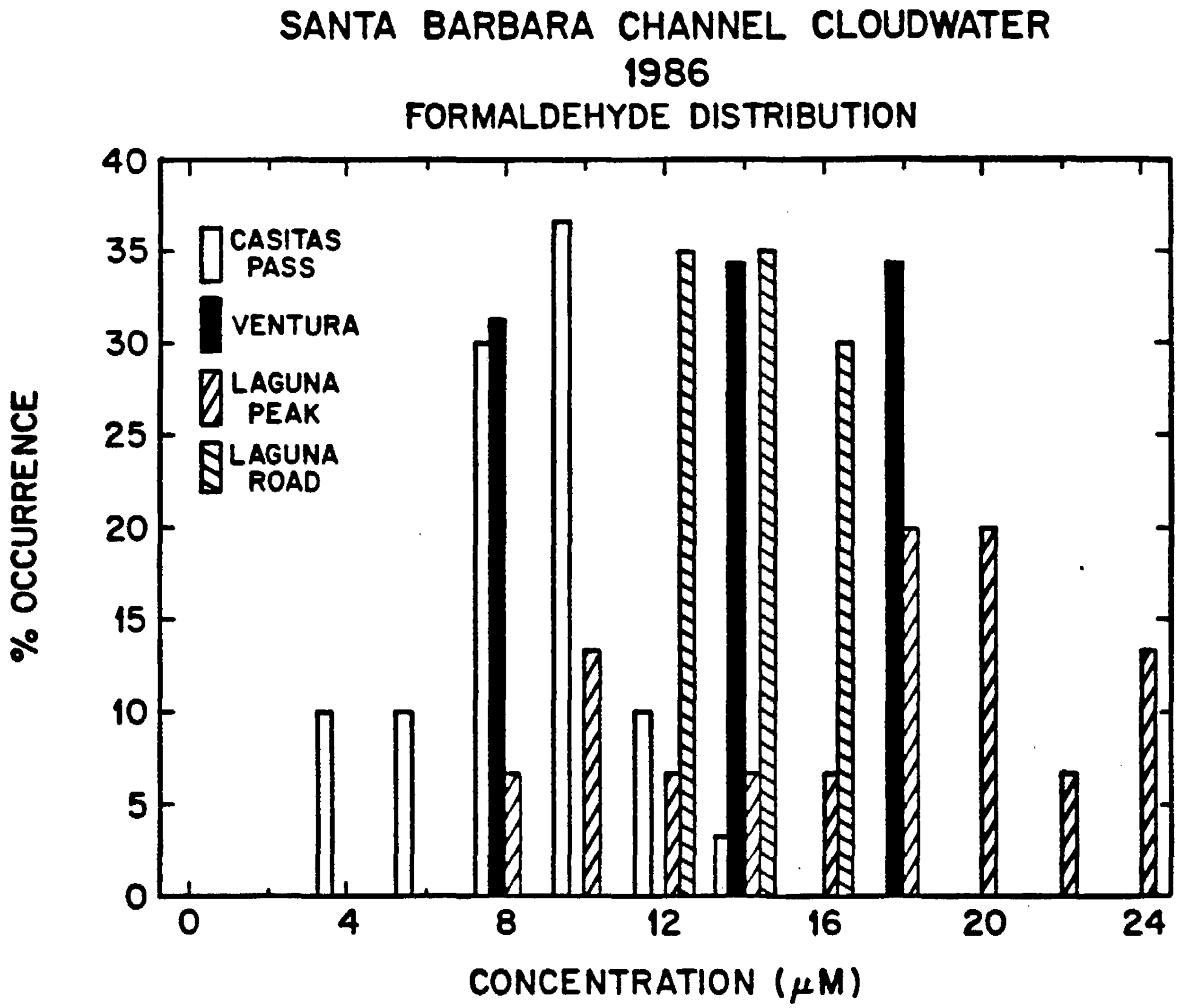

Figure 7. Distribution of CH_2O concentrations in intercepted stratus cloud samples from four sites along the Santa Barbara Channel coast.

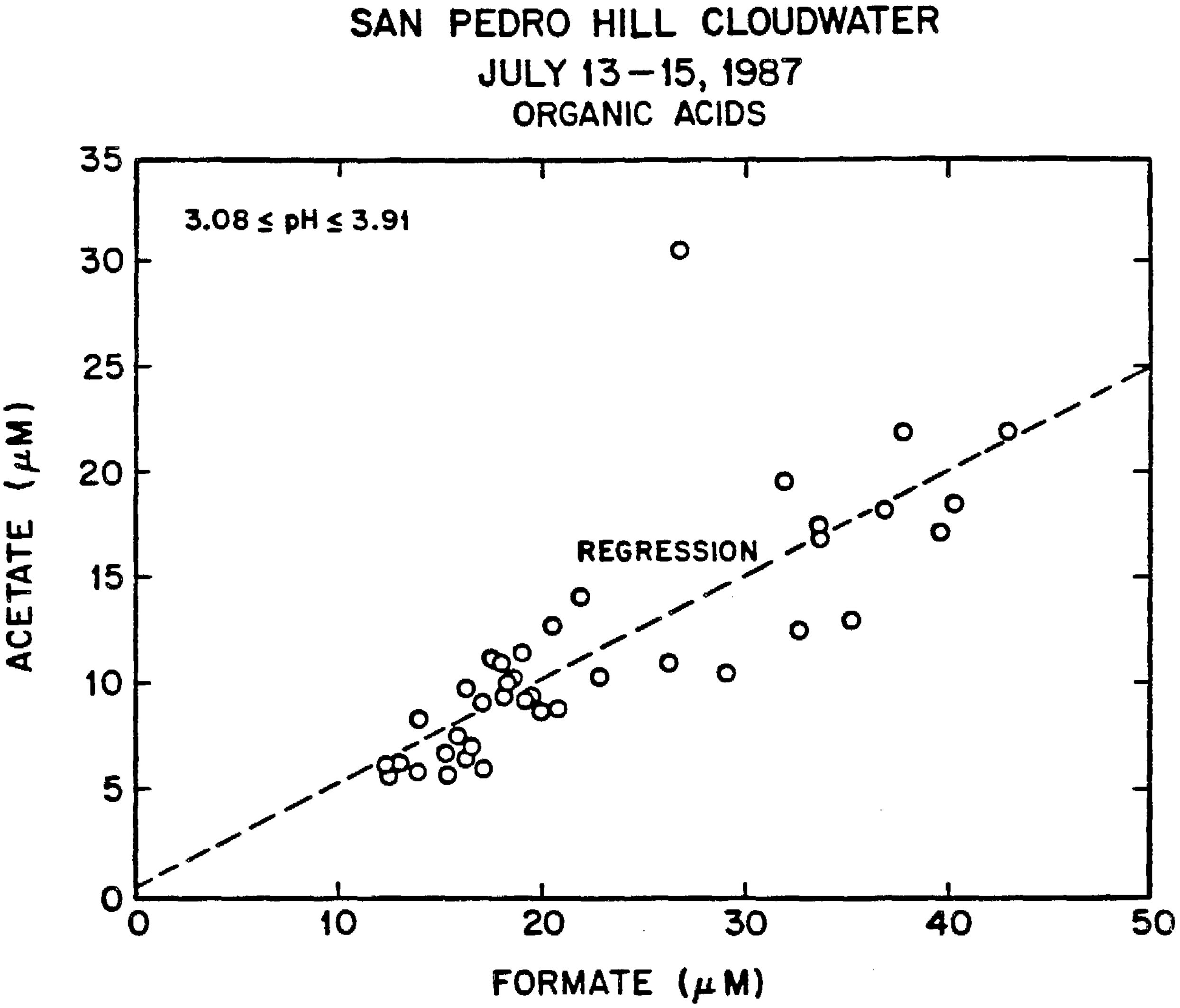

Figure 8. Formic and acetic acid concentrations in samples of intercepted stratus clouds on San Pedro Hill. The range of sample pH is indicated at the upper left of the figure.

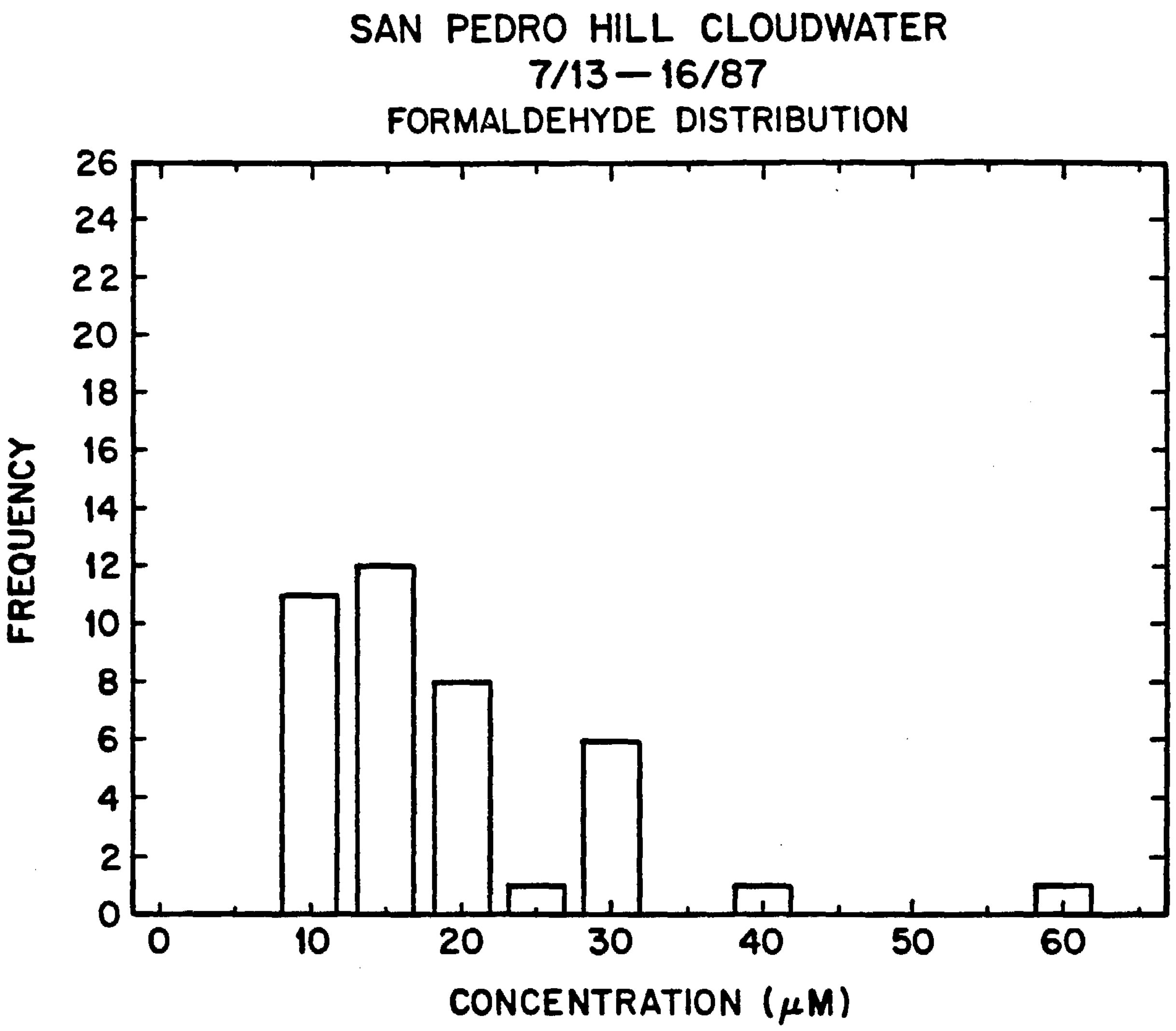

Figure 9. Distribution of CH_2O concentrations in intercepted stratus cloud samples from San Pedro Hill.

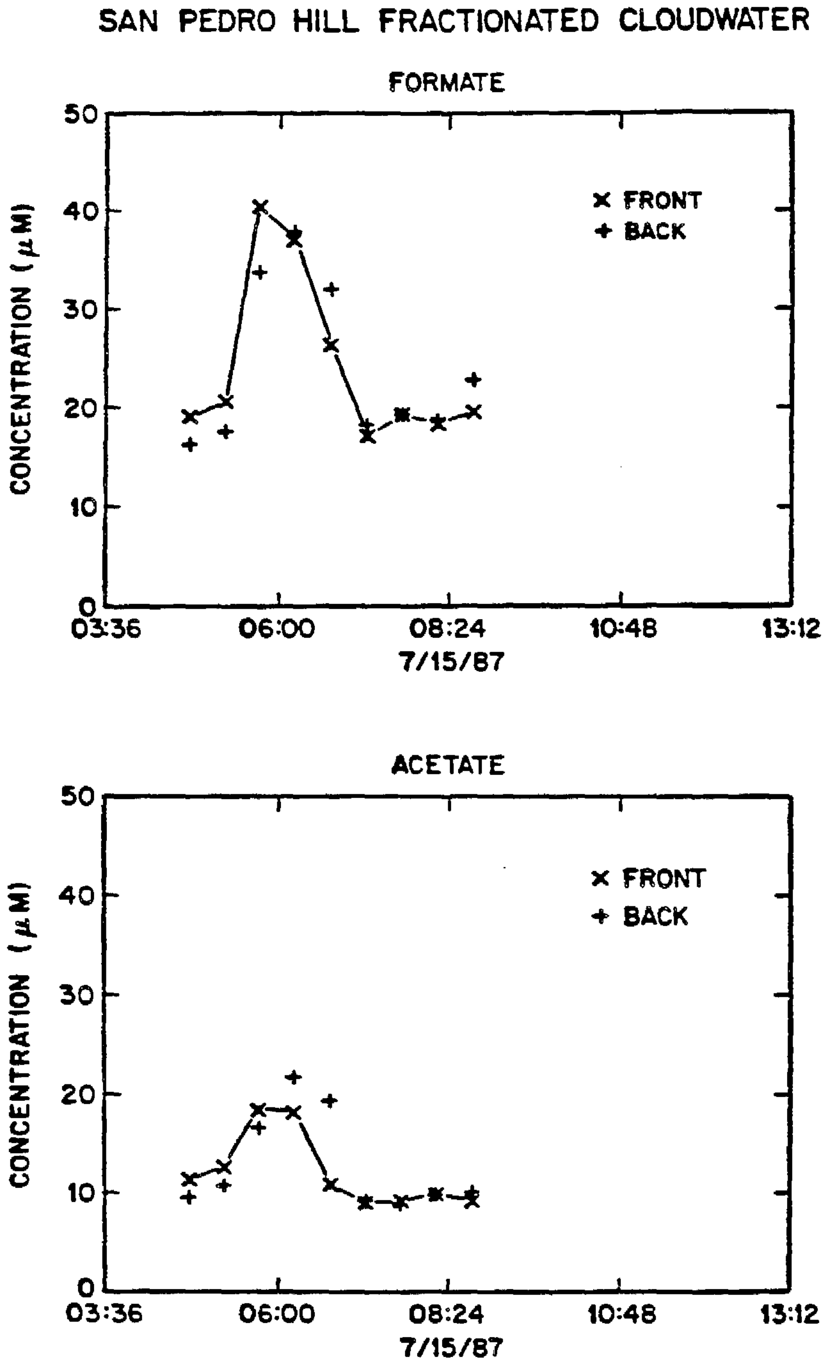

Figure 10. Formate (A) and acetate (B) concentrations in size–fractionated cloudwater samples from San Pedro Hill. Large droplets are collected in the front fraction; small droplets are collected in the back fraction.

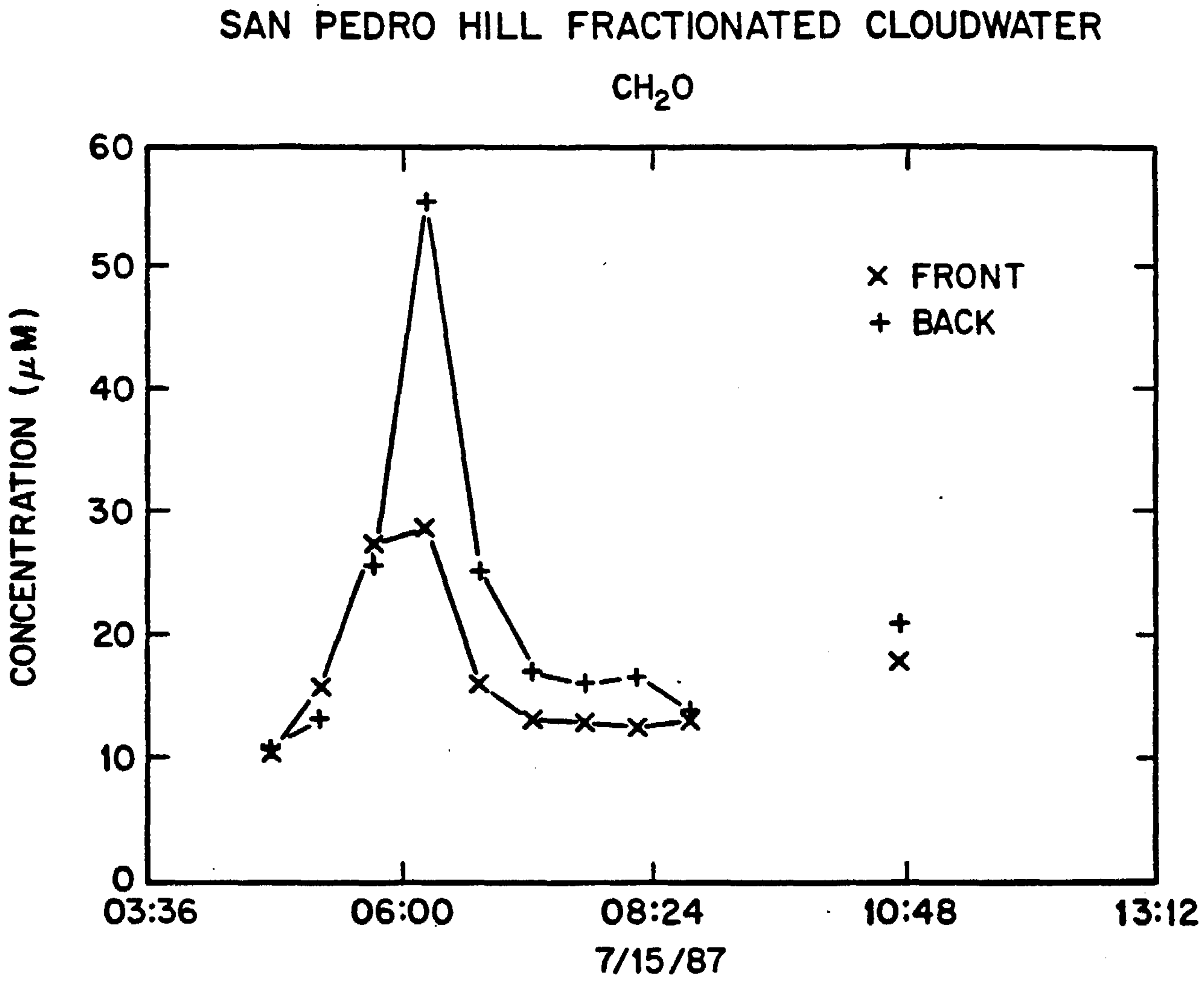

Figure 11. Formaldehyde concentrations in the size–fractionated cloudwater samples from San Pedro Hill. Large droplets are collected in the front fraction; small droplets are collected in the back fraction.

CHAPTER 14

Fogwater Chemistry at Riverside California

by

J. William Munger[‡], Jeff Collett, Jr., Bruce Daube, Jr., and Michael R. Hoffmann*

Environmental Engineering Science
W. M. Keck Laboratories, 138–78
California Institute of Technology
Pasadena, CA 91125

Submitted to: *Atmospheric Environment*

May 11, 1988

Revised: January 10, 1989

[‡]Present Address:
Dept. of Earth and Planet. Sci.
Harvard University
Pierce Hall, 29 Oxford St.
Cambridge, MA 02138

* To whom correspondence should be addressed

ABSTRACT

Fog, aerosol, and gas samples were collected during the winter of 1986 at Riverside, California. The dominant components of the aerosol were NH_4^+, NO_3^-, and SO_4^{2-}. Gaseous NH_3 was frequently present at levels equal to or exceeding the aerosol NH_4^+. Maximum levels were 3800, 3100, 690, and 4540 neq m^{-3} for NH_4^+, NO_3^-, SO_4^{2-}, and $NH_{3(g)}$, respectively. The fogwater collected at Riverside had very high concentrations, particularly of the major aerosol components. Maximum concentrations were 26000, 29000, and 6200 μN for NH_4^+, NO_3^-, and SO_4^{2-}, respectively. pH values in fogwater ranged from 2.3 to 5.7. Formate and acetate concentrations as high as 1500 and 580 μM, respectively, were measured. The maximum CH_2O concentration was 380 μM. Glyoxal and methylglyoxal were found in all the samples; their maximum concentrations were 280 and 120 μM, respectively. Comparison of fogwater and aerosol concentrations indicates that scavenging of pre–cursor aerosol by fog droplets under the conditions at Riverside is less than 100% efficient.

The chemistry at Riverside is controlled by the balance between HNO_3 production from NO_x emitted throughout the Los Angeles basin and NH_3 emitted from dairy cattle feedlots just west of Riverside. The balance is controlled by local mixing. Acid fogs result at Riverside when drainage flows from the surrounding mountains isolate the site from the NH_3 source. Continued formation of $HNO_{3(g)}$ in this air mass eventually depletes the residual $NH_{3(g)}$. A simple box model that includes deposition, fog scavenging, and dilution is used to assess the effect of curtailing the dairy cattle feedlot operations. The calculations suggest that the resulting reduction of NH_3 levels would decrease the total NO_3^- in the atmosphere, but nearly all remaining NO_3^- would exist as HNO_3. Fogwater in the basin would be uniformly acidic.

Keywords: fogwater composition, aerosol composition, atmospheric acidity, ammonia emissions, nitric acid formation

Introduction

Previous studies of fogwater chemical composition show a direct relation to ambient air quality. High aerosol and pollutant gas concentrations lead to highly concentrated fogs. Conversely, highly concentrated fog or clouds contribute to high aerosol loading. We have previously termed this relationship the "smog–fog–smog cycle" [Munger et al., 1983]. In polluted locations such as Los Angeles and the southern San Joaquin Valley, nitrate and sulfate are the dominant anions in fog and cloudwater. Ammonium or hydrogen ion are the major cations. Droplet acidity depends on the balance between NH_3 emissions and NO_x and SO_2 emissions and oxidation [Jacob et al., 1986; Munger et al., 1983]. In addition to these major inorganic ions, fog and cloudwater contain important organic species derived from pollutant and natural sources. Carbonyls such as formaldehyde, glyoxal, and methylglyoxal and organic acids such as formic and acetic acid are produced by photochemical oxidation of hydrocarbons and are emitted directly. These highly soluble organic species have been observed at high concentrations in fog and cloudwater [Munger et al., 1983; Steinberg and Kaplan, 1984; Kawamura et al., 1985; Jacob et al., 1986].

Topography, meteorology, and the distribution of emissions in the South Coast Air Basin (SoCAB) combine to produce extreme pollutant levels in the eastern portion of the basin. Air pollution monitoring stations in and around Riverside and San Bernardino measure some of the highest levels of O_3 and particulate NO_3^- and SO_4^{2-} in the SoCAB [Hoggan et al., 1980]. Dairy operations around Chino (see Fig. 1), which are the major NH_3 source for the entire SoCAB [Russell and Cass, 1986], are responsible for producing extreme concentrations of NH_3 gas and NH_4^+ aerosol in the the eastern basin. Predominant daytime winds advect pollutants from central and coastal Los Angeles and Orange County through the Santa Ana Canyon near Anaheim into the eastern basin. Pollutants also are transported eastward through the San Gabriel Valley. Temperature inversions keep the pollutants trapped near the ground by restricting vertical mixing. Air passing through the basin during the day is recycled at night by drainage flows from the surrounding mountains.

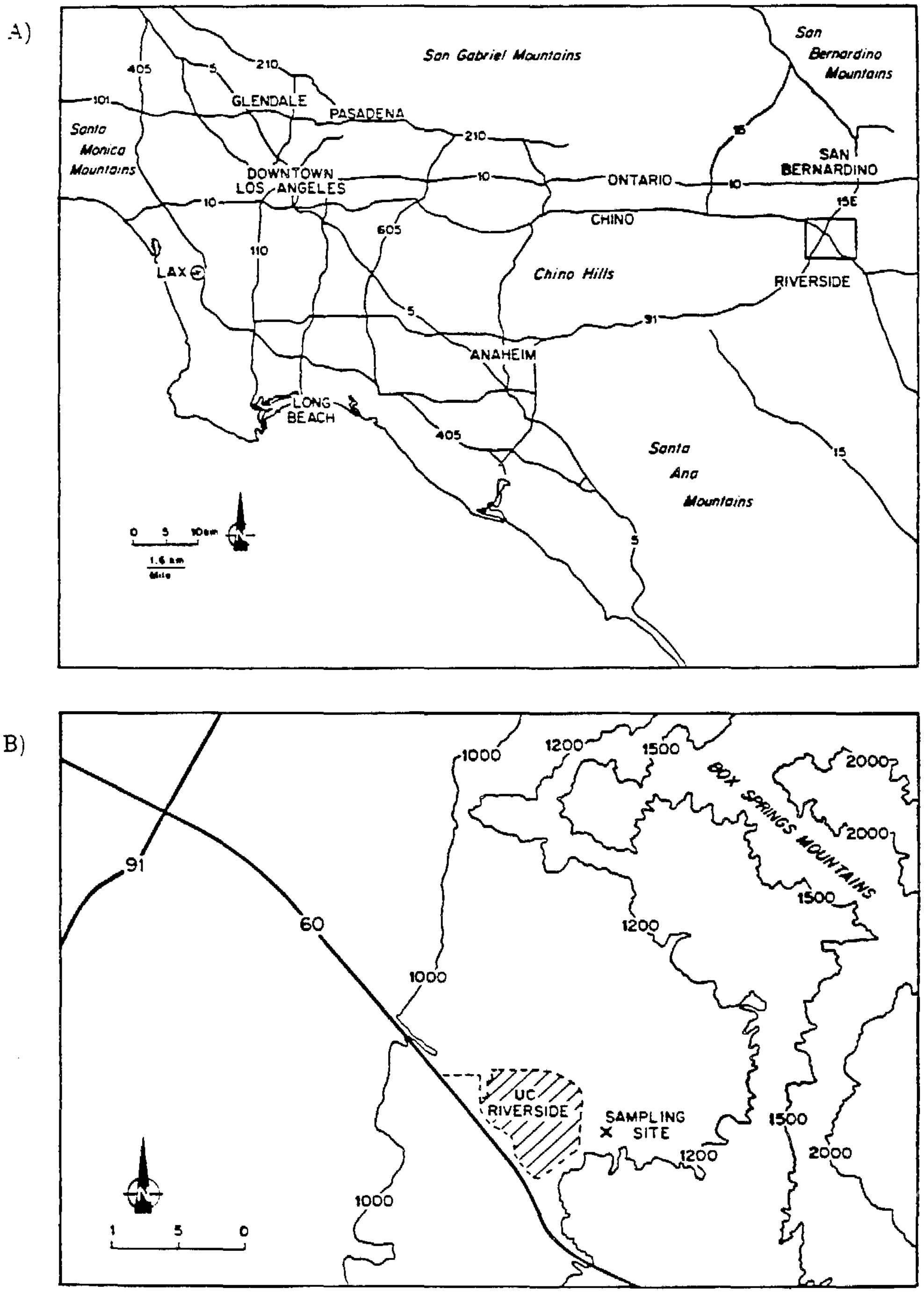

Figure 1. A. Map of the South Coast Air Basin indicating the location of major freeways and the surrounding mountains. B. Map of the Riverside sampling site and its immediate surroundings. The area of this map is outlined by the small box in panel A.

Fog and low clouds are frequently observed in the eastern SoCAB. Marsh [1984] reports 60 days of fog per year in the Riverside area. The frequency of low ceilings or restricted visibility at March Air Force Base near Riverside exceeds 25% during the periods of February through June and September through October [March Air Force Base Climate summary]. Because Riverside frequently experiences both high pollutant levels and fog, it is an ideal location to identify smog/fog interactions. Previous results indicate a potentially wide range of pH in fog and cloud from the eastern basin [Munger et al., 1983]. A sample collected in Upland had a pH near 2.0, whereas a sample from Ontario, downwind of the dairy cattle feedlots in Chino, had a pH near 7. More extensive sampling is required to determine the balance between acid and base inputs and to characterize interactions between fogwater and atmospheric composition. Baseline data on the chemistry of fog and clouds in the region are required to assess the impacts of future development and to identify potential health effects. Aerosol, gases, and fogwater were collected during the winter of 1985–86 to meet these objectives.

Methods

Sampling Site

Samples were collected from the roof of a one story building on the eastern edge of the campus of the University of California at Riverside (elevation 350 m) (see Figure 1 for map of the area). The site was bordered by undeveloped land covered with grass and shrubs. The Box Spring Mountains rise to nearly 1000 m to the north and east of the collection site. A major freeway passes within 600 m of the sampling site; access roads to parking lots on the campus are about 100 m away.

Fogwater was collected using the Caltech Active Strand Collector (CASC) illustrated in Figure 2 [Daube et al., 1987]. Droplets are collected by inertial impaction on an angled bank of six rows of 508 μm teflon strands. The collected droplets coalesce, and are drawn down the strands by gravity and aerodynamic drag into a Teflon trough. A Teflon tube delivers the sample from the trough to a collection bottle, which was emptied at 30 to 60 minute intervals. The 50% collection efficiency lower size–cut, predicted from impaction theory [Friedlander, 1977], corresponds to a droplet diameter of 3.5 μm. The flow rate of air through the CASC is 24.5 $m^3 min^{-1}$, yielding a collection rate of approximately 1 $ml\ min^{-1}$ when the liquid water content of the fog is 0.1 $g\ m^{-3}$. Prior to sample collection, the strands and sample tube were rinsed thoroughly with distilled deionized water. The first 15 minutes of sample were discarded to avoid any bias due to residual rinse water.

Aerosol and selected gases were sampled using the automated filter pack sampler illustrated in Figure 3. Teflon filters (Gelman Zefluor, 1 μm pore size) were used to collect aerosol for inorganic analysis. HNO_3 was collected on a nylon filter (Gelman Nylasorb) placed behind a teflon filter. NH_3 was collected on two oxalic acid–impregnated glass fiber filters behind a second teflon filter. The third filter holder contained a base–impregnated quartz filter preceded by a teflon filter. Because base–impregnated filters have been shown to collect artifact organic acids [Keene et al., 1988], the results for these filters are not included here. A flow rate of 10 to 11 $l\ s^{-1}$ was maintained with a critical orifice. Flow rates were checked with a calibrated rotameter. Denuder difference methods were not used in this study because liquid water collected during fog events would destroy the coating of the denuder. The interferences associated with filter pack methods [Hering, 1987] are minimized by the short collection times used in this study and the relative constancy of temperature and humidity during the sampling periods. Aerosol samples collected during fog contain both aerosol and fog droplets. In order to minimize loss of volatile components, wet filters were extracted immediately after collection. Sedimenting fog and rain droplets were excluded by a cover over the filter packs. Collection of large fog droplets may be negatively biased due to the close proximity of the cover to the tops of the filter packs.

In order to collect samples of interstitial aerosol (the aerosol not scavenged by the fog drops), one of the filter cassettes was connected via a short 0.6 cm diameter tube to a port on

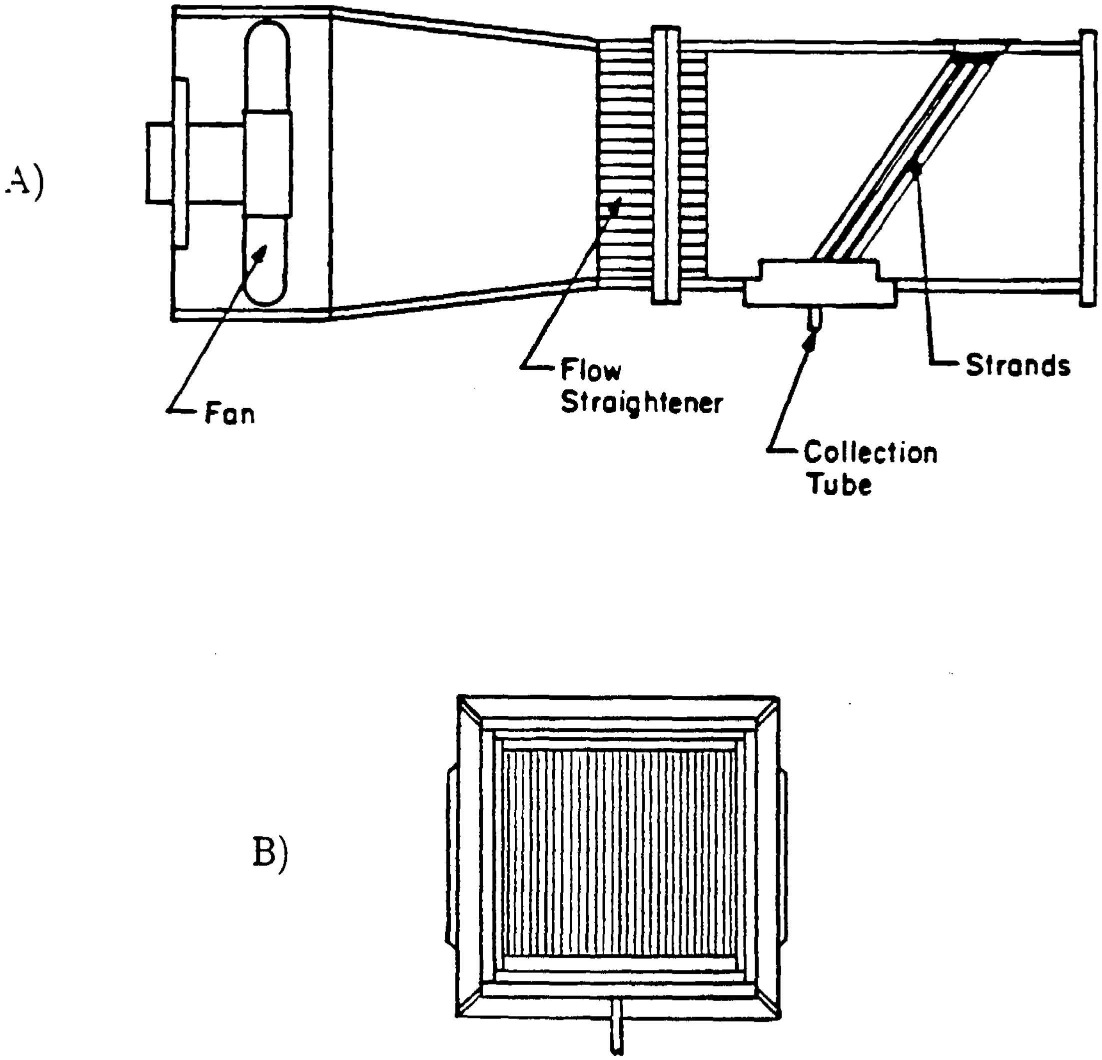

Figure 2 Diagram of the Caltech Active Strand Cloudwater Collector used in the Riverside sampling program. A. Side view. B. Front view.

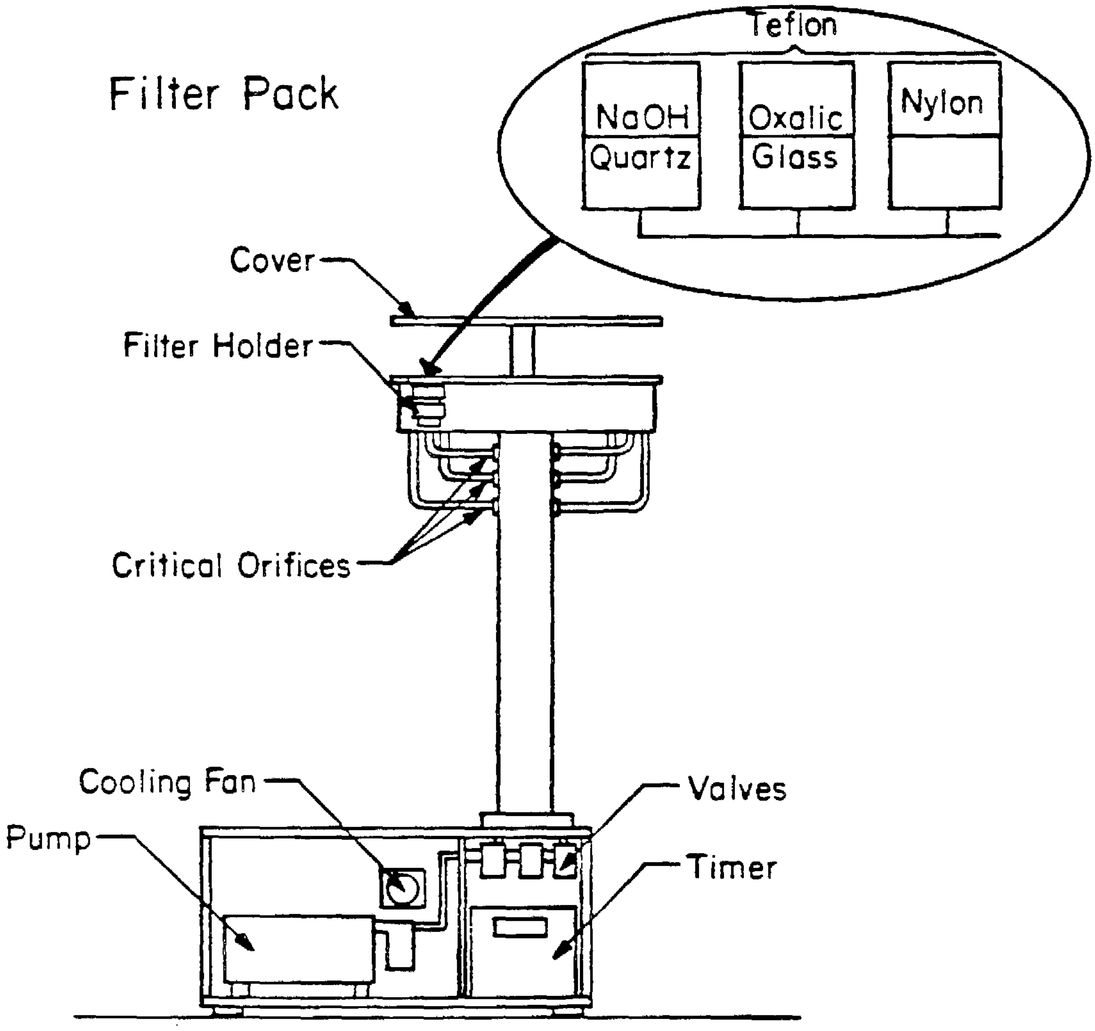

Figure 3. Diagram of the aerosol filter pack used in the Riverside sampling program.

the side of the CASC, downstream of the collection strands, during some foggy periods. Nearly all fog droplets with diameter greater than 16 μm are excluded from this filter; however, a fraction of the fog droplets with diameter less than 16 μm will enter the sampling tube and penetrate to the filter. This fraction should remain quite small since wall losses of these droplets to the sampling tube are large. The contribution due to small fog droplets would be greatest when the mass median diameter of the fog droplets was small, which might occur as the fog dissipates. The total collection efficiency of the strands upstream of the inlet (calculated from impaction theory) is 50% for 3.5 μm diameter droplets and rises sharply to greater than 80% for droplet diameters greater than 10 μm. The total fraction of the initial droplet distribution that is collected is limited to a maximum of 86% – the fraction of incoming air swept by the strands. The combined action of the strands and the aerosol inlet to remove droplets with diameter greater than 2 μm minimizes the influence of droplets on the interstitial aerosol sample.

Analytical Procedures

At the end of each sampling interval the collected fogwater was transferred to a sample bottle and weighed. The pH of an aliquot from the sample was determined at the field site using a Radiometer pHM 80 meter with a combination electrode calibrated against pH 4 and pH 7 buffers. Small aliquots of sample were removed and treated to stabilize reactive species. S(IV) was stabilized as the hydroxymethanesulfonate by adding buffered CH_2O [Dasgupta et al., 1980]. CH_2O was reacted with NH_4^+–acetylacetone [Nash, 1953] to form 3,5–dihydro–1,4-dihydrolutidine (DDL), which is stable for several weeks [Reitz, 1980]. A buffered solution of p–OH phenylacetic acid (POPA) and peroxidase was used to preserve peroxides (H_2O_2 and ROOH) [Lazrus et al., 1985] by formation of the dimer. Carboxylic acids were preserved by addition of chloroform [Keene et al. 1984]. Carbonyls were derivatized with 2,4–dinitrophenylhydrazine in acidic solution [Grosjean and Wright, 1983].

The samples and preserved aliquots were stored in a refrigerator at 4 °C until analysis. Major anions were determined by ion chromatography with a Dionex AS4A separator column and a micromembrane suppressor. The eluent was 2.8 mM HCO_3^-/ 2.2 mM CO_3^{2-}. The metallic cations were determined by atomic absorption spectrophotometry. An air/acetylene flame was used for Na^+ and K^+, while N_2O/acetylene was used for Ca^{2+} and Mg^{2+} to minimize interferences. NH_4^+ was determined by flow injection analysis employing the indophenol blue method.

The stabilized CH_2O concentration was determined by absorption measurement at 412 nm after addition of I_2 to accelerate the decomposition of sulfonates [Smith and Erhardt, 1975]. The results for standards prepared from hydroxymethanesulfonate (HMSA), the S(IV) adduct of CH_2O, were comparable to CH_2O standards. The results from the Nash determination, therefore, are total CH_2O concentrations. S(IV) was analyzed by the pararosaniline method [Dasgupta, 1981], adapted for flow injection analysis. This method also is intended to give a total concentration; Na_2SO_3 and $NaCH_2OHSO_3$ gave equivalent responses. Peroxide was determined from the fluorescence of the POPA enzyme solution [Lazrus et al., 1985]. The method is sensitive both to H_2O_2 and to some organic peroxides; however, the significantly lower Henry's law coefficients of CH_3OOH and peroxoacetic acid suggest that they will not be important in fog and cloud water [Lazrus et al., 1985]. Carboxylic acids were determined by ion exclusion chromatography (Dionex ICE–AS1) with dilute HCl as the eluent.

The dinitrophenylhydrazone derivatives of carbonyls were extracted 3 times in 60/40 hexane/dichloromethane after adding cyclohexanone 2,4–dinitrophenylhydrazone (Aldrich) as an internal standard. The organic fraction was washed with H_2O to remove excess acid and unreacted DNFH, and then evaporated to dryness under a stream of N_2. The extracted and dried hydrazones were stored in a refrigerator until analysis. Immediately before analysis the residue was dissolved in tetrahydrofuran (THF). The derivatized carbonyls were separated by HPLC on a C18 column (Alltech Spherisorb ODS–2), using 45/27.5/27.5

(v/v/v) $H_2O/CH_3CN/THF$ as the mobile phase. Aldehydes and ketones were determined by absorbance at 365nm; each analysis was repeated at 430 nm to determine the dicarbonyls, which absorb at a higher wavelength. Stored and fresh standards gave comparable peak areas at the time of analysis, indicating that the derivatives were stable during storage. The spectra taken at the peaks of selected samples (see Figure 4) were compared to sample spectra to aid in identification of the compounds present. Standards were prepared from carbonyl hydrazones that were previously synthesized and purified. The DNPH determination of carbonyls is not sensitive to carbonyls bound by S(IV). Therefore, only free carbonyls are measured by this method.

The α–OH alkanesulfonates were determined in selected samples by an ion–pairing chromatographic method developed by Munger et al. [1986]. Separation is accomplished on a Dionex MPIC column using tetrabutylammonium chloride/HCl in dilute aqueous CH_3OH or CH_3CN as the mobile phase. Because background interferences were more pronounced in the Riverside fogwater samples than had been observed in previously sampled fogs and clouds, some samples were not analyzed for sulfonates.

The teflon and oxalic acid–impregnated filters were extracted in distilled deionized water (DDH_2O) on a shaker table. A small volume of ethanol was added to the filter prior to extraction to wet the filter surface more effectively. The nylon filters were extracted in HCO_3^-/CO_3^{2-} IC eluent. The composition of the extracts was determined by the same procedures used for the fogwater samples, with the exception of additional buffer in the complexing reagent and oxalic acid in the rinse solution of the ammonia analysis to account for the effect of the oxalic acid in the filter extracts. The precision, accuracy, and detection limits for the major analyses are given in Table 1.

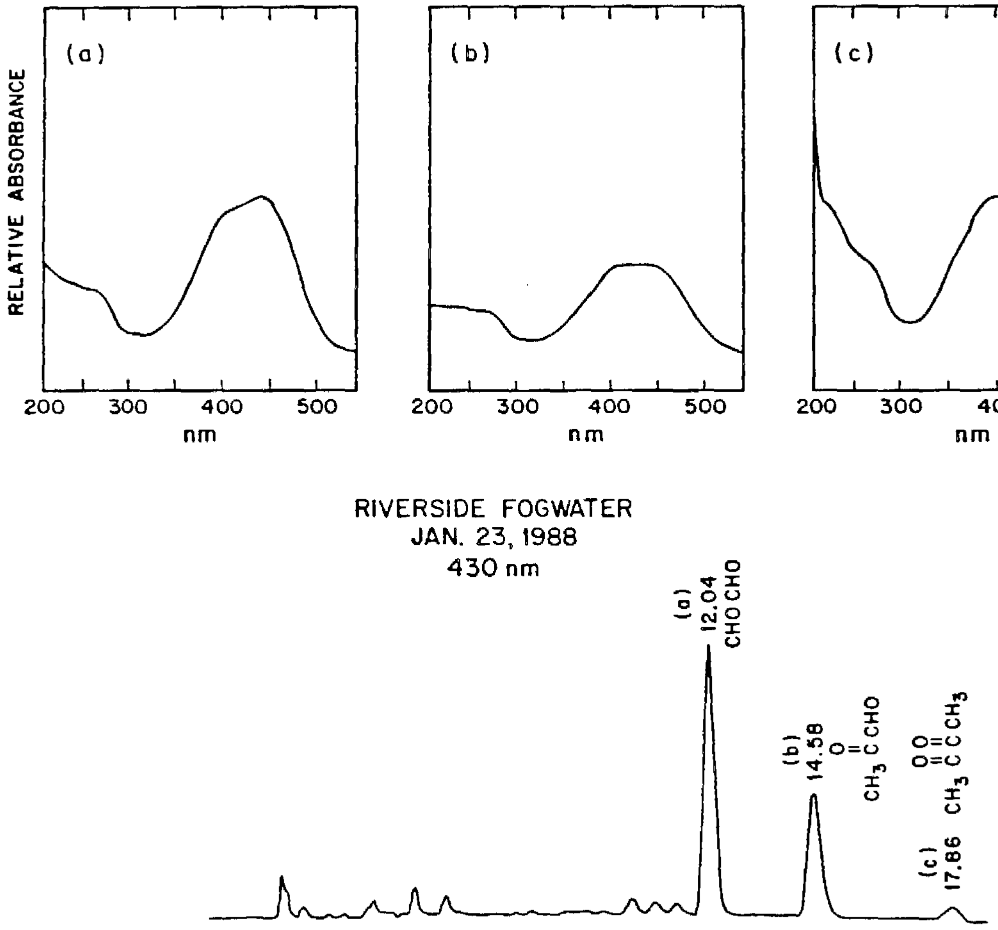

Figure 4. Chromatogram and peak spectra for derivatized samples of Riverside fogwater. Note the distinct spectra of glyoxal, methylglyoxal and 2,3 butanedione (biacetyl). Comparison of sample spectra with standards is an aid to identification of unknown peaks.

Table 1. **Precision, Accuracy, and Minimum Detection Limit.**

Aqueous Phase

Species	Nominal conc. μN	Acc.[1] μN	Prec.[2] μN	RSD[3] %	MDL[4] μN
NH_4^+	20	0.28	0.58	2.92	1.75
Na^+	10.9	0.13	0.45	4.15	1.36
Ca^{2+}	12.5	–0.42	0.87	6.97	2.61
Mg^{2+}	10.2	0.30	0.48	4.66	1.43
Cl^-	20	0.26	2.04	10.2	6.12
NO_3^-	20	0.11	0.92	4.60	2.76
SO_4^{2-}	20	0.20	0.86	4.29	2.57
Cl^-	2	0.87	2.22	111	6.66
NO_3^-	2	0.31	0.35	17.7	1.06
SO_4^{2-}	2	0.26	0.38	19.13	1.15

Gas Phase (4 hour run)

Species	Nominal conc. neq/m3	Acc. neq/m3	Prec. neq/m3	RSD %	MDL neq/m3
NH_4^+	69.4	0.96	2.90	4.18	8.70
Na^+	37.8	0.44	1.95	5.16	5.86
Ca^{2+}	43.4	–1.46	3.28	7.56	9.84
Mg^{2+}	35.6	1.04	1.99	5.61	5.98
Cl^-	69.4	0.90	7.40	10.6	22.2
NO_3^-	69.4	0.38	3.83	5.52	11.5
SO_4^{2-}	69.4	0.69	3.66	5.27	11.0
NH_3	69.4	0.96	2.90	4.18	8.70
HNO_3	69.4	0.38	3.83	5.52	3.69
Cl^-	6.9	3.02	7.71	111	23.1
NO_3^-	6.9	1.09	1.23	17.7	3.69
SO_4^{2-}	6.9	0.91	1.33	19.1	3.98

---

[1] Acc. = Accuracy, the deviation of the mean of replicate analyses from the nominal concentration

[2] Prec. = Precision, the standard deviation of replicate analyses of a standard

[3] RSD = Relative Standard Deviation, the standard deviation of replicate analyses of a standard divided by their mean

[4] MDL = Minimum detection limit.

Results

Meteorology and Sampling Conditions

Sampling was initiated when fog was forecast for the Riverside area. During the winter of 1985–86, aerosol, gases, and fog were collected during four periods at the Riverside site. The first two sampling periods, 26 November and 16 January, were not foggy, although visibility was reduced by dense haze. Sampling on 26 November was preceded by light rain the previous day. Fog was present during the subsequent sampling periods, which are described below.

Aerosol sampling began at 2230 on 22 January, with visibility limited to about 2 miles by thick haze. Fog formed at the site prior to 0545 on 23 January. Fogwater sampling commenced at 0555 and continued until the fog dissipated at 1000. A single aerosol sample was collected during the foggy period. Two more aerosol samples were collected in the thick haze that remained after the fog dissipated. Aerosol collection continued the following night. Visibility the second night was reduced to about 1 mile by haze. Fog formed over much of the inland basin that night, but did not penetrate as far inland or rise as high as the sampling site.

Two aerosol samples were collected during hazy conditions in the early morning of 28 February. Fog formed between 0600 and 0730, and four fogwater samples were collected between 0744 and 1000. Two aerosol samples were taken during the fog; one post–fog aerosol sample was collected during the following afternoon. Fog formed before midnight the following night. Four samples of fogwater were collected between 0000 and 0400. Light drizzle was observed during this event. After 0400, the fog layer rose above the sampling site, but it remained overcast well into the following morning. Two aerosol samples were obtained during the fog; one aerosol sample was collected immediately after the fog lifted. Interstitial aerosol samples were collected during the fog events on both days.

Aerosol samples were collected at Pasadena to determine the composition of aerosol away from point NH_3 sources. Samples were collected at Pasadena when fog was expected at other sampling sites in the basin. During the day, Pasadena is generally upwind of the Riverside–San Bernardino area. Drainage flows from the nearby mountain slopes and eastern San Gabriel Valley affect the site at night. Conditions were generally hazy during sampling at Pasadena.

The concentrations of major air pollutants are measured at a network of stations throughout the SoCAB by the South Coast Air Quality Management District. Data for two sites near the Riverside sampling site are shown in Figure 5 for the periods during which fog samples were obtained. Because the CO, O_3, and NO_2 concentrations are quite similar at the two sites, it is probable that these measurements are also representative of the air mass at the Riverside sampling site. Active photochemistry is indicated by the high daytime O_3 concentrations. The marked differences in the NO concentrations at Rubidoux and Fontana may be due to their proximity to automobile traffic. The decreasing concentrations of all species on 1 March are due to dilution by strengthened onshore flow and a deeper mixed layer, which was indicated by the rising cloud layer.

Aerosol and Gas Concentrations

The aerosol measured at Riverside (Table 2) was dominated by NH_4^+, which constituted 78 to 99% of the total cation loading. Calcium and sodium were at least an order of magnitude less concentrated. Nitrate was the major anion; it exceeded SO_4^{2-} by a factor ranging from 1.5 to 6. The range of nitrate concentrations was greater than that for sulfate. In the most dilute aerosol samples, those with less than 1000 neq m^{-3} NH_4^+, there was a close balance between the acidic anions and basic cations. The remaining samples generally had excess NH_4^+ ($NH_4^+ > NO_3^- + SO_4^{2-}$). The two Riverside samples with an excess of acid were both collected during the night, and both nights had fog present, either at the site or covering

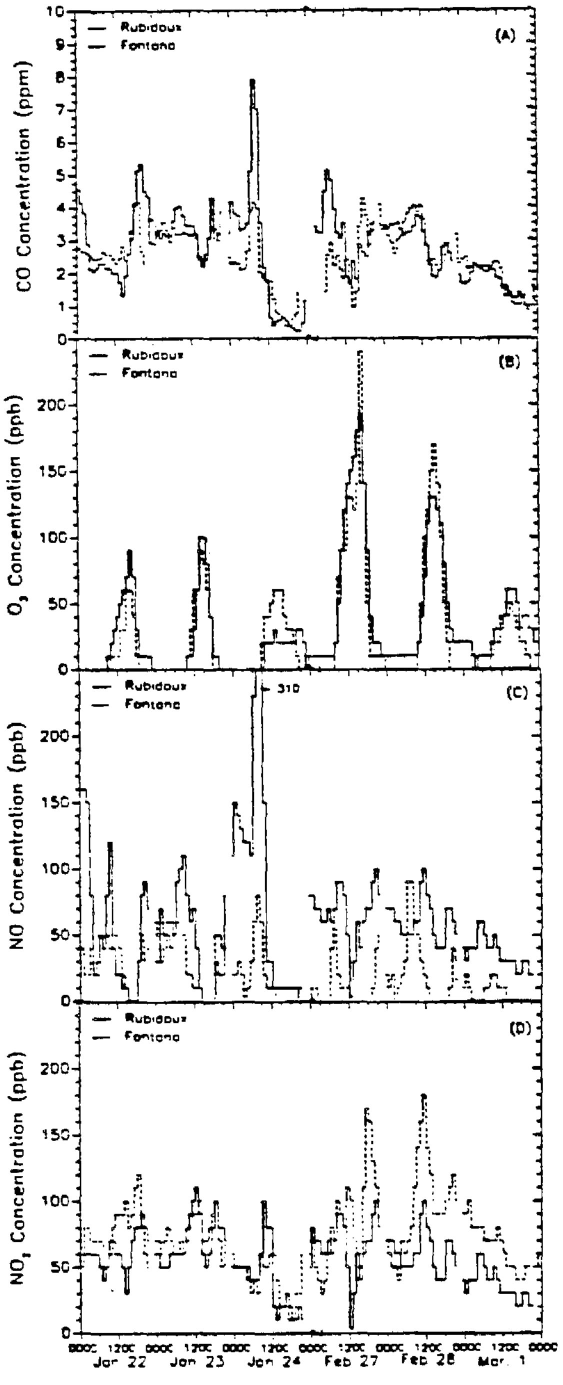

Figure 5. Concentration profiles of CO, O_3, NO, and NO_2 at South Coast Air Quality Management District monitoring stations near the Riverside sampling site. Rubidoux is ≈ 10 km W and Fontana is ≈ 20 km NW of the Riverside sampling site.

Table 2 Major aerosol and gas concentrations at Riverside, California

Date	Seq	Start Time	Stop Time	Na^+	NH_4^+	Ca^{2+}	Mg^{2+}	Cl^-	NO_3^-	SO_4^{2-}	NH_3	HNO_3
				neq m^{-3}								
11/26	A	22:20	02:05	36.3	791	53.8	12.2	40.8	464	319	NA	28.0
11/27	B	02:18	05:38	25.3	841	63.0	7.6	50.3	521	256	NA	17.1
01/16	A	21:30	00:00	82.6	705	81.4	29.4	73.7	519	192	507	21.0
01/17	A	00:00	04:00	39.7	1112	64.5	17.0	20.1	779	178	433	16.0
01/22	A	22:30	01:59	64.3	2564	79.4	27.5	52.6	1860	5657	1144	18.8
01/23	A	06:03	09:35	11.1	2354	20.7	4.5	42.4	1969	326	32	20.8
01/23	B	11:05	14:00	143	3779	138	42.4	202	3104	612	NA	NA
01/23	C	14:10	17:15	18.0	3648	113	23.3	67.6	2593	517	1498	76.9
01/23	D	23:00	03:00	26.8	3349	50.0	11.8	15.3	3072	550	91	28.0
02/28	A	01:45	04:00	456	3787	83.8	36.7	16.5	2922	688	69	44.6
02/28	B	04:01	06:30	402	2957	72.2	21.4	95.2	2410	430	123	24.9
02/28	C	07:36	09:26	11.7	3141	65.7	7.4	71.6	2134	599	179	20.6
02/28	D	09:33	10:42	8.1	3002	35.7	17.2	135	2278	616	183	43.7
02/28	E	13:00	16:00	168	2920	13.2	20.8	49.8	1654	406	4537	50.5
03/01	A	20:00	02:00	63.3	2051	13.2	1.7	49.8	1870	470	1097	13.9
03/01	B	02:10	04:05	56.5	2602	21.8	7.0	104	2219	443	903	8.5
03/01	C	04:15	06:15	11.0	2384	17.4	3.1	38.6	1934	309	855	15.1
Minimum				8.	704	13.	2.	15	463	178	32	8
Maximum				456	3787	139	42	202	3104	688	4537	77
Arith. Avg.				95	2470	62	17	66	1900	440	832	28

the remainder of the basin. Concentrations of NH_3 ranged from 32 to 4540 nmole m^{-3} (0.7 to 100 ppb) at Riverside. All the concentrations were well above the detection limit. The maximum observed NH_3 concentration of 4540 nmole m^{-3} exceeded the maximum NH_4^+ concentration. Nitric acid levels were comparatively low.

In general, the concentrations in the Pasadena aerosol, shown in Table 3, were less than those at Riverside. The fraction of cation charge contributed by NH_4^+ in the Pasadena aerosol ranged from 42 to 96%, while the NO_3^-:SO_4^{2-} ratio ranged from 0.36 to 5.0. Free HNO_3 was present at the Pasadena site, and on several occasions its levels exceeded those of aerosol NO_3^-. Gaseous NH_3 was present in Pasadena at much lower levels than in Riverside.

Fogwater Composition

Riverside fogwater samples contained such a high level of suspended solids that the collected samples appeared black. These particles were hydrophobic with an affinity for surfaces. The collector strands, sampling tube and sample bottles became visibly soiled with black particulate matter during a sampling event. The fogwater composition, shown in Table 4, was dominated by NH_4^+, NO_3^-, and SO_4^{2-}. The concentrations of NH_4^+ and NO_3^- exceeded 0.02 N in several samples. The pH of the samples ranged from 2.33 to 5.68. The first event was the most acidic; the fogwater pH dropped from 3.7 in the first sample collected to 2.33 at the end of the event. The 28 February event was only moderately acidic, with the fogwater pH dropping from 5.0 to 4.25 over the course of the event. Fog the following night was not acidic at all; it had a pH > 5, even though it had some of the highest concentrations of NO_3^- and SO_4^{2-} observed during the study. The drop in pH and the increase in solute concentration were due partly to the concentrating effect of droplet evaporation as the fog dissipated; however, some of the variation occurred during periods with stable LWC (as estimated from sample collection rate).

Except for the final sample collected during the 1 March fog event, the anion/cation

Table 3 Major aerosol and gas concentrations at Pasadena, California

Date	Seq	Start Time	Stop Time	Na^+	NH_4^+	Ca^{2+}	Mg^{2+}	Cl^-	NO_3^-	SO_4^{2-}	NH_3	HNO_3
				neq m^{-3}								
12/27	A	22:00	02:00	23.9	913	61.9	19.0	32.1	756	159	192	37.4
01/16	A	22:25	01:59	42.4	572	32.9	13.2	28.2	437	137	152	16.5
01/17	A	02:00	06:00	29.4	520	25.9	11.2	20.1	409	130	124	12.6
01/17	B	14:20	17:00	96.7	1859	187	56.1	61.3	2033	410	541	638
01/17	C	20:00	00:00	28.2	633	47.5	18.2	18.7	553	105	168	44.0
01/18	A	02:00	06:00	57.9	150	20.7	5.2	33.2	114	6.6	116	25.3
01/19	A	15:40	18:00	61.6	736	61.6	15.9	69.1	653	265	116	398
01/19	B	19:00	23:00	45.6	614	37.9	14.1	28.6	442	180	59	67.0
01/20	A	00:00	04:00	30.5	664	21.6	9.7	9.7	392	271	13	305
02/26	A	20:00	00:00	13.9	780	29.7	6.2	4.6	521	300	33	100
02/27	A	02:00	06:00	8.5	834	21.6	5.8	25.5	572	239	46	29.9
02/28	A	00:00	03:00	48.0	1228	24.6	15.2	42.0	624	741	5	358
02/28	B	03:01	06:00	15.4	1002	20.2	9.3	8.8	494	540	10	339
02/28	C	07:01	08:33	30.9	1521	40.0	10.9	8.6	761	810	5	771
02/28	B	08:00	10:50	4.9	894	33.8	5.5	3.8	545	223	30	190
02/28	D	04:00	17:00	38.7	1102	85.0	23.2	12.1	1312	545	64	891
03/01	A	00:00	04:00	41.9	688	40.9	9.1	3.9	219	607	10	832
03/01	B	08:00	11:31	19.8	808	31.0	8.5	5.3	379	464	16	650
03/04	A	20:00	23:00	22.1	1098	84.1	15.8	32.3	637	490	173	59.5
03/05	A	01:00	04:00	23.2	468	36.0	6.7	11.6	226	183	65	20.6
03/05	B	09:29	12:04	5.1	650	43.4	7.7	6.0	408	171	457	472
03/05	C	14:45	16:45	131	950	75.9	18.6	14.2	324	644	49	757
03/05	D	20:00	23:00	146	790	42.7	15.2	8.2	NA	654	7	268
03/06	A	01:00	04:00	159	951	39.1	11.6	21.9	415	554	5	340
Minimum				3.3	150	14.0	1.8	3.8	NA	3.5	5	0.0
Maximum				159	1859	187	56.1	69.1	NA	810	541	891
Arith. Avg.				44.3	851.0	48.8	13.7	21.3	NA	330	108	283

Table 4 Major ion concentrations in fogwater samples from Riverside, California.

Date	Seq	Start Time	Stop Time	Vol	pH	Na^+	NH_4^+	Ca^{2+}	Mg^{2+}	Cl^-	NO_3^-
				ml		µN					
01/23	A	05:55	06:30	58	3.70	123	10600	303	86	206	8230
01/23	B	06:30	07:00	59	3.65	37	10300	124	33	178	8290
01/23	C	07:00	07:30	55	3.08	30	8660	118	27	165	7580
01/23	D	07:30	08:00	37	3.35	41	12200	212	41	<100	9890
01/23	E	08:00	08:30	45	2.90	37	11300	158	35	<100	10900
01/23	F	08:30	09:00	48	2.78	32	10500	100	27	<100	10600
01/23	G	09:00	09:35	22	2.66	47	14000	181	45	176	12500
01/23	H	09:35	10:12	18	2.33	106	19800	362	81	371	20100
			N	8	8	8	8	8	8	8	8
			Minimum	18	2.33	30	8660	100	27	<100	7580
			Maximum	59	3.70	123	19800	362	86	371	20100
			Vol. Wt. Avg		2.99	52	11096	175	43	158	819
02/28	A	07:44	08:20	89	5.22	64	8340	131	26	130	6090
02/28	B	08:20	08:45	67	4.88	35	8380	109	23	170	6050
02/28	C	08:45	09:30	92	4.24	43	10400	106	26	190	7850
02/28	D	09:30	10:00	16	4.25	54	18100	209	55	384	13300
			N	4	4	4	4	4	4	4	4
			Minimum	16	4.24	35	8340	106	23	130	6050
			Maximum	92	5.22	64	18100	209	55	384	13300
			Vol. Wt. Avg		4.59	48	9588	122	27	178	7050
03/01	A	00:00	01:00	40	5.68	188	25800	396	103	380	18800
03/01	B	01:00	02:06	87.8	5.53	103	21200	164	49	370	15300
03/01	C	02:06	03:00	37.5	5.36	62	23200	129	37	370	17200
03/01	D	03:00	04:05	11.5	5.20	91	24000	294	73	750	28900
			N	4	4	4	4	4	4	4	4
			Minimum	11	5.20	62	21200	129	37	370	15300
			Maximum	87	5.68	188	25800	396	103	750	28900
			Vol.Wt. Avg		5.48	112	22926	217	60	396	17400

Table 4 continued

Date	Seq	SO_4^{2-} µN	S(IV)	CH_2O	H_2O_2	HFo	HAc	HMSA	−/+	LWC $g\ m^{-3}$
			µM							
01/23	A	2030	57	165	0	178	95	83	0.93	0.09
01/23	B	1650	64	187	0	—*	—*	92	0.94	0.11
01/23	C	1430	33	193	0	—*	—*	49	0.95	0.10
01/23	D	1810	53	218	0	182	122	103	0.90	0.07
01/23	E	1920	32	187	0	—*	—*	66	1.00	0.08
01/23	F	1850	13	186	0	106	56	52	1.01	0.09
01/23	G	2840	20	279	0	—*	—*	64	0.94	0.04
01/23	H	3960	14	207	0	346	237	86	0.98	0.03
N		8	8	8	8	8	4	8	8	
Minimum		1430	13	165	0	106	56	49	0.90	
Maximum		3960	64	279	0	346	237	103	1.01	
Vol.Wt. Avg		1929	40	194	0	—	—	73	0.96	0.074
02/28	A	1890	5	175	6	480	167	158	0.95	0.14
02/28	B	1810	12	223	17	451	161	NA	0.94	0.15
02/28	C	2300	15	234	15	357	134	NA	0.97	0.11
02/28	D	3660	10	370	25	576	267	NA	0.94	0.03
N		4	4	4	4	4	4	NA	4	
Minimum		1810	5	175	6	357	134	NA	0.94	
Maximum		3660	15	370	25	576	267	NA	0.97	
Vol.Wt. Avg.		2096	11	221	14	444	163		0.95	0.109
03/01	A	4900	60	309	19	NA	NA	NA	0.91	0.04
03/01	B	3770	12	205	21	1408	581	NA	0.90	0.07
03/01	C	3830	11	254	0	1293	417	NA	0.91	0.04
03/01	D	6230	26	384	15	1517	462	NA	1.47	0.01
N		4	4	4	4	4	4		4	
Minimum		3770	11	205	0	NA	NA	NA	0.90	
Maximum		6230	60	384	21	NA	NA	NA	1.47	
Vol.Wt. Avg		4199	24	252	15	0	0		0.94	0.040

* —indicates invalid data
NA —indicates not anlyzed
HFo = $CHOOH + CHOO^-$
HAc = $CH_3COOH + CH_3COO^-$

balance was between 0.99 and 1.10 which suggests that all major species were determined. It is likely that the NO_3^- determination for sample 301–D was too high or the NH_4^+ determination was too low; however, because the sample volume was small, it could not be reanalyzed.

The concentration of CH_2O determined by the Nash method varied from 165 to 384 μM. Dong and Dasgupta [1987] found similar concentrations of CH_2O in several of these samples that they analyzed by a flow–injection fluorimetric method. The S(IV) concentrations determined by the automated pararosaniline method were lower than the concentrations determined by Dasgupta and Yang [1986] in separate aliquots of several samples. The S(IV) concentrations reported here appear to be too low because of negative interference caused by the background matrix in the samples. This interference has not been a problem in samples from other locations.

The large number of carbonyls present in the Riverside fogwater samples is indicated by the number of peaks shown in Figure 6. Concentrations of the species that have been identified and quantified are given in Table 5. Note that the CH_2O concentrations determined by the DNPH derivatization are lower than those determined by the Nash method (Table 4). As noted above, the Nash method determined total CH_2O, while the DNPH derivative only forms from free carbonyls. In some cases the dicarbonyl concentration exceeds the formaldehyde concentration. The samples from 1 March are the most extreme example of this. A third dicarbonyl, 2,3 butanedione (biacetyl), was also present at low levels in most of the samples.

Peroxide was not detectable in the samples from 23 January. The two fog events on 28 February and 1 March contained peroxide up to 25 μM. Hydroxymethanesulfonate (HMSA) was observed in the 23 January samples at levels of 50 to 100 μM. Sample "A" from 28 February had 160 μM HMSA. Unfortunately, the HMSA concentration in the remaining samples, which had the higher H_2O_2, could not be determined because of interferences.

Formate and acetate had high concentrations in the Riverside fogwater. The highest

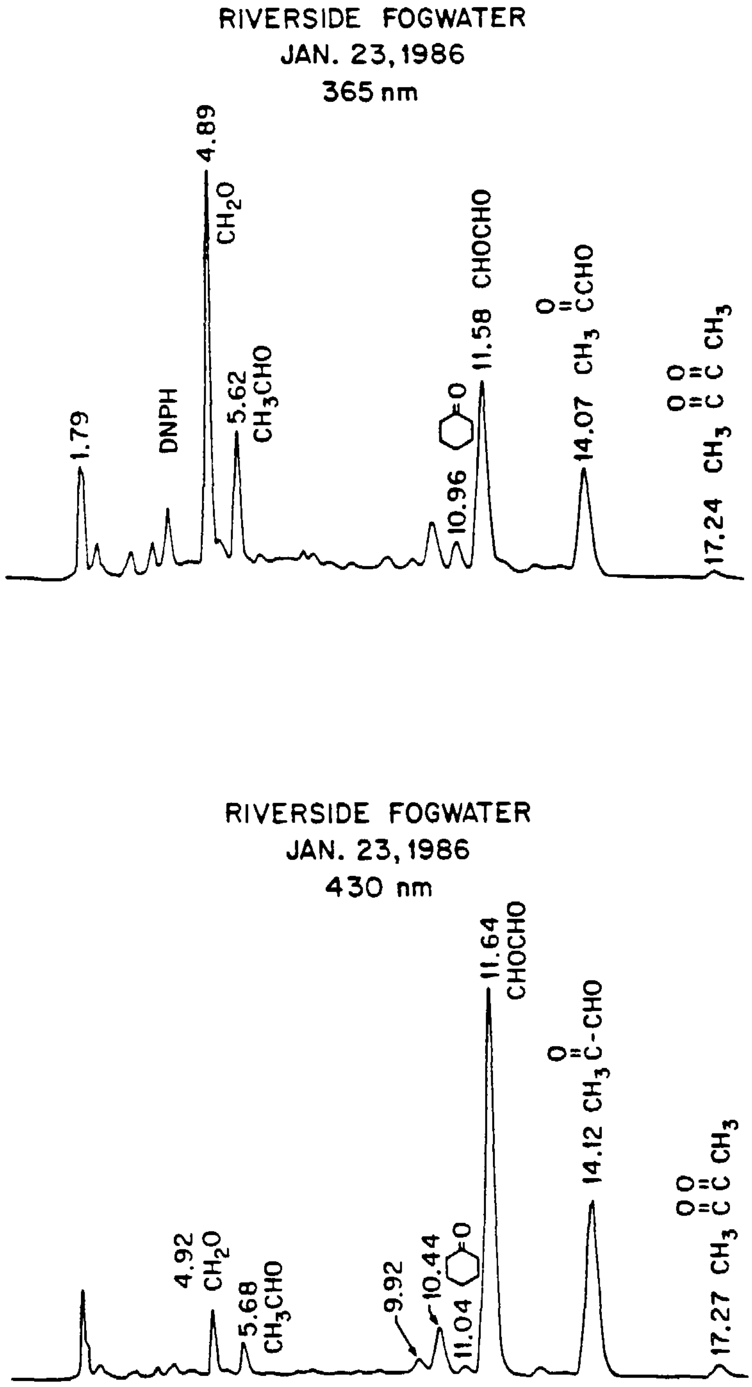

Figure 6. HPLC chromatograms of DNPH derivatives of Riverside fogwater at two wavelengths. Several–fold greater sensitivity for dicarbonyls is achieved by monitoring the absorbance at 430 nm, which is near the absorbance maximum for these compounds.

Table 5 Carbonyl concentrations in Riverside fogwater samples determined by HPLC analysis of DNPH derivatives

Date	ID	Start Time	Stop Time	Vol[1]	CH_2O	CHOCHO	CH_3COCHO	$(CH_3CO)_2$
				(ml)	μM			
01/23	A	05:55	06:30	3	109	65.3	45.9	4.7
01/23	B	06:30	07:00	3	122	32.3	25.8	3.7
01/23	C	07:00	07:30	3	162	34.6	26.7	3.5
01/23	D	07:30	08:00	2	228	59.9	44.1	5.8
01/23	E	08:00	08:30	2	119	55.3	42.7	5.1
01/23	F	08:30	09:00	2	142	56.8	47.7	5.8
01/23	G	09:00	09:35	1	104	121	83.9	1.4
01/23	H	09:35	10:12	1	84	139	108	0.0
01/23		Blank		3	0.4	0.0	0.0	0.0
01/23		Blank		2	14.7	0.4	0.0	0.0
01/23		Blank		2	17.2	0.5	0.0	0.0
02/28	A	07:44	08:20	2	36.3	38.6	35.5	3.9
02/28	B	08:20	08:45	2	40.8	45.0	41.1	4.9
02/28	C	08:45	09:30	2	57.3	77.1	60.5	6.6
02/28	D	09:30	10:00	1	107	198	128	14.0
02/28		Blank		2	21.0	0.8	0.0	0.0
03/01	A	00:00	01:00	2	4.1	147.8	79.1	8.8
03/01	B	01:00	02:06	2	8.7	142.3	74.9	8.9
03/01	C	00:06	03:00	2	8.2	144.1	77.4	8.8
03/01	D	03:00	04:05	1	36.0	276.2	124	17.7
03/01		Blank		2	13	0.6	0	0

[1] Volume of sample that was derivatized

Sample Concentrations are corrected for blank concentrations. The concentrations given for the blanks are the actual concentrations in the blank.

concentrations, 1520 and 580 μM ,respectively, were observed in the 1 March samples, which had pH > 5. Even the 23 January samples, which were quite acidic, had formate and acetate concentrations up to 350 and 340 μM, respectively. In all cases, HCOOH exceeded CH_3COOH, though the ratio varied substantially.

Discussion

Aerosol and Gas Data

The results presented here are an example of the coincidence between severe air pollution and fog. This of course does not necessarily imply a causal relationship. The sampling periods affected by fog represent extreme pollution events. The overall average SO_4^{2-} concentration of 440 neq m^{-3} is 80% of the California State Air Quality Standard for SO_4^{2-} (25 μg m^{-3} as a 24–hr average). The nitrate concentrations reported here are 6 – 10 times the monthly averages for January and February [Hoggan et al., 1980;1986]. The two sampling periods not affected by fog, 26–27 November and 16–17 January, exhibited lower aerosol concentrations.

Russell and Cass [1984] performed a series of detailed aerosol measurements in the SoCAB during August of 1982. Their results for Rubidoux, which is 8 km west of UC Riverside, also indicated that NH_4^+, NO_3^-, and SO_4^{2-} were the dominant inorganic components of the aerosol. The concentrations they observed were considerably lower, although they also observed high NH_3 and low HNO_3 concentrations. Higher wind speeds and a deeper mixed layer during the August study could account for the difference in the observed concentrations.

The acid–base balance of the aerosol is illustrated in Figure 7A. At Riverside, which is adjacent to the major NH_3 source region, most of the aerosol had an excess of NH_4^+. On the other hand, Pasadena appeared to have neutral aerosol. When NH_3 and HNO_3 in the gas phase were included (see Fig. 7B), the alkaline excess at Riverside was enhanced and the most concentrated of the Pasadena samples appeared acidic. This observation is consistent with the distribution of sources and prevailing winds in the SoCAB. Emissions of NO_x are highest along the coast and over downtown Los Angeles, where automobile traffic density is greatest. The region downwind is affected by HNO_3 formed from the oxidation of NO_x. When the air mass reaches the vicinity of Chino, it is mixed with NH_3 emissions, neutralizing the HNO_3.

Scavenging Ratios

The extent to which fog is affected by the pre–existing aerosol and gas phase composition depends on the scavenging efficiency. At humidities $\geq$ 100%, nearly all hygroscopic aerosol larger than a critical size will be activated and form droplets. The critical size for nucleation decreases as the supersaturation ratio is increased [Pruppacher and Klett, 1978]. For conditions typical of fog, the critical size is $\simeq 0.1\ \mu$m. This phenomenon would allow for scavenging efficiencies less than 100% if a large mass of aerosol smaller than the critical size were present. Scavenging efficiency would thus be related to the degree of supersaturation. Aerosol smaller than the critical size are scavenged by existing droplets through diffusion and impaction, which are less efficient processes. Soluble gases rapidly exchange across the air/water interface. The characteristic time for mass transfer across the interface is typically less than the lifetime of droplets; thus, the extent of scavenging from the gas phase can be predicted from thermodynamic considerations [Schwartz and Freiberg, 1981].

The aqueous–phase concentrations in the fogwater samples have been multiplied by the liquid water content (LWC), estimated from the collection rate of the CASC, to give the concentration on a mass per volume of air basis (Table 6), referred to as fogwater loading. The uncertainty of the calculated LWC is estimated to be ± 20%. The comparison of

Table 6 Concentration of aqueous–phase solutes per volume of air [1]

Date	Seq	LWC[2]	H^+	Na^+	NH_4^+	Ca^{2+}	Mg^{2+}	Cl^-	NO_3^-
		$g\ m^{-3}$				$neq\ m^{-3}$			
01/23	A	0.09	18.5	11.4	984	28.1	7.9	19.1	764
01/23	B	0.11	24.6	4.0	1132	13.6	3.6	19.6	912
01/23	C	0.10	84.6	3.1	881	12.0	2.8	16.8	771
01/23	D	0.07	30.6	2.8	836	14.5	2.8	<6.9	678
01/23	E	0.08	106	3.2	953	13.3	3.0	<8.4	920
01/23	F	0.09	149	2.8	941	9.0	2.4	<9.0	950
01/23	G	0.04	78.1	1.7	500	6.5	1.6	6.3	446
01/23	H	0.03	128	2.9	542	9.9	2.2	10.2	551
N			8	8	8	8	8	8	8
Minimum			18.5	1.7	500	6.5	1.6	<6.3	446
Maximum			149	11.4	1132	28.1	7.9	19.6	950
02/28	A	0.14	0.8	8.9	1155	18.1	3.6	18.0	843
02/28	B	0.15	2.0	5.3	1258	16.4	3.5	25.5	908
02/28	C	0.11	6.6	4.9	1196	12.2	3.0	21.8	903
02/28	D	0.03	1.7	1.7	554	6.4	1.7	11.8	407
N			4	4	4	4	4	4	4
Minimum			0.8	1.7	554	6.4	1.7	11.8	407
Maximum			6.6	8.9	1258	18.1	3.6	25.5	908
03/01	A	0.04	0.08	7.0	963	14.8	3.8	14.2	702
03/01	B	0.07	0.22	7.7	1579	12.2	3.6	27.6	1140
03/01	C	0.04	0.17	2.4	902	5.0	1.4	14.4	669
03/01	D	0.01	0.06	0.9	238	2.9	0.7	7.4	286
N			4	4	4	4	4	4	4
Minimum			0.08	0.9	238	2.9	0.7	7.4	286
Maximum			0.22	7.7	1579	14.8	3.8	27.6	1140

Table 6 continued

Date	Seq	SO_4^{2-}	S(IV)	CH_2O	H_2O_2	HFo[3]	HAc[4]	HMSA
		neq m^{-3}	nmole m^{-3}					
01/23	A	188	5.3	15.3	0.0	16.5	8.8	7.7
01/23	B	181	7.0	20.6	0.0	—[5]	—	10.1
01/23	C	146	3.4	19.6	0.0	—	—	5.0
01/23	D	124	3.6	14.9	0.0	12.5	8.6	7.1
01/23	E	162	2.7	15.8	0.0	—	—	5.6
01/23	F	166	1.2	16.7	0.0	9.4	5.0	4.8
01/23	G	101	0.7	10.0	0.0	—	—	2.3
01/24	H	108	0.4	5.7	0.0	9.5	6.5	2.4
N		8	8	8	8	4	8	8
Minimum		101	0.4	5.7	0.0	2.8	0.0	2.3
Maximum		188	7.0	20.6	0.0	16.5	8.8	10.1
02/28	A	262	0.73	24.2	0.85	66.5	23.1	—
02/28	B	272	1.76	33.5	2.61	67.6	24.2	—
02/28	C	264	1.77	26.9	1.75	41.0	15.4	—
02/28	D	112	0.32	11.3	0.76	17.6	8.2	—
N		4	4	4	4	4	4	0
Minimum		112	0.32	11.3	0.76	17.6	8.2	—
Maximum		272	1.77	33.5	2.61	67.6	24.2	—
03/01	A	183	2.23	11.54	0.69	NA	NA	—
03/01	B	281	0.88	15.27	1.53	105	43.3	—
03/01	C	149	0.42	9.88	0.00	50.3	16.2	—
03/01	D	62.	0.26	3.80	0.15	15.0	4.6	—
N		4	4	4	4	4	4	0
Minimum		62	0.26	3.80	0.15	15.0	4.6	—
Maximum		281	2.23	15.27	1.53	105.0	43.3	—

---

[1] $C_{air} = C_{aq} \cdot LWC$

[2] LWC is estimated from the sample collection rate

[3] HFo = $CHOOH + CHOO^-$

[4] HAc = $CH_3COOH + CH_3COO^-$

[5] — indicates sample not analyzed

fogwater loading (Table 6) with the aerosol concentration (Table 2) suggests that scavenging of aerosol by fogwater under these conditions is not 100% efficient. It is unlikely that the LWC values are underestimated by enough to account for the discrepancy, but we can not exclude this possibility since no alternate, confirming method of measuring the LWC was used. The existence of a significant fraction of unactivated aerosol is supported by the results for the interstitial aerosol filters (Table 7). The concentrations of interstitial aerosol are comparable to the fogwater loadings. If the CASC and aerosol inlet perform as expected, considerably more than half the solute mass would have to be in the smallest droplets to account for this result, without having any unactivated aerosol.

The scavenging ratios for individual events are computed by three different methods and presented in Table 8. The scavenging ratios computed by method one, which compares the loading in the fog with the concurrent total aerosol concentration, are less than 0.5. The ratio decreases at the end of the fog event as the droplets are evaporating. Method two, which compares the fogwater loading to the aerosol concentration measured prior to formation of the fog, yields similar results. In method three, the difference between total and interstitial aerosol concentrations is divided by the total. The calculation by method three does not depend on the estimated LWC. If the interstitial aerosol measurement includes a significant fraction of small droplets, the scavenging ratios computed by method 3 will underestimate the true scavenging ratios. The scavenging ratios calculated by method 3 are somewhat higher than the others, but the pattern of decreased scavenging efficiency as the fog dissipates is preserved. Because of the inherent uncertainties in the scavenging calculations, these values are qualitative; however, the consistently low values suggest that radiation fogs in highly polluted air may not scavenge aerosol at 100% efficiency.

Low scavenging efficiencies were also reported by Waldman and Hoffmann [1987] in a study of radiation fog in the San Joaquin Valley. That study also showed a weak positive correlation between scavenging ratio and LWC. ten Brink et al. [1987], however, observed

Table 7 Interstitial Aerosol Concentrations at Riverside, California.

Date	Seq	Start	Stop	Na^+	NH_4^+	Ca^{2+}	Mg^{2+}	Cl^-	NO_3^-	SO_4^{2-}
				neq m^{-3}						
02/28	C	07:36	09:26	579	986	78	9	61	735	138
02/28	D	09:33	10:42	825	2338	140	20	110	1733	415
03/01	A	00:00	02:00	4	664	3	0	15	569	100
03/01	B	02:10	04:05	4	1225	6	5	11	1034	150

Table 8. Scavenging Ratios for Riverside Fogwater.

Method 1: $R = [C_{fog}]/[C_{aerosol}]$

Date	Seq	Start	Stop	Na^+	NH_4^+	Ca^{2+}	Mg^{2+}	Cl^-	NO_3^-	SO_4^{2-}	N(−III)[1]	N(V)[1]
01/23	A	06:03	09:35	0.38	0.38	0.68	0.78	—[2]	0.39	0.47	0.37	0.39
02/28	C	07:36	09:26	0.54	0.38	0.23	0.45	0.30	0.41	0.44	0.36	0.41
02/28	D	09:33	10:42	0.21	0.18	0.18	0.10	0.09	0.18	0.18	0.17	0.18
03/01	A	00:00	02:00	0.12	0.63	1.02	2.20	0.43	0.50	0.50	0.41	0.49
03/01	B	02:10	04:05	0.03	0.21	0.18	0.15	0.10	0.21	0.23	0.15	0.21

Method 2: $R = [C_{fog}]/[C_{aerosol}]_{pre\text{-}event}$

Date	Seq	Start	Stop	Na^+	NH_4^+	Ca^{2+}	Mg^{2+}	Cl^-	NO_3^-	SO_4^{2-}	N(−III)	N(V)
01/22	A	22:30	01:59	0.18	0.38	0.35	0.29	0.36	0.41	0.33	0.27	0.41
02/28	B	04:01	06:30	0.02	0.39	0.25	0.17	0.19	0.35	0.61	0.37	0.35

Method 3: $R = (1-[C_{interstitial}]/[C_{total}])$

Date	Seq	Start	Stop	Na^+	NH_4^+	Ca^{2+}	Mg^{2+}	Cl^-	NO_3^-	SO_4^{2-}	N(−III)	N(V)
02/28	C	07:36	09:26	—	0.69	—	—	0.15	0.66	0.77	0.70	0.66
02/28	D	09:33	10:42	—	0.22	—	—	0.18	0.24	0.33	0.27	0.25
03/01	A	00:00	02:00	0.93	0.68	0.74	0.82	0.69	0.70	0.79	0.79	0.70
03/01	B	02:10	04:05	0.92	0.53	0.72	0.36	0.89	0.53	0.66	0.65	0.54

[1] N(−III) = $NH_3 + NH_4^+$, N(V) = $HNO_3 + NO_3^-$

[2] — indicates data invalid for calculating scavenging ratios.

nearly complete scavenging of aerosol SO_4^{2-} and of total aerosol in clouds, based on measurements of the scattering coefficient. We also have observed high scavenging efficiencies for intercepted marine stratus and mountain clouds [Munger et al., 1989; Collett et al., 1989]. Because the aerosol number concentration, size distribution, and saturation conditions in clouds are much different than those at the ground, we do not see a conflict in these results.

Temporal Variations

The aerosol, gas and fogwater concentrations of major ions and alkalinity are plotted together in Figures 8A–C and Figure 9. During the night of 22 January, the N(–III) concentration decreased, mostly due to a decline in the concentration of NH_3. The NO_3^- concentration was constant over the period, while the SO_4^{2-} concentration decreased. The following morning concentrations of all three species increased as the fog dissipated. The timing of this increase coincided with the onset of a westerly wind, which advected fresh emissions to the site, and with an increase in automobile traffic throughout the basin. NH_4^+ and NH_3 concentrations declined the following night, when the site was above the fog layer, but NO_3^- and SO_4^{2-} levels remained high. During the night of 28 February, NO_3^- and NH_4^+ concentrations declined. The gas phase contributions of HNO_3 and NH_3 were small during this period. The NO_3^- concentration remained low the following morning, but the concentration of NH_3 rose to the highest level observed during the study. The concentrations were similar the following night, but NH_3 made a larger contribution to the total N(–III). The alkalinity plot, shown in Figure 9, indicates that the gas phase is the major reservoir of alkalinity at Riverside. The acidity of the fog is not completely explained by the precursor aerosol and gas phase species. Prior to the 23 January fog event, the atmosphere contained over 1000 neq m^{-3} total alkalinity. This alkalinity was almost completely dissipated by the time the fog formed; however, the atmosphere was still more alkaline than the fog. High

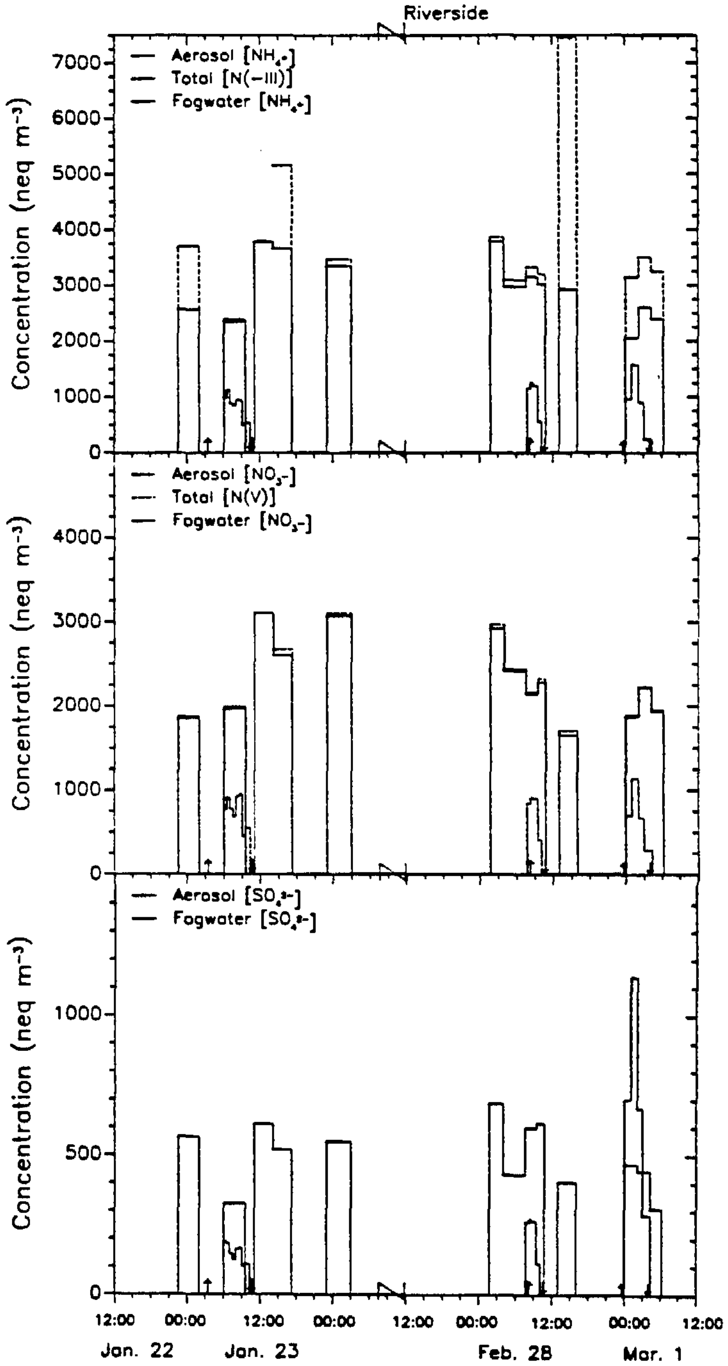

Figure 8. Plot of aerosol, gas and fogwater concentrations of N(–III), N(V), and SO_4^{2-} at Riverside. Fogwater concentrations are calculated from the aqueous phase concentrations and liquid water content estimated from the collection rate of the CASC. The start and end of a fog event are indicated by ↑ and ↓.

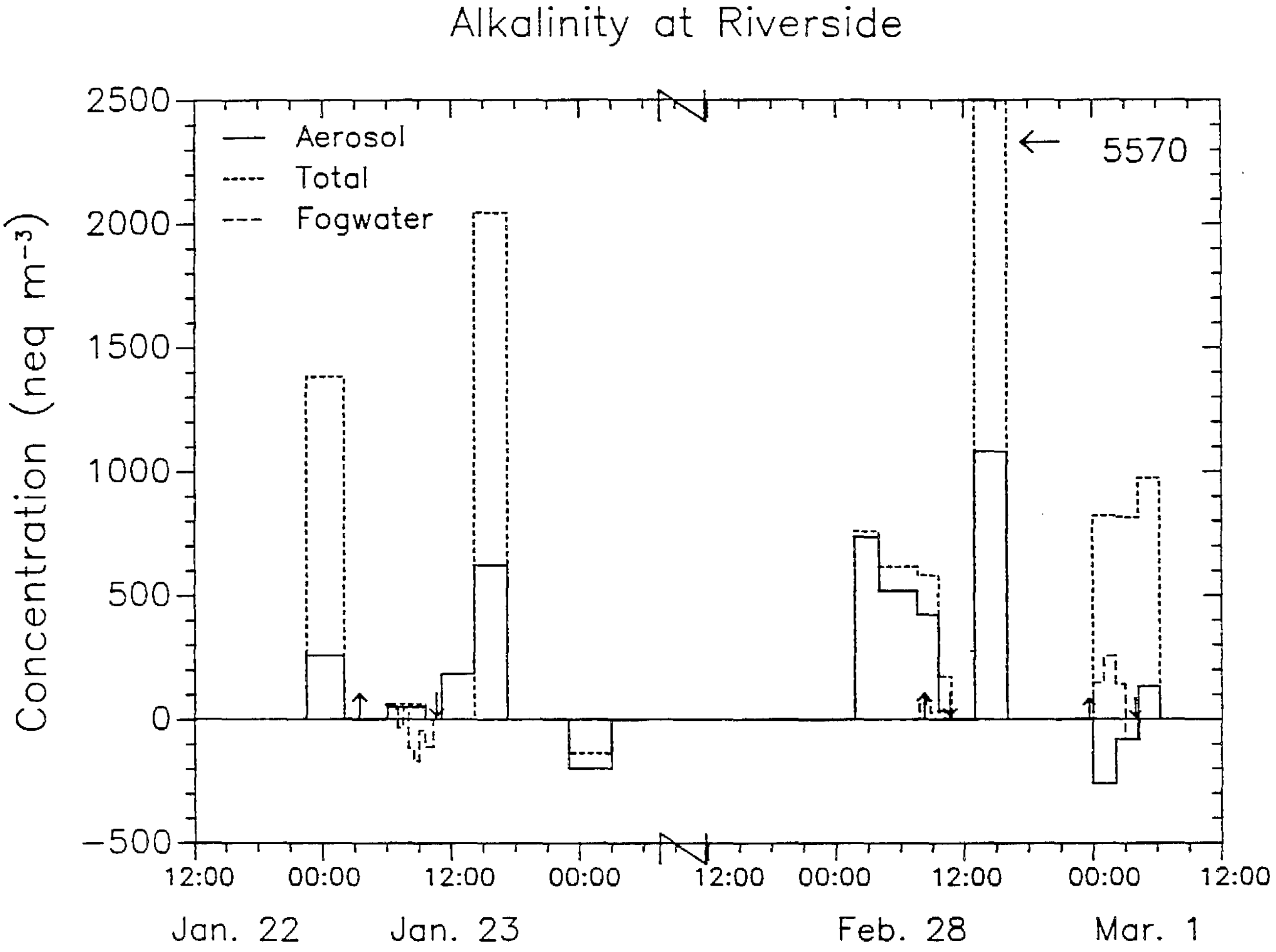

Figure 9. Plot of atmospheric alkalinity at the Riverside sampling site. The aerosol and fogwater lines are computed from the equation: Alk = Σcations − Σanions. The total alkalinity is the aerosol alkalinity plus the contribution from gas phase NH_3 and HNO_3. The start and end of a fog event are indicated by ↑ and ↓.

atmospheric alkalinity levels were observed the following afternoon. The air mass was acidic the following night. An alkaline air mass generated a moderately acidic fog again on 28 February. On 1 March the alkalinity of the fog was supported by an excess of NH_3 in the gas phase. The aerosol measurements alone seem to imply that emissions of NH_3 in the basin exceed the production of HNO_3 from NO_x emissions, but the fogwater data are not consistent with this argument.

The resolution of this apparent contradiction lies in the meteorology of the basin and the location of the emission sources relative to the sampling site. During the day, the sea breeze creates a westerly flow through the basin. Nitric acid is continually produced, but NH_3 emissions near Chino are more than sufficient to neutralize the air mass by the time it reaches the Riverside sampling site. Convective mixing distributes the NH_4NO_3 and NH_3, as well as unreacted NO_x, throughout the mixed layer. At night, the wind reverses direction and a shallow nocturnal inversion forms, which effectively isolates the site from the NH_3 emissions. The air present at the site at night is polluted air that was isolated from the boundary layer by the nocturnal inversion. Nitric acid is produced in this air mass via $NO_3\cdot$ and N_2O_5 mechanisms:

$$NO_2 + O_3 \rightarrow NO_3\cdot + O_2 \qquad (1)$$

$$NO_3\cdot + NO_2 \rightarrow N_2O_5 \qquad (2)$$

$$NO_3\cdot + RH \rightarrow HNO_3 + R\cdot \qquad (3)$$

$$NO + O_3 \rightarrow NO_2 + O_2 \qquad (4)$$

$$NO + NO_3\cdot \rightarrow 2NO_2 \qquad (5)$$

The concentrations of $NO_3\cdot$ and N_2O_5 are enhanced in this air mass because it is also isolated from NO emissions, which would consume O_3 and $NO_3\cdot$ via reactions 4 and 5. Over the course of the night, production of HNO_3 titrates the residual NH_3 in the air mass. This is observed on the nights of 22–23 January and 28 February. The conditions on 23 January are an extreme example of this. The sampling site was above the fog layer on this date, clearly indicating that it was isolated from the NH_3 sources. This was the only sampling period when the aerosol was observed to be acidic. We did not observe a decrease in alkalinity or formation of acid fog on the night of 1 March when there was no wind reversal. This scheme implies that the source of HNO_3 in the fog is above the fog layer. Its logical consequence is that acid fog may form at the margins of the basin while fog in the center is neutral or alkaline. Because the hillsides are some of the most desirable sites for housing developments, this is of particular concern for assessing potential health effects of fogwater in the Riverside area.

The concentrations of carbonyls in the Riverside fogwater samples are plotted in Figure 10. On 23 January, the concentration of CH_2O reached its maximum at the midpoint of the collection period, which is between 0730 and 0800. Subsequent to this time, the concentration of CH_2O decreases while concentrations of the dicarbonyls, CHOCHO and $CH_3C(O)CHO$, increase. The increase in dicarbonyl concentrations coincides with the morning rush hour, which contributes hydrocarbon precursors, and with increased sunlight. This pattern is repeated on 28 February. The presumed source of dicarbonyls in the atmosphere is the gas–phase oxidation of aromatic compounds, such as toluene. The observed concentrations of carbonyls and dicarbonyls are consistent with their solubilities. CH_2O, CHOCHO, and $CH_3C(O)CHO$, which have the highest concentrations, all have large effective Henry's Law constants because of their large hydration constants [Betterton et al., 1988]. Acetaldehyde, which has been reported at levels comparable to CH_2O in Los Angeles air [Grosjean, 1982], but is one thousand times less soluble, was not observed above the blank concentration in these samples.

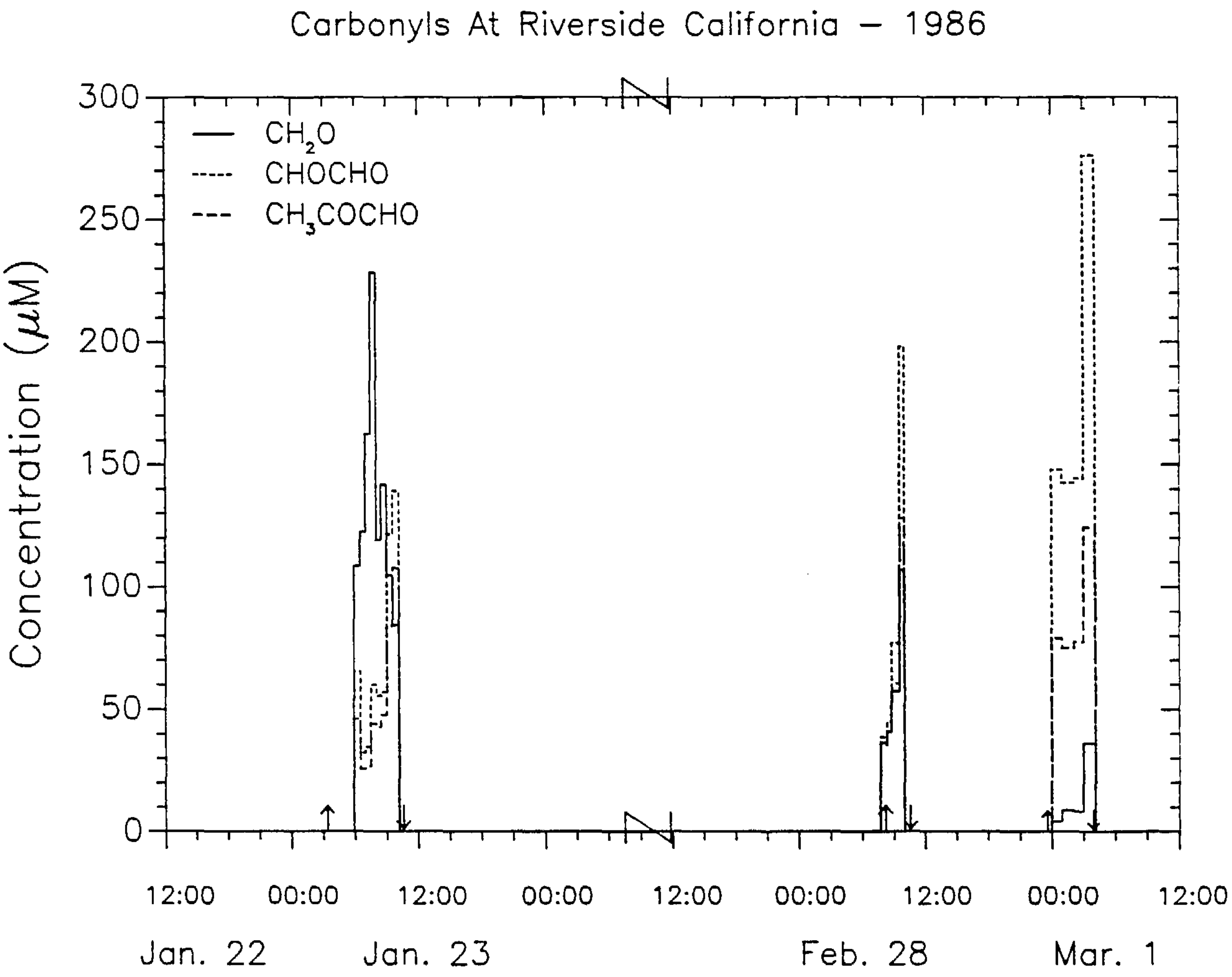

Figure 10. Plot of carbonyl concentrations determined by the DNPH derivatization method. The start and end of a fog event are indicated by ↑ and ↓.

Several lines of evidence indicate the importance of sulfonates in the Riverside fog. Direct measurements of HMSA in some samples indicate the presence of HMSA. The disparity between concentrations of free CH_2O (DNPH measurement, Table 5) and total CH_2O (Nash measurement, Table 4) implies the presence of HMSA. In addition, the apparent coexistence of S(IV) with peroxide suggests that the S(IV) was present as the sulfonate [Munger et al., 1984]. HMSA was observed in the 23 January samples at levels of 50 to 100 μM, and in the first sample from 28 February at 160 μM. Unfortunately, the HMSA concentration in the remaining samples, which had higher concentrations of H_2O_2, could not be determined because of interferences.

Because the kinetics of sulfonate formation are slow compared to the reaction of S(IV) with H_2O_2 [Boyce and Hoffmann, 1984; Deister et al., 1986, Kok et al., 1986], the sulfonates probably formed prior to being scavenged by the fog. Although the dicarbonyls found in these samples could also react with S(IV) to form the corresponding sulfonates [Betterton and Hoffmann, 1987; Olson and Hoffmann, 1988], it is not clear whether they were present as sulfonates.

The physical and chemical processes that drive the observed concentration changes are horizontal advection, vertical mixing (by turbulence), deposition, emission, and chemical reaction. These processes can be represented in differential form by:

$$\frac{dC_i}{dt} - \vec{u}\cdot\nabla C_i = \kappa\frac{dC_i}{dz} + \frac{E}{H} - \frac{C_i V_{d,i}}{H} + R_i \qquad (6)$$

where C_i is the concentration of species i, $\vec{u}$ is the horizontal wind vector, κ is the turbulent eddy diffusion coefficient, E is the emission flux, H is the height of the mixed layer, $V_{d,i}$ is the species dependent deposition velocity, and R_i is the net reaction rate ($R_i = \Sigma k_j C_j - k_i C_i$, where k_j and C_j are the pseudo–first order rate constants and the reactants that form species i, and k_i is the pseudo–first order rate constant for destruction of species i). Diffusion is not included in equation 6 because its contribution is small relative to the contributions of the other terms. All the phases that a species can exist in must be considered together. Clearly this becomes a very complex system of equations even when one considers only the major species found in the fog (NH_4^+, H^+, NO_3^-, SO_4^{2-}) and their precursors. Equation 6 is presented as a guide to evaluating the observed compositional changes, rather than as an equation to be solved.

This equation can be used to establish some bounds on the magnitude of the advection and source terms for N(–III) and N(V). The analysis is simplified for N(–III) and N(V) because $R = 0$ for N(–III) and $E = 0$ for N(V). During periods with constant concentration, the net transport equals the difference between deposition and emission (or atmospheric reaction). For sampling intervals on 22 January and again on 1 March, the aerosol NO_3^- concentration was constant at about 2000 neq m^{-3}. Assuming a deposition velocity of 0.1 cm s^{-1} [Waldman and Hoffmann, 1987], the change in concentration due to deposition would range from 18 to 36 nmole m^{-3} hr^{-1} for mixing heights of 200 to 400 m. In fog, however, with an assumed deposition velocity of 1 cm s^{-1} (a lower limit reported by Waldman and Hoffmann [1987] for San Joaquin Valley fog), and a scavenging fraction of 0.5, the deposition term would increase to 180 nmole m^{-3} hr^{-1} for a 200 m mixing height. For an NH_4^+ concentration of 3000 neq m^{-3}, the deposition term would be 27 to 54 nmole m^{-3} hr^{-1}, in the absence of fog, for the same mixing heights. Assuming a deposition velocity of 1 cm s^{-1} for NH_3 gives values of 90 to 180 nmole m^{-3} hr^{-1} for a 1000 nmole m^{-3} concentration. As was predicted for N(V), N(–III) deposition is enhanced by the formation of fog, which scavenges the NH_4^+ aerosol and deposits it at a faster rate.

Impact of Development

Because the eastern SoCAB is undergoing rapid development, which is likely to force the curtailment of dairy operations in the Chino area, it is important to consider the effect of reduced NH_3 inputs on fogwater chemistry. In order to evaluate the role of fog formation, dry deposition, and changes in emissions, a simple box model of the Riverside basin was developed. It is not sufficient merely to subtract the NH_4^+ and NH_3 from the present results to predict the effect of reduced NH_3 emissions because changes in the N(V) speciation, which is partly dependent on the concentration of N(–III), will have a pronounced effect on its fate. The model is described by the following equation:

$$\frac{dC_i}{dt} = \frac{E_i}{H} + P_i - \frac{(\alpha_f \cdot C_i \cdot v^f_{d,i} + \alpha_a \cdot C_i \cdot v^a_{d,i} + \alpha_g \cdot C_i \cdot v^g_{d,i})}{H} - \frac{C_i}{\tau_f} \qquad (7)$$

where P_i represents the rate of chemical production of species i in the atmosphere. The rates of chemical destruction of HNO_3 and NH_3 are assumed to be negligible; therefore, P_i has been substituted for R_i, the net reaction rate for species i. The advection and vertical mixing terms in equation 6 have been combined and approximated as a first–order dilution, described by the inverse of the flushing time, τ_f, in order to obtain equation 7. The coefficients α_f, α_g, and α_a, are the fractions present as fog, gas, and aerosol, respectively; $v^f_{d,i}$, $v^g_{d,i}$, and $v^a_{d,i}$ are the deposition velocities associated with each phase. Integration was performed using a 4th–order Runge–Kutta method.

The model simulation is programmed to run for a two day period, beginning at midnight. The initial conditions, deposition velocities, and production and emission terms are listed in Table 9. The value chosen for P_{HNO_3} represents an overall average for production of HNO_3 from NO_x by all mechanisms reported by Russell et al. [1985]. The emission flux for NH_3 was selected to balance its deposition rate and give a steady state concentration matching the observed value. This flux is consistent with the NH_3 budget of Russell et al. [1985]. At each time step the species are partitioned into aerosol and gas phases by an acid–base balance. Because either NH_3 or HNO_3 is usually present in large excess, it is not necessary to explicitly include the dissociation of NH_4NO_3. Fog is present between 0200

Table 9 Simulation conditions

Initial Concentrations

S(VI)	750 neq m^{-3}
N(–III)	2000 neq m^{-3}
N(V)	1000 neq m^{-3}

Deposition Velocities

Aerosol	$v_d{}^a =$	0.1 cm s^{-1}
Gas	$v_d{}^g =$	1.0 cm s^{-1}
Fog	$v_d{}^f =$	1.0 cm s^{-1}

Inputs

P =	$NO_x \longrightarrow HNO_3$	5.3 x 10^{-11} mole m^{-3} s^{-1}
E =	$F^0_{NH_3}$	4.0 x 10^{-8} mole m^{-2} s^{-1}

Mixing Height	H = 250 m
Flushing time	τ = 12 hr

For Low NH_3 case, all conditions are the same except $F_{NH_3} = 0.1 \cdot F^0_{NH_3}$

and 1000, and is assumed to scavenge half the aerosol and 100% of the gas phase species. This is valid for HNO_3 at all expected pH values and for NH_3 in acidic fog. During the period 2000 to 0800, the NH_3 source is shut off (to model a wind reversal), and the dilution term is included. Ten percent of the base case ammonia emissions was chosen for the low ammonia case because the elimination of dairy operations would reduce NH_3 emissions drastically, but would not eliminate them entirely.

Although the results of the simulation (Fig. 11) do not exactly mimic the Riverside observations (and were not intended to), they are qualitatively similar and show a comparable range of concentrations. The depletion of NH_3 by nighttime production of HNO_3 is exaggerated in the simulation. The presence of fog acts to slightly enhance the deposition of NH_4NO_3 aerosol. When NH_3 emissions are decreased, both N(–III) and N(V) are lower than the base case (Fig. 12). However, nearly all the N(V) is present as HNO_3, yielding a highly acidic atmosphere. A balance between production of HNO_3 and its rapid dry deposition quickly leads to a steady state concentration of HNO_3 around 1000 neq m^{-3}. A 0.1 g m^{-3} fog forming in the low NH_3 case would be uniformly acidic ($pH \simeq 2$), whereas the same fog in the base case would only approach pH 2 towards the end of the event. The variable pH levels that were observed in the fog are simulated by the base case. Without the NH_3 source, the model predicts uniform acidity, unlike the present situation with highly variable fogwater acidity. Under this scenario, any portion of the basin that is influenced by advection from Los Angeles is likely to have acid fogwater.

Acknowledgements

This work was supported by the California Air Resources Board, Contract # A4–075–32. We thank R. Musselman of UC Riverside for permission to sample at UC Riverside.

References

Betterton, E. A. and Hoffmann, M. R. (1987) The kinetics, mechanism, and thermodynamics of the reversible reaction of methylglyoxal (CH_3COCHO) with S(IV). *J. Phys. Chem.* **91**, 3011–3020.

Betterton, E. A., Erel, Y., and Hoffmann, M. R. (1988) Aldehyde–bisulfite adducts: Prediction of some of their thermodynamic and kinetic properties. *Environ. Sci. Technol.* **22**, 92–99.

Boyce, S. D. and Hoffmann, M. R. (1984) Kinetics and mechanisms of the formation of hydroxymethanesulfonic acid at low pH. *J. Phys. Chem.* **88**, 4740–4746.

Collett, J., Jr., Daube, B. C., Jr., Munger, J. W., and Hoffmann, M. R. (1989) Cloudwater chemistry in Sequoia National Park. *Atmos. Environ.* in press.

Dasgupta, P. K. (1981) Determination of atmospheric sulfur dioxide without tetrachloromercurate(II): Further refinements of a pararosaniline method and a field application. *J. Air Pollut. Cont. Assoc.* **31**, 779–782.

Dasgupta, P. K., DeCesare, K. and Ullrey, J. C. (1980) Determination of atmospheric sulfur dioxide without tetrachloromercurate (II) and the mechanism of the Schiff reaction. *Anal. Chem.* **52**, 1912–1922.

Dasgupta, P. K. and Yang, H.–C. (1986) Trace determination of aqueous sulfite, sulfide and methanethiolate by flourimetric flow injection analysis. *Anal. Chem.* **58**, 2839–2844.

Daube, B. C., Jr., Flagan, R. C., and Hoffmann, M. R. (1986) *Active Cloudwater Collector.* United States Patent #4,697,462. Oct.6, 1987.

Deister, U., Neeb, R., Helas, G. and Warneck, P. (1986) Temperature dependence of the equilibrium $CH_2(OH)_2 + HSO_3^- = CH_2(OH)SO_3^- + H_2O$ in aqueous solution. *J. Phys. Chem.* **90**. 3213–3217.

Dong, S. and Dasgupta, P. K (1987) Fast flourimetric flow injection analysis of formaldehyde in atmospheric water. *Environ. Sci. Technol.* **21**, 581–588.

Friedlander, S. K. (1977) *Smoke, Dust and Haze*, p. 107. John Wiley and Sons, New York.

Grosjean, D. (1982) Formaldehyde and other carbonyls in Los Angeles ambient air. *Environ. Sci. Technol.* **16**, 254–262.

Grosjean, D. and Wright, B. (1983) Carbonyls in urban fog, ice fog, cloudwater and rainwater. *Atmos. Environ.* **17**, 2093–2096.

Hering, S. V. (1987) Field comparison of measurement methods for nitric acid, ARB Final Report, Contract #A4–164–32, California Air Resources Board, Sacramento, CA. 69 pp.

Hoggan, M., Davidson, A., and Shikiya, D. (1980) Seasonal and diurnal variation in air quality in California's South Coast Air Basin, South Coast Air Quality Management District, El Monte, CA. 103 pp.

Jacob, D. J., Munger, J. W., Waldman, J. M., and Hoffmann, M. R. (1986) The H_2SO_4–HNO_3–NH_3 system at high humidities and in fogs: I. Spatial and temporal patterns in the San Joaquin Valley of California, *J. Geophys. Res* **91**, 1073–1088.

Kawamura, K., Steinberg, S. and Kaplan, I. R. (1985) Capillary GC determination of short–chain acids in rain, fog and mist. *Intern. J. Environ. Anal. Chem.* **19**, 175–188.

Kok, G. L., Gitlin, S., N., and Lazrus, A. L. (1986) Kinetics of the formation and decomposition of hydroxymethanesulfonate. *J. Geophys. Res.* **91**, 2801–2804.

Keene, W. C., Talbot, R. W., Andreae, M. O., Beecher, K. Berresheim, J., Castro, M., Farmer., J. C., Galloway, J. N., Hoffmann, M. R., Li, S.–M., Maben, J. R., Munger, J. W., Norton, R. B., Pszenny, A. A. A. P., and Puxbaum, H. (1988) An intercomparison of measurement systems for vapor and particulate phase concentrations of formic and acetic acids, *J. Geophys Res.* (submitted).

Lazrus, A., Kok, G. L., Gitlin, S. N., Lind, J. A., and McLaren, S. E. (1985) Automated fluorometric method for hydrogen peroxide in atmospheric precipitation. *Anal. Chem.* **57**, 917–922.

Marsh, S. L., Jr. and Bergman, L. D. (1984) Meteorological factors influencing the acidity of fog in the Los Angeles Basin, Presentation at 77th Annual Meeting of the Air Poll. Cont Assoc., San Francisco, CA, June 24–29, 1984.

Munger, J. W., Jacob, D. J., Waldman, J. M., and Hoffmann, M. R. (1983) Fogwater chemistry in an urban atmosphere. *J. Geophys. Res.* **88,** 5109–5121.

Munger, J. W., Jacob, D. J., and Hoffmann, M. R. (1984) The occurrence of bisulfite–aldehyde adducts in fog– and cloudwater. *J. Atmos. Chem.* **1,** 335–350.

Munger, J. W., Tiller, C. T., and Hoffmann, M. R. (1986) Determination of hydroxymethanesulfonate in fog water. *Science* **231,** 247–249.

Munger, J. W., Collett, J., Jr., Daube, B., Jr., and Hoffmann, M. R. (1989) Chemical composition of coastal stratus clouds: dependence on droplet size and distance from the coast. *Atmos. Environ.* (submitted).

Nash, T. (1953) The colorimetric estimation of formaldehyde by means of the Hantszch reaction, *Biochem. J.* **55**, 416–421.

Olson, T. M. and Hoffmann, M. R. (1988) The kinetics, mechanism and thermodynamics of glyoxal–S(IV) adduct formation, *J. Phys. Chem.* **92** 533–540.

Pruppacher, H. R. and Klett, J. D. (1978) *Microphysics of clouds and precipitation*, pp. 139–140. D. Reidel, Dordrecht.

Reitz, E. B. (1980) The stabilization of small concentrations of formaldehyde in aqueous solutions. *Anal. Lett.* **13**, 1073–1084.

Russell, A. G. and Cass, G. R. (1984) Acquisition of regional air quality model validation data for nitrate, sulfate, ammonium ion and their precursors. *Atmos. Environ.* 18, 1815–1827.

Russell, A. G. and Cass, G. R. (1986) Verification of a mathematical model for aerosol nitrate and nitric acid formation and its use for control measure evaluation. *Atmos. Environ.* **20**, 2011–2025.

Russell, A. G., McRae, G. J., and Cass, G. R. (1985) The dynamics of nitric acid production and the fate of nitrogen oxides. *Atmos. Environ.* **19**, 893–903.

Schwartz, S. E. and Freiberg, J. E. (1981) Mass–transport limitation to the rate of reaction of gases in liquid droplets: Application to oxidation of SO_2 in aqueous solutions. *Atmos. Environ.* **15**, 1129–1144.

Smith, R. V., and Erhardt, P. W. (1975) Nash determination for formaldehyde in the presence of bisulfite. *Anal. Chem.* **47**, 2462–2454.

Steinberg, S. and Kaplan, I. R. (1984) The determination of low molecular weight aldehydes in rain, fog, and mist by reversed phase liquid chromatography of the 2,4–dinitrophenyl hydrazone derivatives. *Intern. J. Environ. Anal. Chem.* 18, 253–266.

ten Brink, H. M., Schwartz, S. E., And Daum, P. H. (1987) Efficient scavenging of aerosol sulfate by liquid–water clouds. *Atmos. Environ.* **21**, 2035–2052.

Waldman, J. M. and Hoffmann, M. R. (1987) Depositional aspects of pollutant behavior in fog and intercepted clouds, in *Sources and Fates of Aquatic Pollutants.* Advances in Chemistry Series **216**, 80–129.